UNIVERSITAT DE
BARCELONA

Organ-on-a-chip microfluidic devices mimicking human splenic functions

Luis Guillermo Rigat Brugarolas

Tesis Doctoral

Organ-on-a-chip microfluidic devices mimicking human splenic functions

Memoria presentada por

Luis Guillermo Rigat Brugarolas

Para optar al grado de **Doctor en Biomedicina**

Universitat de Barcelona
Departament d'Enginyeries: Electrònica

Programa de Doctorado en Biomedicina
2012-2016

Tesis dirigida por: **Prof. Josep Samitier Martí**

Dr. Antoni Homs Corbera

Tutor: **Prof. Josep Samitier Martí**

Barcelona, 2016

General Index

## 2.	Materials and methods: engineering the microfluidic devices.

3. A functional microengineered model of the splenon hydrodynamic properties.

4. Mimicking splenic functions and vascular scenarios *in vitro.*

5. Usage of 3D printing techniques to build a splenon-like microfluidic platform.

6. General conclusions.

List of Figures

Abbreviations

2D/3D	Two/Three-dimensional
AFM	Atomic Force Microscopy
BSA	Bovine serum albumin
CA	Central arteriole
CAD	Computer-aided design program
CFP	Co-flow phenomenon
CQ	Chloroquine
D_C	Critical diameter
DC	Dendritic cell
DLP	Digital light projector
$D_{M\%}$	Deformation measurement
ECM	Extracellular matrix
EDTA	Ethylenediamitetraacetic acid
EP	Erythrophagocytosis
FDA	Food and Drug Administration
FITC	Fluorescein isothiocyanate
GFP	Green fluorescent protein
GTA	Glutaraldehyde
HCT	Haematocrit
$H_{L\%}$	Percent haemolysis difference
HpS	Heparin sodium
hSEC	Human splenic endothelial cell
IBEC	Institute for BioEngineering of Catalonia
IES	Interendothelial slits
iRBC	Infected red blood cell
iRET	Infected reticulocyte
LOC	Lab-on-a-Chip
L_{RM}	Length in the pillar matrix
L_S	Length in the slit
MCD	Minimum cylindrical diameter
MD	Human macrophages
M_{ed}	Median
MEMS	Micro electro-mechanical system
mØ	Specialized macrophage
OCD	Organ-on-a-Chip biomimetic model

OD	Optical density
PBS	Phosphate buffered saline
PDMS	Poly(dimethylsiloxane)
PEG-DA	Poly(ethyleneglycol) diacrylate
PFZ	Perifollicular zone
P. falciparum	*Plasmodium falciparum*
P. vivax	*Plasmodium vivax*
P. yoelii	*Plasmodium yoelii*
PTFE	Poly(tetrafluoroethylene)
R&D	Research and development
RBC	Erythrocyte or red blood cell
R_D	RBCs density
Re	Reynolds number
RET	Reticulocyte (immature erythrocyte)
R_H	Hydraulic resistance
RP	Red pulp
RPMI	Roswell Park Memorial Institute medium
S/V	Surface area-to-volume ratio
SEM	Scanning electron microscopy
SOAC	Splenon-on-a-Chip
TEM	Transmission electron microscopy
TV	Trabecular vein
UV	Ultra-violet
WBC	White blood cell
WP	White pulp
µTAS	MicroTotal Analysis System

x

Chapter 1. General Introduction

SUMMARY

The development of the first microengineered model of a human splenon-on-a-chip will be the principal focus of this study. Before the presented work, no research in the Organ-on-a-Chip field was centered on the splenic red pulp, to the best knowledge of the authors: only few in vitro or ex vivo approaches were exhibited. Hence, the creation of such a microfluidic device may have a significant impact, and could help in future evaluation of some biological hypotheses and screening strategies in the ambit of splenic haematological disorders.

1.1. MicroTotal Analysis Systems:
from microdevices to Lab-on-a-Chip platforms.

1.1.1. Introducing MicroTotal Analysis Systems.

MicroTotal Analysis Systems (µTAS), formally defined as miniaturized devices able to perform continuous and fast-response measurements and analysis using small sample volumes, have recently gained considerable importance, in part as a consequence of the improvements made in the field of microfabrication and integration.[1-5]

However, the considered beginning of micro/nano-technologies dates back from the middle of the twentieth century, several decades ago. A visionary speech given by the Novel Prize winner Richard P. Feynman in 1959, titled "There is plenty of room at the bottom", laid the foundation of what was going to be the origin of the application of nano technologies.[4,5]

Nowadays, half a century after, it is possible to miniaturize (nearly) all sorts of mechanisms, and µTAS platforms and devices are fabricated for chemical, biological or even medical applications, to name but a few.[5] These devices could make use of fluid flows operating at the microscale, under particular conditions, and fostered the creation of a novel discipline: "microfluidics".[5,6]

The term µTAS was later expanded and included into a broader concept known as Lab-on-a-Chip (LOC) devices, which encompassed any well-defined laboratory task performed and fully integrated on a single microdevice.[7] The main and principal goal of LOC systems is to achieve a higher efficiency through working in smaller scales, or to perform duties that cannot be done adequately by other means, in a short space of time.[8-12]

Due to the intrinsic nature of these systems, there are several advantages that come as a result of working at the microscopic scale, such as to have the possibility of: (*i*) using smaller samples volumes, (*ii*) improving, or facilitating, the transport of particles through the channels (using, for example, capillary forces),[13] (*iii*) handling cells in a more efficient manner (since it is feasible to work in their dimensional scale)[14,15] and/or (*iv*) integrating several micro-structures (that could facilitate the operability) in a single device, or set of devices; everything, in a cost-effective way, with storage facilities and with the possibility of improving the sensitivity of the sensors.[5,6,11]

Furthermore, the small sizes of its components could be critical to develop portable or handheld apparatus, with potential applications to point-of-care (POC) devices or in-the-field setups.[5,11,12]

1.1.2. Lab-on-a-Chip beginnings and first microfluidic devices.

The possibility to conduct laboratory analysis on miniaturized devices could be seen as highly attractive. These artificial systems could perhaps, not only reduce the time taken to synthesize and/or analyze a product(s), but also could expand the chances to reproduce cell environments, and to maybe study certain diseases in a more closer-to-reality scenario.[5,6,11,12,15]

In this framework, the first described microfluidic-like technology emerged in the 1950's[10], when efforts were made in order to be able to administer minute amounts of samples, providing the

technological basis for actual ink-jet printers.[10,16] For its part, the first proposed micro-fabricated device was presented years later, by S.C. Terry *et al.* in the lates 1970's.[17] However, it was not until the 1990's, time when A. Manz *et al.*[1] proposed the "µTAS concept", that the miniaturization processes and the Micro Electro-Mechanical Systems (MEMSs) stepped forward, thus opening, posteriorly, a new era for LOC devices and microfluidic systems fabrication[5] (in conjunction with the development of micropumps, microvalves or micropippetes, to name a few).[5,10-12,15,16]

Researchers have created platforms for several different applications: droplets generators, for performing a variety of "digital microfluidics" operations on a chip,[18] plasma separation steps, for POC apparatus,[19,20] or even massive parallelization of particle focusing channels, enabling high-efficiency flow cytometry,[21,22] to give some examples.

1.1.3. The concrete impact of microfluidics on biomedicine.

Despite the major advances in fabrication and cell culturing processes, there is still a long way to walk in order to match with the enthusiasm related to the LOC microfluidic technology, in the framework of diagnosis disciplines, biological evaluation, or drug testing.[5,6,12,23,24] Hence, efforts are being directed towards creating novel structures and platforms that could help and/or assist in the research of bioengineering investigators.[6,12,24]

Albeit the reality is that the immense majority of new work related to microfluidics is (commonly) published in "engineering-focused" journals, it is worth saying that (not surprisingly) over the last years, the number of publications strictly focused on LOC systems for biology and/or medicine, have slightly increased, suggesting that these platforms could be starting to gain importance in some routine laboratory assays.[24]

Therefore, it could be stated that platforms for performing cell analysis and/or blood studies are gradually beginning to be recognized and taken into account, partly thanks to several interesting advantages that microfluidics could perhaps provide.[12,15,24]

1.1.4. Lab-on-a-Chip devices for the study of blood rheology and its associated diagnostic applications.

Blood, as a biofluid, is an important source of information about the human body status. Hence, analyzing blood samples is of great interest for many medical applications, in order to minutely evaluate the correct functioning of an organ or vascular system. However, exploiting and taking advantage of all the possibilities that this source of data could give is not simple, so it requires, besides a deep biological knowledge, the usage of appropriate techniques.[25]

Many LOC devices have been developed recently for studying and/or characterizing this type of samples. Some of the methodologies that may be implicated could be classified whether as cell phenotyping or cell isolation techniques (for plasma separation or enrichment of particles).[26-30]

In this regard, mechanobiology, that could be defined as the measurement, or characterization, of the mechanical and/or the adhesive properties of cells and its membranes, could be useful to identify or diagnose some diseases, by examining specific changes in the cellular structures.[30]

Several blood disorders are well-known to induce changes, not only from the properly biological point of view, but also in the intrinsic physical properties of the cells.[30,31] Hence, those structural modifications could result in a change in cells capacity to deform (increasing or decreasing cell stiffness), which may be significant enough to cause a failure in the organic functions.[30] In those scenarios, erythrocytes, or red blood cells (RBCs), could experience an aggravated rigidity.

To study this effect, and cell's rheological properties in different status, several platforms, with integrated capillary-like structures, have been recently developed. These microconstrictions can be shaped either funnel-like fashion or straight, depending on the parameter to examine, or because of microfabrication matters. One of the first microfluidic studies that geared towards modeling RBCs deformability was presented by J.P. Shelby *et al.*[32] This innovative microdevice allowed visualizing the behavior of different RBCs when crossing through micrometer clefts.[32] Another example could be found in the work of A.T. Santoso *et al.*,[33] that fabricated a so-called "cell-phoresis device", with a mechanism analogous to gel electrophoresis, to estimate the RBC stiffness.[33]

1.1.5. Microfluidic strategies for *in vitro* cell cultures.

Microfluidic systems gives also the opportunity to be able to create novel and interesting testing grounds to study and/or monitor (for instance) cellular behavior, growth and/or proliferation, in a (exhaustively) controlled environment and geometries, under different stimuli.[6,12,15,34]

These bio-mimics could, perhaps, also have the ability (*i*) of reproducing physiological scenarios and/or (*ii*) to more closely translate organic biochemical signals.[6,12,15,34]

Moreover, these devices could be valuable for cell assays for a variety of reasons; possibly, the most practical is the resemblance, in terms of dimensions, between cells and the blood vessels, with the channels often built in the LOC devices. Also, they may facilitate the scaling and usage of external sources commonly used for cell manipulation.[6,12,15,34]

Thus, it could be reasonable to state that microfluidic technology has great potential to positively disrupt in the field dedicated to the *in vitro* cell cultures (very relevant to medical disciplines and, possibly, one of the keystones of the modern biology). They could, perhaps, assist in answering and assault, in the future, some biomedical questions.[6,12,15,35]

In this regard, there are many examples of works addressed to this connection. It is possible to found several novel two/three-dimensional (2D-3D) microfluidic strategies that researchers have used, or discovered, to potentiate cell cultures operativity. As an example, neuronal research is extensively performed using LOC devices, since the possibility of defining micrometer channels allows the study of axon behavior and growth in "realistic" scenarios.[36] Besides, it is feasible to build macro-structures no perform pumpless perfusion systems.[37]

Also, although cells in suspension are usually flowing in the near media, they can be physically retained in devices using different strategies.[12,15] A microfluidic device with integrated pneumatic valves, capable of isolating single cells and then release them, was presented by H.S. Kim *et al.*[38] However, the use of non so sophisticated traps are also commonly employed: architectures such as C-like structures[39] or posts could also be used to retain cells in certain positions against flow, basically considering deformability or dimensional characteristics.

Therefore, it is clear that great advances have been made, in the last years, in the "microfluidic cell culturing approach", with the final aim of perhaps utilizing, in the future, these platforms for: personalized medicine, to design organ mimic devices, for implementation in toxicity or efficacy screening (to name a few examples).[6,15,24,40]

1.1.6. Technologies for fabricating polymeric-based LOC devices.

To highlight, possibly one crucial point to take into consideration in the commercial development and/or utilization of several LOC platforms (both in the laboratories and in the industry), is the usage of sophisticated manufacturing technologies, derived from the semiconductor fabrication, that with the passage of time have become accessible, cost-affordable and easy-to-use.[2,5,6,11]

The vast majority of these methodologies were developed in the 1970s-80s for the production of MEMS devices.[2,5,6,11] In addition, with the view to cover a wider range of applications, apart from microfabrication procedures, novel materials (aside from glass) were analyzed and finally added to the existing listing.[2] Nevertheless, although there are many polymers (such as polycarbonate, poly(methylmethacrylate), cyclic olefin copolymer, to name but a few) much more interesting for mass-fabrication and commercialization, most of the microfluidic devices fabricated in research laboratories are made using a compound named poly(dimethylsiloxane) (PDMS).[5,6,41,42] In fact it was not until G. Whitesides *et al.* introduced this silicon-based organic polymer,[42] that research in LOC microfluidic devices stepped forward. Due to its favorable properties, most researchers in this field commonly use PDMS as molding material: it is low-cost, transparent, biocompatible and simple to produce, to name just a few advantages.[2,5,6,24,41,42]

However, depending on the selection of material(s), and the individual needs, the choice for a particular micromachining technology may vary substantially.[43] Even so, the standard procedure for most LOC fabrication processes is "photolithography" (a scheme is shown in Figure 1.1).[5,44] It is one commonly selected and utilized method for building microchannels on top of a planar substrate, due to its ease of use.[5,44] The process entails working with either negative or positive photoresists (normally photocurable epoxy SU-8 or AZ).

A device design, previously "created" in a computer-aided design (CAD) program, is printed on a transparency (called "photomask", normally made of acetate or chrome-on-glass), that will be disposed in contact with the photoresist to produce a relief on a substrate, after illuminating with ultra-violet (UV) light. This will make possible to obtain what is referred as "master".[5] The master will then be used for the casting of, for example, PDMS-LOC devices (soft lithography process).
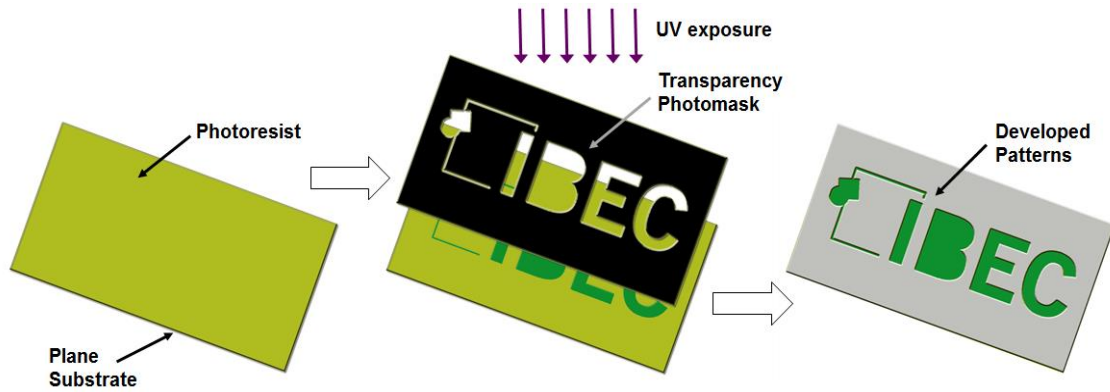
Figure 1.1. Photolithography process. *A positive/negative photoresist is disposed on a plane substrate, and after the incidence of UV light, that passes through a photomask, the drawn design is transferred when developed.[44] (Figure adapted from Reference 44).*

However, because of demands of different specifications (such as faster prototyping, interesting for the disposables market),[5,11] other processes have been developed in parallel to the polymer-based technologies (such as for example, 3D printing, hot embossing or injection molding).[5,43-45]

1.1.7. Hydrodynamics of fluids in small channels of microfluidic systems.

Along with new LOC fabrication methods, it is worth mentioning that these platforms could also benefit from some fundamental physical fluidic properties, that appear when working in small geometries. In that sense, there are several features that differentiate macro *versus* microfluidic systems, being one the most important the absence of turbulent regime, hence laminar flow.[5,6]

In addition, in microsystems, fluids do not usually merge (something that occurs convectively at the macroscale). When several fluid streams flow in a microchannel, they flow in parallel, and the only mixing that occurs is the result of diffusion across the interface between them, after a determined period of time.[5,6] This fact has proven to have (some) advantages in many particular circumstances (such as co-flow devices[46] or hydrodynamic focusing[47]).[5]

It is also important to highlight the role that plays the ratio of inertial-to-viscous forces on fluids, characterized by the dimensionless Reynolds number (*Re*), whose value is typically lower than one in many LOC systems, "setting" the mentioned laminar flow regime.[5]

Hereafter are detailed some physical phenomena and representative equations related to these particular microchannels, to summarize, to the extent possible, the behavior of microfluidic networks and the hydrodynamics of fluids at this scale.[5,48,49] For further information, please refer to Reference 49 (K.W. Oh *et al.*, 2012).

1.1.7.1. Navier-Stokes equation.

When it is possible to consider a continuum of fluid, and the flow is not excessively far removed from the thermodynamic equilibrium, the Navier-Stokes equation could, then, be considered as representative of the fluidic reality being studied.

In microfluidic geometries, fluids could be well approximated as incompressible. So, for uniform-viscous pressure-driven Newtonian fluids, at constant temperatures and with no forces acting throughout the volume, the incompressible (defined when the velocity of the fluid is much lower than the speed of sound)[5] Navier-Stokes equation, dictating velocity, could be defined as:[5,49]

$$D_f (\partial u/\partial t) = - D_f u\nabla u - \nabla p + \mu\nabla^2 u \qquad\qquad \text{(Eq. 1)}$$

where u [m·s^{-1}] is the velocity field; D_f [kg·m^{-3}] is the fluid density; p [Pa] is the pressure, and μ [Pa·s] is the viscosity.

1.1.7.2. The Reynolds number.

To characterize the fluidic behavior in these channels, the *Re* value is normally utilized. Laminar flow occurs at low *Re* (*i.e. Re*<2300). As said, fluid flows in microchannels are, typically, at low *Re*, because of the small geometries, and the common usage of low flow rates, and the inertial effects.[5,49] The *Re* is:

$$Re = \text{(inertia force)} / \text{(viscous force)} = D_f VD/\mu \approx D_f UD_H/\mu \qquad\qquad \text{(Eq. 2)}$$

where V [m·s^{-1}] is the characteristic velocity; U [m·s^{-1}] the area-averaged velocity; D [m] the characteristic length and D_H [m] the hydraulic diameter of a microchannel.[49]

1.1.7.3. Poiseuille flow.

The Poiseuille flow happens at low *Re*, when there is a steady pressure-driven flow, describing a parabolic velocity profile. Hence, the velocity of flow in the center of a channel is greater than the one found in the walls.[49] So, given a long smooth channel, in a steady-state, and completely developed fluid flow, the velocity field of the fluid could be then considered as (*i*) unidirectional, (*ii*) laminar and (*iii*) with no acceleration.[5,49] Consequently, those parameters of the Equation (1) corresponding to the unsteady and convection terms, become zero:

$$\nabla p = \mu\nabla^2 u \qquad\qquad \text{(Eq. 3)}$$

The pressure-driven motion in a microchannel, termed Poiseuille flow, is described as parabolic due to the geometric simplifications and the boundary condition.[49] In this case:

$$u = ((R^2-r^2)/4\mu) (-\partial p/\partial x) = u_{max}(1-r^2/R^2) \qquad\qquad \text{(Eq. 4)}$$

where R,r [m] is the radius; u_{max} is the maximum velocity: $u_{max}=R^2/4\mu (-\partial p/\partial x)$ at r=0, and u=0 at r=R. The X direction is defined as the one along the axis of a microchannel.[49]

When the conditions of the Poiseuille flow apply, behaviour of fluids in microchannels could be approximated by the Ohm's law equivalent solution.

1.1.7.4. The hydraulic resistance.

To calculate hydraulic resistance (R_H, the resistance to flow) in the different branches of a LOC, the following Equation (5) for microfluidic microchannels could be used:[49-51]

$$\Delta P = Q\bullet R_H \qquad\qquad \text{(Eq. 5)}$$

It establishes a relationship, for this type of devices, between Q [$m^3 \cdot s^{-1}$], the volumetric rate of flow of liquid between two points in a microchannel, and ΔP [Pa or $kg \cdot m^{-1} \cdot s^{-2}$], the difference in pressure between those two points. Both terms are proportional to R_H [$Pa \cdot s \cdot m^{-3}$].[50,51]

In a microfluidic channel, with a rectangular cross-section, the laminar flow of the liquid sample may follow Equation (6). In this case *a* is a dimensionless parameter dependant on *W/H* aspect ratio, as shown in Equation (7).[50,51]

$$\Delta P = a\mu QL/WH^3 \qquad \text{(Eq. 6)}$$

$$a = 12\{1-(192H/\pi5W)\ tanh(\pi W/2H)\}^{-1} \qquad \text{(Eq. 7)}$$

where *L* [m] is the length of a microchannel, *W* [m] is the width of a microchannel, *H* [m] is the height of a microchannel.[51]

The presence of bubbles or impediments (*i.e.* obstacles or obstructions) in the microchannel(s) structure could vary the calculated resistance values.[51]

1.1.7.5. Electric circuit analogy.

Electric circuit analogy could be used to help or facilitate a LOC device design, since Hagen-Poiseuille's law (used to calculate the volumetric flow rate Q [$m^3 \cdot s^{-1}$] in a channel), corresponds to Ohm's law (Equation 8):[49,50]

$$Voltage = Current \cdot Resistance \qquad \text{(Eq. 8)}$$

Therefore, the pressure drop is analogous to the voltage drop [V, $kg \cdot m^2 \cdot s^{-3} \cdot A^{-1}$], the volumetric flow rate to the current [A], and the R_H to the electric resistance [Ω, $kg \cdot m^2 \cdot s^{-3} \cdot A^{-2}$] (Figure 1.2). This recognized correspondence could be used to define the fluidic parameters relation in some complex LOC networks, based on electric circuit theory.[49,50]
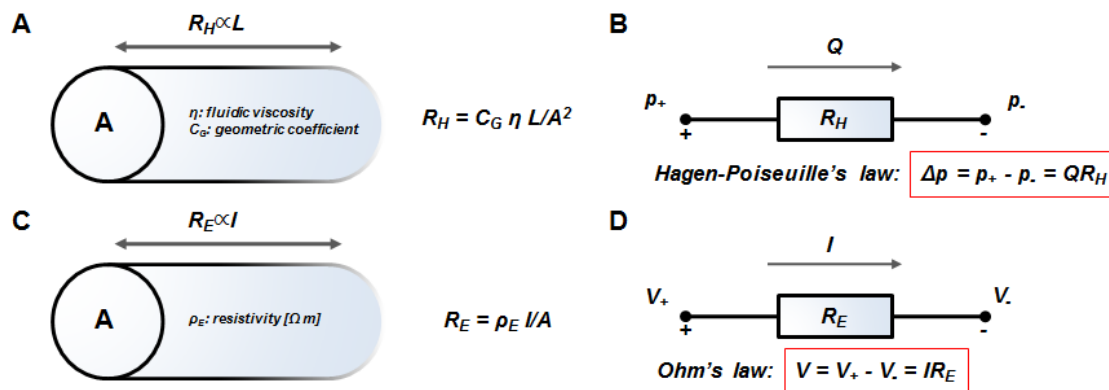
Figure 1.2. The physical similarities between the flow of a fluid and the flow of electricity. *(A) The hydraulic resistance of a microchannel. (B) Equivalent circuit symbol of a fluidic resistance. (C) The electric resistance of a conductive wire. (D) Circuit symbol of the resistor for the electric resistance.[49] (Figure adapted from Reference 49).*

1.2. Blood: structure, rheology and circulatory patterns.

1.2.1. Blood and its components.

Blood, a mixture of cells suspended in a liquid called "plasma" (essentially water with dissolved proteins), is the fluid that circulates within vertebrates, hence being essential to maintain life. Its main key role is to transport ions, gases and nutrients to the different organs, as well as waste products that will have to be filtered out by the kidneys, for elimination. Apart from containing hormones, clotting agents, proteins and immune factors, the basic cell components of blood consists of three main classes: RBCs, white blood cells (WBCs) and platelets.[19,52-54]

A healthy human RBC (that is a specialized cell that delivers oxygen to the body tissues through the vascular system), the dominant blood constituent, which represents *circa* 35-55% by volume of whole blood has, at rest, a biconcave/discoid-like shape with, normally, an average diameter of approximately 7 μm, and a thickness of ~2.5 μm in the outer diameter of the cell, and ~1 μm in the centre.[52,55] Its lipid bilayer membrane, highly deformable, encloses a nucleus-free cytosol, formed by a haemoglobin solution.[52,56,57]

When flowing through the vascular system, and under normal physiological flow conditions[52,56] (for instance, with no clot formation), the hydrodynamic behavior of whole blood is ruled, and regulated, by the interaction of these RBCs with its natural environment comprised, mainly, by the vessel walls and the plasma that surrounds it (apart from other cellular components). In this regard, it is important also to highlight the fact that, due to its nature, blood is not homogeneous (it is a suspension), so it behaves as a non-Newtonian fluid.[56] Thus, its viscosity coefficient is no longer a constantly defined property.[52,54,56]

1.2.2. Blood rheology and haemodynamics.

Thanks to the research carried out by R. Fahraeus, a Scandinavian pathologist, in the early part of past century,[58] and, posteriorly, through the development and usage of adequate techniques to study RBCs bending capacities and blood hydrodynamic behavior and rheological properties, it became possible the emergence of a new discipline applied to the practice of haematology, that was termed blood rheology or "haemorheology".[52,54,56,58]

From a biological viewpoint, blood could be defined as a liquid containing various elements, and blood cells themselves. Therefore, plasma (*i.e.* the suspending phase), is clearly one of the key players determining the properties of blood, in the sense that a variation in its state could affect the blood viscosity (independently of other factors such as, for instance, the properties of the components). It has been identified that the higher viscosity values are commonly seen in non-physiological scenarios, closely related to the protein, or phase reactants, content (for example, fibrinogen) of plasma.[52,54,56]

In large vessels, blood rheological behavior and viscosity could be considered, besides, mainly dependent on blood volume percentage of RBCs in the blood (*i.e.* haematocrit).[54,56] However, in smaller vessels, such as the capillaries (where cells have to significantly stretch to pass through

narrow geometries), cell deformability and aggregation could play a major role in opposing fluid movement (so, resistance to flow).[59] In that sense, since the extraordinaries bending properties of RBCs (essentially linked to its structure)[52,56] are pivotal for cell lifespan in the circulation, any biomechanical alteration in its structure is likely to influence and impact in blood flow demeanor, as could happen in several haematological disorders (as detailed in Chapter 1.1.4.).[56,59,60] Thus, RBCs rheological properties could be highly significant for that matter.

RBCs orientation is also a leading factor affecting blood rheological behavior. In that sense, flow streamlines perturbation or alteration by non-deformable RBCs or cell aggregates also seems to affect to blood viscosity.[56,61,62]

1.2.3. Erythrocytes in microcirculation.

Blood non-Newtonian behavior, both in large and small blood vessels, could then be related to the intrinsic RBCs properties (basically deformability/rigidity), and aggregation.[56,63,64] The impact of other cells types on the macroscopic flow could be defined as "no significant", due to their low concentration in blood, or small dimensions. However, this picture changes in microcirculation, where they could contribute notably to blood flow resistance and hydrodynamics.[56] At the scale close to a microvascular network, blood could be considered as a cell suspension flowing inside a Newtonian plasma.[56,65,66]

1.2.3.1. Single-cell dynamics.

Plasma flow in microvasculature is mainly laminar; however, the *Re* value may oscillate several orders of magnitude.[65] RBCs are known to display distinct hydrodynamic behaviors/movements (named "tumbling", "tank-treading" and "swinging") and even adopt different "forms" depending on the *Re* and the magnitude of the acting shear forces (the RBC inner/outer fluid viscosity ratio could also contribute).[65,67-69] They also have, as detailed, an extraordinary stretching capacity, due to its deformable membrane, which is valuable to undergo micrometer constrictions.[52.65] To remark is that, at branching points in fine blood vessels, every single RBC will likely flow into the branch with less resistance to flow, and therefore with a higher flow rate. This effect is known as "Zweifach-Fung effect" (named in honor of its discoverers).[70-72]

1.2.3.2. Blood parabolic profile in microfluidic-like channels.

RBCs, that are small and deformable, while flowing, tend to migrate to the channel center (axial migration) due to pressure gradients imposed by the non-uniform flow velocity profile across the channel.[54,56,65,73,74]

In this kind of small geometries, the walls of the vessel/channel provokes a slowing down and brake of the blood fluid motion and its consequent velocity, that gradually increases towards the axis, where there are no physical barriers. This fact promotes the apparition of a parabolic cross sectional profile, under laminar flow, known as Poiseuille flow (as detailed in Chapter 1.1.7.3.). This phenomenon causes the RBC scrolling towards the centre of the geometry. As a result, the average RBC speed in the centre is greater that the axial velocity to be found in the adjoining plasma.[54,56,65,75]

1.2.4. Erythrocytes deformability and its implications in haematological disorders.

1.2.4.1. RBCs membrane aiding deformability scenarios.

As mentioned, RBCs are able to greatly modify its shape under different flow conditions and/or applied forces, by virtue of its high ability to deform (*i.e.* RBCs deformability). This behavior is mainly a function of three cellular properties:[50,52,56,76-79] the intracellular viscosity, the geometry of the cell, or its surface area-to-volume ratio (S/V),[80] and also the viscoelastic properties of the cytoplasmic membrane;[50,52,56,76,81] this last one could become compromised as a result of some diseases, inducing permanent plastic modifications to the membrane.[56] Notwithstanding, RBCs principally behaves as an elastic entity, which means that those changes are reversible and the cell membrane will be able to return to its original shape, in physiological conditions.[52,56,79]

Therefore, RBCs are able to rapidly change its shape while keeping its structural integrity intact. And this feature is of enormous interest for the maintenance of body blood homeostasis. The excess surface area of its membrane structure (in comparison with a sphere) gives to the RBCs the capacity to deform and pass through capillaries and narrow constrictions with ease.[52,56,59,82]

1.2.4.2. Erythrocytes deformability in pathological/physiological scenarios.

The study of cells biomechanical properties could provide valuable data and perspectives about the human body function,[26,83-85] and in the framework of the RBCs,[52,56] structural changes in its rheological properties has been closely associated with several haematological disorders.[59] As RBC deformability affects blood rheology and its movement along capillaries/microconstrictions, implications could take place when membrane properties vary over physiological tresholds.[52,59]

Since the status of the environment in which the RBCs are flowing could affect its rheological demeanor (apart from the metabolic functionality), changes in the physiological conditions could perhaps also induce pathological changes to the RBCs biomechanical settings.[52,56,59]

Some diseases are derived from losses in the RBCs physical properties. Other haematological disorders, however, affect RBC deformation more directly (then, its survival), such as hereditary spherocytosis, sickle cell anemia,[59] or malaria.[52,86] In this last, several complications could take place derived from RBCs sequestration by *Plasmodium* parasite, and an increase of membrane shear modulus could also be appreciated, which could lead to a multiorgan failure, anemia or an enlargement of the spleen, named splenomegaly.[52,54,60,87]

In normal healthy context, RBCs, that are continuously flowing in the body vascular system[52,56] experimenting, therefore, persistent mechanical/chemical stresses could, at some point, loss membrane properties that could directly affect its deformability, due to a decrease in size and in the S/V.[52,88] This phenomenon has been observed in aged-RBCs.[52,56,76,87] In those cases, RBCs could tend to resemble to a sphere, rather than its characteristic biconcave shape, resulting in a poor deformation capacity.[52,59,82] This leads to the fact that non-fresh or unhealthy RBCs would be likely removed from circulation by the spleen, and more specifically in its red pulp histological region, where some main blood filtration mechanism are located.[52,56,76,89,90]

1.3. The importance of blood filtering: the role of the spleen in the human body.

1.3.1. Introduction.

The spleen is, probably, one of the most lesser-known organs in the body. However, nowadays, it is being recognized the importance of this organ in several haematological disorders.[89-93] This is thanks to the research conducted by scientists during the past centuries. In this regard, one should highlight (*i*) the importance of M. Malpighi's research, that studied the splenic capsule,[92] and proved the division of this organ into two main sections, red and white pulp (terminology still used in these times)[92] or (*ii*) the identification of the reticular structure of the splenic red pulp, by A. Tigri.[92] The conception and understanding of the functions of the human spleen is something that has been evolving over the years.[90,92,94]

1.3.2. Structure and function of the spleen.

The spleen, located in the left section of the abdomen, is the largest lymphoid organ and filter of the blood in the human body, thanks to its unique architecture.[89,90,95-98]

It is able to perform many functions that are vital to maintain a correct homeostasis in the body, regarding mainly to RBCs, and the immune system. It is responsible of, (very) selectively, clear from circulation those elements that should not be in the blood stream, such as pathogens and non-healthy/aged/parasitized-RBCs.[89,92,90,98] In addition, due to the presence of several immune cell types in its structure (for instance, B/T-cells, or macrophages), also combines an essential innate and adaptive immune response.[89,90,95,98] These "defense mechanisms" makes the spleen a necessary element to face some haematological disorders.

However, there are several factors that impede a systematic investigation of some important splenic functions, that could help to deepen in the knowledge of the mechanisms involved[89,90] to perform the previously described "duties"; the most limiting ones are, probably, that (*i*) there are clear anatomical and physiological differences between the spleen of a mouse and of a human, and (*ii*) the difficulty to examine the human organ in healthy scenarios.[89,98,99]

In terms of morphology, it could be said that the human spleen is defined to be basically formed of two main sections: the red pulp and the white pulp. In addition, also could be considered the marginal zone, that is the region that divides both pulps.[89,97,99]

The red pulp acts, mainly, as the splenic blood filter, able to remove non-healthy RBCs from the blood stream. For its part, the white pulp, located near the central arterioles, is responsible, for example, for immune response processes.[89,97,100]

Hereafter, the splenic compartments are (briefly) detailed (with special attention to the red pulp). For more information, please refer to References 89 to 102.

1.3.2.1 The white pulp.

The white pulp, that is organized as lymphoid sheaths around arterial vessels, is one lymphoid tissue holding the majority of immune effector cells.[99] It is divided into different sections, named the periarteriolar lymphoid sheath (also known as T-cell zone) and the follicles.[89,90,97,99]

1.3.2.2. The marginal zone.

The marginal zone could be identified as a histological region dividing the two pulps, although some authors consider it as part of the white pulp.[97] The major role of this region is (*i*) to actively search and capture pathogens, and also is (*ii*) key in antigen processing.[89,90,97,99]

1.3.2.3. The red pulp.

The red pulp is the zone of the human spleen that represents the major part of its volume, and it happens to be, mainly, the blood filtering mechanism of the organ.[89,90,99,101] It is formed by:

> (*i*) Sinuses, and the
>
> (*ii*) Splenic cords (or the cords of Billroth, an "open" blood system without an endothelial lining, containing numerous specialized and highly phagocytic macrophages).[89,90,97,99]

It displays a complex structure that permits to accomplish its tasks, with the assistance of the characteristic splenic dual network.[89,90,97,99] The macrophages inhabiting in the splenic red pulp open circulation, apart for playing a key role in iron recycling processes, are responsible for the removal of senescent RBCs, and microorganisms (such as bacteria), from the splenic or global blood circulation.[89,90,97,99,102-105]

The venous sinuses, that consists on a parallel arrangement of endothelial cells,[89] "collects" the blood samples once they have passed through the human splenic cords.[89,99] This endothelium is connected to components of the extracellular matrix (ECM) by stress fibers, forming multitude of micrometer-sized constrictions, named interendothelial slits (IES), that are known to be the narrowest constriction in the human body.[50,89,90,97,99] The crossing through those slits becomes a (last) stringent "deformability test" for cells, in the sense that, for instance, unhealthy rigid RBCs will likely be unable to pass through the IES.[89,90,97,99,103]

In terms of hydrodynamic behavior, once blood enters the spleen, through a central artery, it is divided into trabecular arteries, where the small branching vessels finally enter the splenic red pulp.[99] Recently, the circulation patterns of the spleen has been investigated, *in vivo*, by means of ultrasonography.[50,104] In this work,[104] the obtained data showed and confirmed a dual splenic circulatory organization:[50,89,99,104,105]

> (*i*) Closed/fast circulation (bypassing the reticular meshwork of the red pulp, entering the marginal zone, flowing through the adjacent venous sinuses),[90,97,99] and the
>
> (*ii*) Open/slow circulation (flowing, mainly, through the cordal open system of the splenic red pulp).[89,90,97,99,104,105]

These circulations hold, respectively, the ~90% and the remaining ~10% of the total blood flow of the spleen.[50,89,90,99,104] This means that only a (small) portion of the total RBCs population that enters, every time, into the spleen are going to be "sensed" for their deformability at some point of the red pulp (as shown in the scheme of Figure 1.3).

The open/slow circulation (termed this way, as detailed, due to the lack of endothelium),[105] has a labyrinthine slow-motion circulatory structure, that allows time for specialized macrophages to clear from circulation the unwanted elements.[92,103] Both fast and slow circulations are connected by the IES, where cells are called upon to squeeze in order to reach the venous system (Figure 1.3).[50,89,99,104,105]

As detailed, RBCs are capable to exhibit high deformability in physiological scenarios, essential virtue to flow through narrow geometries, narrower than their original shape. However, in some diseases, or due to aging, this extraordinary physical property could be compromised, and could lead to RBC retention in the IES, in a process in which the human body maintains physiological scenarios.[52,54,56,59,90,99,104,105]

Posteriorly, it has been described that the splenic macrophages could phagocytize those cells in a "selection process" still not fully understood.[90,97,99,103,104,105]
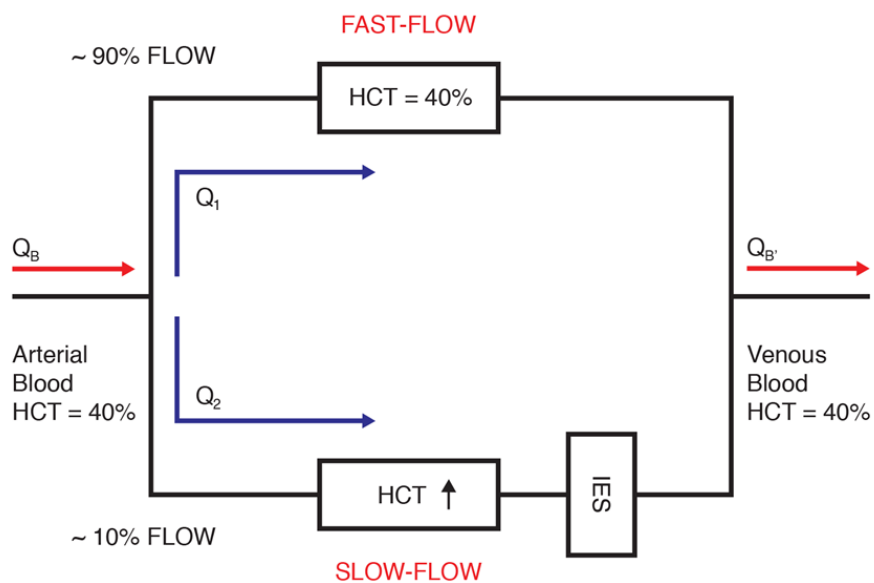
Figure 1.3. Splenic microfluidic network. *Scheme representing the blood flow division that seems to occurs in the human spleen.[50]*
Abbreviations: Q, volume flow; HCT, haematocrit.

Although the overall picture of this organ is, nowadays, clear enough to understand most of its main functions, there are several mechanisms that are important in different diseases that need of further studies. Recent advances in bioengineering and microfluidics could facilitate the task of better understanding the role of the spleen in different scenarios, by helping in the creation of novel disease and physiological models.[50,89,99]

1.4. From 2D/3D cell cultures to living systems on a microfluidic device: Organ-on-a-Chip biomimetic model platforms.

1.4.1. Introduction: changing the paradigm.

Despite their highly demonstrated importance and utility over the last decades in the biomedical field, traditional 2D and more actual 3D cell culture models have not seem to fully cover some of the necessities that could be considered of great importance for the future of the pharmaceutical investigation, such as be able, to some extent, to predict the activity of candidate compound.[106]

The development of (novel) microfluidic strategies, incorporating multiple cell types and/or fluid flow, to resemble, for example, tissue interaction with circulating blood and immune cells, could have great interest for designing dynamic platforms reproducing, to the extent possible, (even) both health and disease scenarios.[106-108] This could perhaps also help in providing novel testing grounds to have the possibility to study some diseases were no robust models exist.

Then, although 2D/3D cell culture strategies signified a considerable technological advance, at that time, improvements could be done in order to (faster) achieve the goal of mimicking more accurately principal organ functions *in vitro*. In this framework, microfluidics has much to say, as the body itself is governed under similar flow regimes, in similar geometries. Together with a "bioengineering improvement", a deeper human (patho)physiology knowledge is also required. This is why, due to the existing limitations in actual cell-based methodologies, there is a strong desire in developing robust *in vitro* alternatives.[106,109-111]

1.4.2. Diagnosing the decline in pharmaceutical R&D efficiency.

Actual analysis and characterization of some disease processes commonly requires, and relies, in the use of animal studies.[109,110] Even so, these models could fail to predict what could happen in human beings when treated with a specific drug, in terms of its toxicity and efficacy.[109,110] This is something that the pharmaceutical industry has already realized. In this framework, studies have shown that, with the passage of time, fewer new drugs are being approved by the Food and Drug Administration (FDA) in recent years.[24,112,113] The usage of alternative methodologies to perform these assays could, ideally, reduce the costs, lengthy processes and ethical issues related to animal testing, and could become, in the future, an attractive alternative in order to be (more) predictive of human results.[106,109,112]

Another reality is that a large number of drug candidates fails in different stages of the clinical trials, due to safety/toxicity problematic,[114,115] and there are also examples of drugs removal or limited use due to adverse effects after the acceptance in the market.[106,109,115]

1.4.3. Approaching the *in vitro* clinical trial: engineering Organs-on-a-Chip.

Scientists working in the field of biomedical engineering have noticed this circumstance, and are beginning to address this problematic by designing and prototyping cell-oriented µTAS platforms that could be able, ideally, to reduce the issues associated to drug development. Progress in the microfluidic technology and in the *in vitro* cell culture methodologies (that is, the junction of engineering and biomedicine) are enabling to microengineer sophisticated chips, seeking to reproduce, to the extent possible, some *in vivo* organ functions, in order to assist in clinical uses with new (routine) tools to deal with essential biological questions.[15,106,109-111] And this new class of microfluidic devices were called "Organ-on-a-Chip" biomimetic models (OCD).[106,109-111,116]

The aim of this technology is to integrate/combine the knowledge acquired from (for instance) microfluidics, physiology, (bio)chemistry and physics into a sole organ model device, to could mimic some relevant physiological mechanisms of the minimal functional subunit of an organ or tissue (to the extent possible), on-a-chip; that is, to artificially mimic aspects of the human organ (like: morphology, movement, flow or rheological properties), *in vitro*.[15,106,109-111,116]

Thus, these newfangled OCD devices may be valuable to expand knowledge in the mechanism of different diseases and could help, in the future, to prioritize animal studies for pharmaceutical trials.[106,109,110,116] So, the idea is to develop platforms that could better approximate the *in vivo* cellular structure, in comparison with traditional culture methods, but without the complexity of animal models. In addition, as it is feasible to work with human cells (cultured in an "organ-like" environment), results could be closer to what is likely to happen in a human being.[15,106,109-111,116]

1.4.4. Organ-on-a-Chip functionalities.

OCDs could be promising tools for the investigation of basic mechanisms of both pathological and physiological organ scenarios. For instance, researchers have, recently, designed devices for studying the kidney,[117] lung,[118] liver,[119] heart,[120] gut,[121] bone marrow[122] and brain,[123] to name a few examples.[106,116]

Also, one of the principal reasons for developing this technology is for their desired implication in drug toxicity-screening methodologies. In this regard, one of the first works/major steps in this framework was conducted by K. Viravaidya *et al.* in 2004 with the creation of a microfluidic multi chambers cell-culture analog, to asses cell response to different chemicals.[106,124] A more recent study using, for instance, the first lung-on-a-chip (by D. Huh *et al.*),[106,118,125] showed that could be viable to use OCDs to test or to find alternative uses to drugs.

Summarizing, taking into account human physiology, it could be possible to "localize" an OCD mimicking nearly every organ in the body. However, though it has a notable importance in many haematological disorders,[99] no studies in this new field were focused on the splenic red pulp (to the best knowledge of the authors). In order to have a deeper knowledge of this organ, different strategies could be employed, and OCD technologies emerges as an interesting methodology to try to deepen in some physiological aspects of the spleen that are still unidentified.[50,99,116]

1.5. Meeting spleen physiology with microfluidics: developing a splenon on-chip.

1.5.1. Introduction and state-of-the-art of spleen-like platforms.

It might be argued that few studies are strictly oriented on the spleen, in comparison with other human organs. As mentioned, some difficulties to examine it in healthy scenarios provoke that little is known about some of its functions in several haematological disorders. Therefore, the development of new strategies that could facilitate the discovery of new clues to elucidate the spleen role in some pathological settings could be a door to understand its usefulness.[89,98,99]

This is why it was considered interesting to focus attention and efforts in building a biomimetic device mimicking, to the extent possible, the structure of the human splenic red pulp. This could ideally facilitate the acquisition of data that could help (*i*) in the development of new drugs, or (*ii*) in the understanding of some mechanisms of action of blood illness and the related pathogens.

As pointed previously, microfluidics could provide extraordinary tools to fabricate and develop a robust platform to achieve the desired goals. Thus, the principal objective of this thesis will be to design, and fabricate, a microengineered OCD model device that could be able to mimic, to the extent possible, both the hydrodynamic blood behaviour and part of the cellular environment of a human splenon. This microfluidic device will be referred to as "Splenon-on-a-Chip",[50] defining the "splenon" as the minimal structural functional unit of the red pulp able to maintain its filtering functions.[105]

Before our study, no OCD microfluidic device mimicked those splenon physiological features (to the best knowledge of the authors). Although some approaches could be found in literature, the devices seemed not to be able to mimic some distinctive features of the splenon.

In one example, C. Lavazec *et al.* developed a system based on beads.[126] Those microspheres, with two different size distributions (5-15 μm and 15-25 μm diameters), were mixed to create an *in vitro* matrix mimicking the human splenic constrictions. After mixing the beads, a micrometer pore size was obtained, resembling the size of the IES.[127] Thus, this device forces the passage of individual RBCs and infected RBCs (iRBCs) through several "slits". In spite of this major difference with the *in vivo* scenario, results on trapping by this device paralleled with the ones obtained on an *ex vivo* model of the human spleen.[50,126,127]

After our first approach, J. Picot *et al.* fabricated a platform that resembled to a filtration unit, aiming to reproduce the physical constrictions that RBCs have to cross on a human spleen.[128] They analyzed, in this study, how stiffer RBCs accumulated in the narrower slits, and verified that the architecture of their device was able to quantify the mechanical properties of different RBCs populations.[128] Notwithstanding, no splenic cell environment was mimicked.

Also, researchers at Wyss Institute (J.H. Kang *et al.*, Harvard University, USA) have created a blood purification system that acts as an "artificial spleen" (this is why they call it "biospleen"), that filters blood samples by using magnetic nanobeads engineered to capture a wide range of toxins and microorganisms.[129]

1.5.2. Objectives and dissertation outline.

The presented thesis, entitled:

 "**Organ-on-a-chip microfluidic devices mimicking human splenic functions**"

aims to make its contribution in the fields of Biomedicine and Biomedical Engineering, were its research will present novel microfluidic devices that mimic, to the extent possible, some human splenon physiological features.

Furthermore, there are several specific objectives:

- Develop an OCD biomimetic platform, with close splenic physiological measurements, using photolithographic and molding techniques with biocompatible materials, that could reproduce, to the extent possible, similar splenon blood hydrodynamic behavior.
- Characterize, calculate and adjust the fluid dynamics of this novel microfluidic platform, using simulations and experimentation.
- Fabricate the device using innovative techniques, to achieve multilayered microfluidic channels, in a cost-effective manner.
- Replicate, to the extent possible, with this device, close filtering functions of the splenon by fabricating micrometer-sized constrictions.
- Create a closed-loop pumping strategy that could facilitate the tests. The entire platform (as a proof of concept) should be able to work at close physiological conditions.
- Describe an on-chip functionalizing protocol, in order to properly coat the sections of the device with appropriate proteins in order to facilitate cell culture.
- Work with human spleen cells in order to mimic part of the cellular environment of the splenon (to the extent possible), to better capture the physiology of the organ.
- Translate vascular tissue-cell and cell-cell interactions, and perform drug trials in order to verify the possible usefulness of the platform for future screening processes.
- Reproduce, to some extent, some disease scenarios, related to the spleen pathological obstruction.
- Deepening in the expertise of 3D printing techniques, to fabricate innovative prototypes that could perhaps, in the future, facilitate different assays.
- Elaborate 3D printed microfluidic devices able to complement with the actual laboratory equipment.

The involved study, so as to achieve these objectives, will be exposed in the following chapters:

Chapter 2. Materials and methods: engineering the microfluidic devices.

Different methodologies and the selection of materials, and building processes, implemented for the development of the microfluidic devices, are introduced. Together with the setups used, the tools employed to perform the different assays will be detailed.

Chapter 3. A functional microengineered model of the splenon hydrodynamic properties.

With the aim of trying to mimic the blood flow behavior and the filtering function of the splenon, it would be introduced a novel microengineered OCD model reproducing, to the extent possible, some hydrodynamic forces and physical properties of the splenon. A description will be given, as a proof of concept, of the evaluated mechanical and physiological responses, using human RBCs and malaria-infected cells.

Chapter 4. Mimicking splenic functions and vascular scenarios *in vitro.*

A second, and enhanced version, of the splenon-on-a-chip, with upgraded filtering constrictions and a secondary inlet, devised to use laminar co-flow properties, will be presented. This version of the functional microengineered model can be completed with a closed-loop pumping station.

Chapter 5. Usage of 3D printing techniques to build a splenon-like microfluidic platform.

A new edition of the splenon-like prototype will be discussed. This time, 3D printing techniques will raise to a concept that aims to facilitate, in the future, laboratory tests. This initial prototype, designed to be user-friendly, is able to function with porous membrane filters.

Chapter 6. General conclusions.

In this chapter, the general conclusions are presented, highlighting the most remarkable results obtained in this work.

1.6 References.

1. A. Manz, N. Graber and H.M. Widmer, *Sensors and Actuators B: Chemical*, 1990, **1**, 244-248.
2. D.R. Reyes, D. Iossifidis, P.A. Auroux and A. Manz, *Anal. Chem.*, 2002, **74**, 2623-2636.
3. A. van den Berg and T.S.J. Lammerink, *Topics in Current Chemistry*, 1998, **194**, 21-49.
4. R.P. Feynman, *Journal of Microelectromechanical Systems,* 1992, **1**, 60-66.
5. P. Tabeling, Introduction to Microfluidics, Oxford University Press, 2005.
6. G.M. Whitesides, *Nature*, 2006, **442**, 368-373.
7. A.E. Guber, M. Heckele, D. Herrmann, A. Muslija, V. Saile, L. Eichhorn, T. Gietzelt, W. Hoffmann, P.C. Hauser, J. Tanyanyiwa, A. Gerlach, N. Gottschlich and G. Knebel, *Chemical Engineering Journal*, 2004, **101**, 447-453.
8. A.J. Mach, O.B. Adeyiga and D. Di Carlo, *Lab Chip*, 2013, **13**, 1011.
9. P.A. Auroux, D. Iossifidis, D.R. Reyes and A. Manz, *Anal. Chem.*, 2002, **74**, 2637-2652.
10. L. Gervais, N. de Rooij and E. Delamarche, *Adv. Mater.*, 2011, **23**, 151-176.
11. S.S. Saliterman, BIOMEMS and Medical Microdevices, SPIE - The International Society for Optical Engineering, 2006.
12. J. El-Ali, P.K. Sorger and K.F. Jensen, *Nature*, 2006, **442**, 403-411.
13. M. Zimmermann, H. Schmid, P. Hunziker and E. Delamarche, *Lab Chip*, 2007, **7**, 119-125.
14. J.P. Wikswo, E.L. Curtis, Z.E. Eagleton, B.C. Evans, A. Kole, L.H. Hofmeister and W.J. Matloff, *Lab Chip*, 2013, **13**, 3496.
15. M.L. Kovarik, P.C. Gach, D.M. Ornoff, Y. Wang, J. Balowski, L. Farrag and N.L. Allbritton, *Anal. Chem.*, 2012, **84**, 516-540.
16. A. Rios, M. Zougagh and M. Avila, *Analytica Chimica Acta*, 2012, **740**, 1-11.
17. S.C. Terry, J.H. Jerman and J.B. Angell, *IEEE Transactions on Electron Devices*, 1979, **26**, 1880-1889.
18. S.Y. Teh, R. Lin, L.H. Hung and A.P. Lee, *Lab Chip*, 2008, **8**, 198-220.
19. M. Kersaudy-Kerhoas and E. Sollier, *Lab Chip*, 2013, **13**, 3323-3346.
20. A.I. Rodriguez-Villareal, M. Arundell, M. Carmona and J. Samitier, *Lab Chip*, 2010, **10**, 211-219.
21. S.C. Hur, H.T.K. Tse and D. Di Carlo, *Lab Chip*, 2010, **10**, 274.
22. H. Amini, W. Lee and D. Di Carlo, *Lab Chip*, 2014, **14**, 2739.
23. G.M. Whitesides, *Lab Chip*, 2012, **13**, 11-13.
24. E.K. Sackmann, A.L. Fulton and D.J. Beebe, *Nature*, 2014, **507**, 181-189.
25. M. Toner and D. Irimia, *Annu. Rev. Biomed. Eng.*, 2005, **7**, 77-103.
26. J. S. Dudani, D. R. Gossett, H. T. Tse and D. Di Carlo, *Lab Chip*, 2013, **13**, 3728-3734.
27. H. Bow, I.V. Pivkin, M. Diez-Silva, S.J. Goldfless, M. Dao, J.C. Niles, S. Suresh and J. Han, *Lab Chip*, 2011, **11**, 1065-1073.
28. S.C. Hur, N.K. Henderson-MacLennan, E.R.B. McCabe and D. Di Carlo, *Lab Chip*, 2011, **11**, 912-920.

29. H.W.H. Hou, A.A.S.B. Bhagat, A.G.L. Chong, P.M. Mao, K.S.W. Tan, J. Han and C.T. Lim, *Lab Chip*, 2010, **10**, 2605-2613.

30. Y. Nematbakhsh and C.T. Lim, *Acta Mech Sin*, 2015, **31**, 268-273.

31. G.Y. Lee and C.T. Lim, *Trends Biotechnol.*, 2007, **25**, 111-118.

32. J.P. Shelby, J. White, K. Ganesan, P.K. Rathod and D.T. Chiu, *Proceedings of the National Academy of Sciences of the United States of America*, 2003, **100**, 14618-14622.

33. A.T. Santoso, X. Deng, J.H. Lee, K. Matthews, S.P. Duffy, E. Islamzada, S.M. McFaul, M.E. Myrand-Lapierre and H. Ma, *Lab Chip*, 2015, **15**, 4451-4460.

34. I. Barbulovic-Nad and A.R. Wheeler, Cell Assays in Microfluidics, Springer, 2014.

35. A.L. Paguirigan and D.J. Beebe, *Integrative Biology*, 2009, **1**, 182-195.

36. J. Park, H. Koito, J. Li and A. Han, *Biomed. Microdevices.*, 2009, **11**, 1145-1153.

37. H.E. Abaci, K. Gledhill, Z. Guo, A.M. Christiano and M.L. Shuler, *Lab Chip*, 2015, **15**, 882-888.

38. H.S. Kim, T.P. Devarenne and A. Han, *Lab Chip*, 2015, **15**, 2467,2475.

39. P.J. Lee, P.J. Hung, V.M. Rao and L.P. Lee, *Biotechnology and Bioengineering*, 2006, **94**, 5-14.

40. V. van Duinen, S.J. Triestsch, J. Joore, P. Vulto and T. Hankemeier, *Current Opinions in Biotechnology*, 2015, **35**, 118-126.

41. A. Mata, A.J. Fleischman and S. Roy, *Biomedical Microdevice*, 2005, **7**, 281-293.

42. J.C. McDonald and G.M. Whitesides, *Accounts of Chemical Research*, 2002, **35**, 491-499.

43. G.S. Fiorini and D.T. Chiu, *Biotechniques*, 2005, **38**, 429-446.

44. Y. Shin, S. Han, J.S. Jeon, K. Yamamoto, I.K. Zervantonakis, R. Sudo, R.D. Kamm and S. Chung, *Nature Protocols*, 2012, **7**, 1247-1259.

45. A.K. Au, W. Lee and A. Folch, *Lab Chip*, 2014, **14**, 1294-1301.

46. C.A. Parra-Cabrera, C. Sporer, I. Rodriguez-Villareal, R. Rodriguez-Trujillo, A. Homs-Corbera and J. Samitier, *Lab Chip*, 2012, **12**, 4143-4150.

47. J.B. Knight, A. Vishwanath, J.P. Brody and R.H. Austin, *Physical Review Letters*, 1998, **80**, 3863-3866.

48. Di Carlo, *Lab Chip*, 2009, **9**, 3038-3046.

49. K.W. Oh, K. Lee, B. Ahn and E.P. Furlani, *Lab Chip*, 2012, **12**, 515-545.

50. L.G. Rigat-Brugarolas, A. Elizalde-Torrent, M. Bernabeu, M. de Niz, L. Martin-Jaular, C. Fernandez-Becerra, A. Homs-Corbera, J. Samitier and H.A. del Portillo, *Lab Chip*, 2014, **14**, 1715-1724.

51. M.J. Fuerstman, A. Lai, M.E. Thurlow, S.S. Shevkoplyas, H.S. Stone and G.M. Whitesides, *Lab Chip*, 2007, **7**, 1479-1489.

52. N. Mohandas and P.G. Gallagher, *Blood*, 2008, **112**, 3939-3948.

53. T.W. Secomb, *Cell Biophysics*, 1992, **1**, 231-251.

54. E.W. Merrill, *Physiological Reviews*, 1969, **49**, 863-888.

55. C. Toumey, *Nature Nanotechnology*, 2011, **6**, 191-193.

56. O.K. Baskurt and H.J. Meiselman, *Blood rheology and hemodynamics*, 2003, **29**, 435-450.

57. M.A. Fedosov, B. Caswell and G.E. Karniadakis, *Biophysical Journal*, 2010, **98**, 2215-2225.

58. H.L. Goldsmith, G. Cokelet and P. Gaehtgens, *Am J Physiol*, 1989, **257**, 1005-1015.

59. G.A. Barabino, M.O. Platt and D.K. Kaul, *Annu. Rev. Biomed. Eng.*, 2010, **12**, 345-367.

60. J. Stuart and G.B. Nash, *Blood reviews*, 1990, **4**, 141-147.

61. H. Schmid-Schönbein, R.E. Wells and J. Goldstone, *Biorheology*, 1971, **7**, 227-234.

62. R. Wells and H. Schmid-Schönbein, *J Appl Physiol*, 1969, **27**, 213-217.

63. S. Chien, *Annu Rev Physiol*, 1987, **49**, 177-192.

64. G. Mchedlishvili, M. Varazashvili and L. Gobejishvili, *Clin Hemorheol Microcirc*, 2002, **26**, 99-106.

65. M. Kersaudy-Kerhoas, R. Dhariwal, M.P.Y. Desmulliez and L. Jouvet, *Microfluid Nanofluid*, 2010, **8**, 105.

66. Y.C. Fung, *Biomechanics*, 2nd edition. Springer, New York, 2004.

67. M. Abkarian and A. Viallat, *Soft Matter*, 2008, **4**, 653-657.

68. M. Abkarian, M. Faivre and A. Viallat, *Phys Rev Lett*, 2007, **98**, 188302.

69. A.M. Forsyth, J. Wan, P.D. Owrutsky, M. Abkarian and H.A. Stone, *Proceedings of the National Academy of Sciences of the United States of America*, 2011, **108**, 10986-10991.

70. K. Svanes and B.W. Zweifach, *Microvascular Res*, 1968, **1**, 210, 220.

71. R.T. Yen and Y.C. Fung, *Am J Physiol*, 1978, **253**, 251-257.

72. Y.C. Fung, *Microvas Res*, 1973, **5**, 34-48.

73. L.E. Bayliss, *J Physiol*, 1959, **149**, 593-613.

74. H.L. Goldsmith and S.G. Mason, *Nature*, 1961, **190**, 1095-1096.

75. A. Narasimhan, Blood Flow and Fahraeus Effect.

76. A. Bransky, N. Korin, Y. Nemirovski and U. Dinnar, *Microvascular Research*, 2007, **73**, 7-13.

77. N. Mohandas and J.A. Chasis, *Semin Hematol*, 1993, **30**, 171-192.

78. N. Mohandas, J.A. Chasis and S.B. Shohet, *Semin Hematol*, 1983, **20**, 225-242.

79. E.A. Evans and P.L. LaCelle, *Blood*, 1975, **45**, 29-43.

80. N. Mohandas, M.R. Clark, M.S. Jacobs and S.B. Shohet, *The Journal of Clinical Investigation*, 1980, **66**, 563-573.

81. G.B. Nash, E. O'Brien, E.C. Gordon-Smith and J.A. Dormandy, *Blood*, 1989, **74**, 855-861.

82. J.P. Brody, Y. Han, R.H. Austin and M. Bitensky, *Biophysical Journal*, 1995, **68**, 2224-2232.

83. S. Suresh, J. Spatz, J.P. Mills, A. Micoulet, M. Dao, C.T. Lim, M. Beil and T. Seufferlein, *Acta Biomater.*, 2005, **1**, 15-30.

84. D. Di Carlo, *J. Lab. Autom.*, 2012, **17**, 32-42.

85. Y. Gambin and A.A. Deniz, *Mol. BioSyst.*, 2010, **6**, 1540-1547.

86. A.M. Dondorp, B.J. Angus, K. Chotivanich, K. Silamurt, R. Ruangveerayuth, M.R. Harderman, P.A. Kager, J. Vreeken and N.J. White, *Am. J. Trop. Med. Hyg.*, 1999, **60**, 733-737.

87. G.D.O. Lowe, *Baillières Clinical Haematology*, 1987, **1**, 597-636.

88. R.E. Waugh, N. Mohandas, C.W. Jackson, T.J. Mueller, T. Suzuki and G.L. Dale, *Am. Soc. Hem.*, 1992, **79**, 1351-1358.

89. R.E. Mebius and G. Kraal, *Nature*, 2005, **5**, 606-616.

90. A.J. Bowdler, The Complete Spleen, Humana Press, 2nd edition, 2002.

91. W.H. Crosby, *Lymphology*, 1983, **16**, 52-55.

92. A. Petroianu, The Spleen, Bentham eBooks, 2011.

93. L. Weiss, *Blood*, 1974, **43**, 665-691.

94. A.C. Groom, E.E. Schmidt and I.C. MacDonald, *Scanning Microsc.*, 1991, **5**, 159-174.

95. G. Kraal, *Int. Rev. Cytol.*, 1992, **132**, 31-73.

96. B. Steiniger and P. Barth, *Adv. Anat. Embryol. Cell Biol.*, 2000, **III-IX**, 1-101.

97. M.F. Cesta, *Toxicologic Pathology*, 2006, **34**, 455-465.

98. P.A. Buffet, G. Milon, V. Brousse, J.M. Correas, B. Dousset, A. Couvelard, R. Kianmanesh, O. Farges, A. Sauvanet, F. Paye, M.N. Ungeheuer, C. Ottone, H. Khun, L. Fiette, G. Guigon, M. Huerre, O. Mercereau-Puijalon and P.H. David, *Blood*, 2006, **107**, 3745-3752.

99. H.A. del Portillo, M. Ferrer, T. Brugat, L. Martin-Jaular, J. Langhorne and M.V.G. Lacerda, *Cellular Microbiology*, 2012, **14**, 343-355.

100. M.H. Ross and W. Pawlina, Histology: a text and atlas, with correlated cell and molecular biology, Lippincott Williams & Wilkins, 6th edition, 2011.

101. J.H. van Krieken, J. Te Velde, J. Hermans and K. Welvaart, *Histopathology*, 1985, **9**, 401-416.

102. A. Chadburn, *Semin Hematol*, 2000, **37**, 13-21.

103. D.Z. de Back, E.B. Kostova, M. van Kraaij, T.K. van den Berg and R. van Bruggen, *Frontiers in Physiology,* 2014, **5**, 1-11.

104. I. Safeukui, J.M. Correas, V. Brousse, D. Hirt, G. Deplaine, S. Mule, M. Lesurtel, N. Goasguen, A. Sauvanet, A. Couvelard, S. Kerneis, H. Khun, I. Vigan-Womas, C. Ottone, T.J. Molina, J.M. Treluyer, O. Mercereau-Puijalon, G. Milon, P.H. David and P.A. Buffet, *Blood*, 2008, **112**, 2520-2528.

105. P.A. Buffet, I. Safeukui, G. Deplaine, V. Brousse, V. Prendki, M. Thellier, G.D. Turner and O. Mercereau-Puijalon, *Blood*, 2011, **117**, 381-392.

106. S.N. Bhatia and D.E. Ingber, *Nat. Biotechnol.*, 2014, **8**, 760-772.

107. T. Mammoto, A. Mammoto and D.E. Ingber, *Annu. Rev. Cell Dev. Biol.*, 2013, **29**, 27-61.

108. D.E. Ingber, *Ann. Med.*, 2003, **35**, 564-577.

109. D. Huh, G.A. Hamilton and D.E. Ingber, *Trends in Cell Biology*, 2011, **21**, 745-754.

110. D. Huh, Y. Torisawa, G.A. Hamilton, H.J. Kim and D.E. Ingber, *Lab Chip*, 2012, **12**, 2156-2164.

111. D. Huh, H.J. Kim, J.P. Fraser, D.E. Shea, M. Khan, A. Bahinski, G.A. Hamilton and D.E. Ingber, *Nat. Protocols*, 2013, **8**, 2135-2157.

112. D.C. Swinney and J. Anthony, *Nat. Rev. Drug Discov.*, 2011, **10**, 507-519.

113. J.W. Scannell, A. Blanckley, H. Boldon and B. Warrington, *Nat. Rev. Drug Discov.*, 2012, **11**, 191-200.

114. H. Ledford, *Nature*, 2011, **477**, 526-528.

115. R.A. Wilke, D.W. Lin, D.M. Roden, P.B. Watkins, D. Flockhart, I. Zineh, K.M. Giacomini and R.M. Krauss, *Nat. Rev. Drug. Discov.*, 2007, **6**, 904-916.

116. F. Zheng, F. Fu, Y. Cheng, C. Wang, Y. Zhao and Z. Gu, *Small*, 2016, DOI: 10.1002/smll.201503208.

117. K.J. Jang, A.P. Mehr, G.A. Hamilton, L.A. McPartlin, S. Chung, K.Y. Suh and D.E. Ingber, *Integr. Biol.*, 2013, **5**, 1119-1129.

118. D. Huh, B.D. Matthews, A. Mammoto, M. Montoya-Zavala, H.Y. Hsin and D.E. Ingber, *Science*, 2010, **328**, 1162-1168.

119. Y. Nakao, H. Kimura, Y. Sakai and T. Fujii, *Biomicrofluidics*, 2011, **5**, 22212.

120. A. Grosberg, P.W. Alford, M.L. McCain and K.K. Parker, *Lab Chip*, 2011, **11**, 4165-4173.

121. H.J. Kim, D. Huh, G.A. Hamilton and D.E. Ingber, *Lab Chip*, 2012, **12**, 2165-2174.

122. Y.S. Torisawa, C.S. Spina, T. Mammoto, A. Mammoto, J.C. Weaver, T. Tat, J.C. Collins and D.E. Ingber, *Nat. Methods*, 2014, **11**, 663-669.

123. Z. Tong, O. Seira, C. Casas, D. Reginensi, A. Homs-Corbera, J. Samitier and J.A. Del Rio, *RSC. Adv.*, 2014, **4**, 54788-54797.

124. K. Viravaidya and M.L. Shuler, *Biotechnol. Prog.*, 2004, **20**, 590-597.

125. D. Huh, D.C. Leslie, B.D. Matthews, J.P. Fraser, S. Jurek, G.A. Hamilton, K.S. Thorneloe, M.A. McAlexander and D.E. Ingber, *Sci. Transl. Med.*, 2012, **4**, 1-8.

126. C. Lavazec, G. Deplaine, I. Safeukui, S. Perrot, G. Milon, O. Mercereau-Puijalon, P.H. David and P. Buffet, *Methods Mol Biol*, 2013, **923**, 291-297.

127. G. Deplaine, I. Safeukui, F. Jeddi, F. Lacoste, V. Brousse, S. Perrot, S. Biligui, M. Guillote, C. Guitton, S. Dokmak, B. Aussilhou, A. Sauvanet, D. Cazals Hatem, F. Paye, M. Thellier, D. Mazier, G. Milon, N. Mohandas, O. Mercereau-Puijalon, P.H. David and P.A. Buffet, *Blood*, 2011, **117**, e88-e95.

128. J. Picot, P.A. Ndour, S.D. Lefevre, W. El Nemer, H. Tawfik, J. Galimand, L. Da Costa, J.A. Ribeil, M. de Montalembert, V. Brousse, B. La Pioufle, P. Buffet, C. Le Van Kim and O. Français, *Am. J. Hematol.*, 2015, **90**, 339-345.

129. J.H. Kang, M. Super, C.W. Yung, R.M. Cooper, K. Domansky, A.R. Graveline, T. Mammoto, J.B. Berthet *et al.* M., A. Kole, A. Jiang, T.M. Valentin, A. Diaz, K. Takahashi and D.E. Ingber, *Nature Medicine*, 2014, **20**, 1211-1216.

Chapter 2. Materials and methods: engineering the microfluidic devices

SUMMARY

In order to fulfil the premise of in vitro mimicking the architecture of the human splenon, the development of OCD platforms, able to mimic, to the extent possible, the splenon filtering properties and part of its most representative cellular microenvironment, will be the final mission.

To meet this objective, the proposal of fabricating the splenon-on-a-chip biomimetic platform, the first functional microengineered OCD model device of the splenon (to the best knowledge of the authors), is a reaffirmation of the commitment to advance in the study of this organ. In this chapter, the different designs proposed to create such a device will be shown. The protocols used to engineer the three different OCD versions will be discussed and further described, taking into account that these platforms were designed in the framework of the splenon hydrodynamic and physiological properties.

2.1. Introduction: concept and design of the microfluidic platforms.

The principal aim of the project is to develop novel microengineered OCD model devices able to reproduce, to the extent possible, the hydrodynamic behavior and haemorheological properties of a human splenon.[1] Figure 2.1 represents an overview of its most representative physiological features. The splenon is mainly composed of two microcirculatory compartments, the fast and the slow-flow channels, holding the ~90% and the remaining ~10% of the flow, respectively, and the IES, the most stringent test for RBCs deformability (please see Chapter 1.3.2.3. for further details).[2-4] These features will be translated into engineering elements, combined to integrate a microfluidic and biomimetic filtering prototype model.

Novel fabrication protocols were established to construct multilayered splenon-on-a-chip OCD devices, as will be detailed hereafter. The platforms were fabricated in transparent materials, to facilitate image acquisition and observation of events happening inside the microchannels. This was done by using techniques such as soft lithography (using PDMS as molding material)[5,6] or stereolithography, which allowed to obtain the 3D printed platforms.[7] These methodologies were briefly introduced in Chapter 1.1.6.
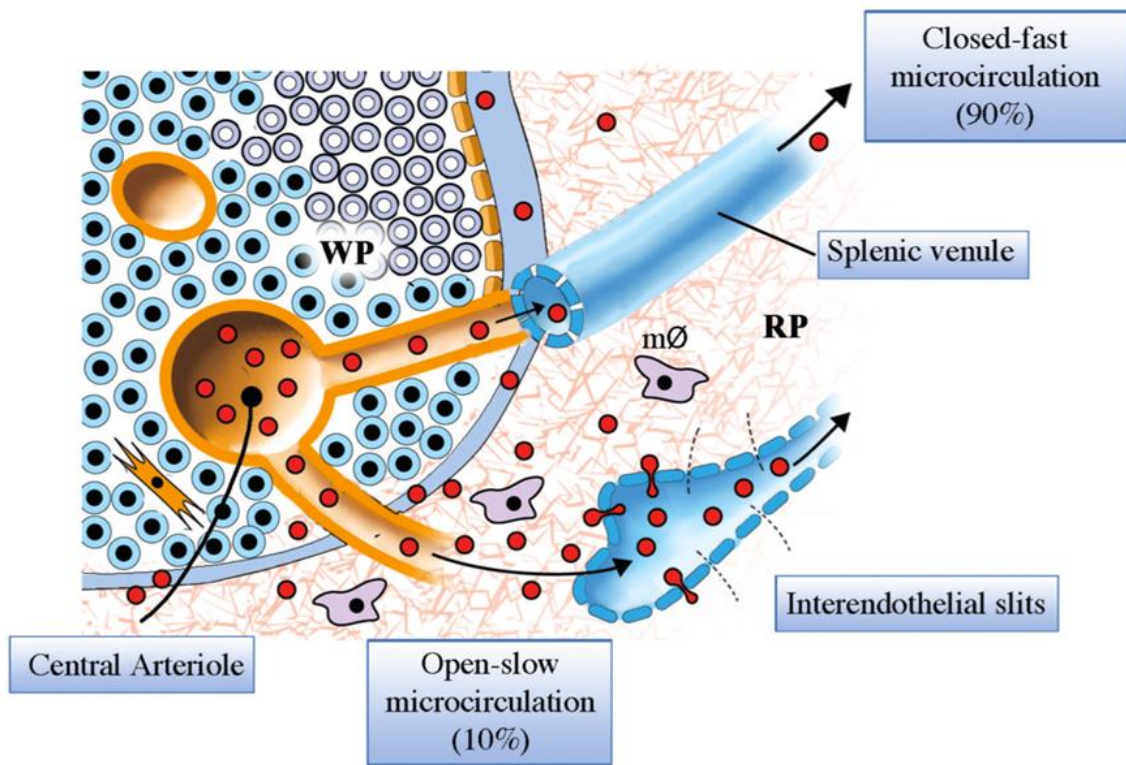
***Figure 2.1. Human splenon model.** Diagram showing the main compartments of the human splenon, representing the closed-fast and open-slow microcirculations, as well as the interendothelial slits (IES). Blood in a central arteriole coming from the splenic artery may follow two different paths: (i) the closed-fast microcirculation, where blood reaches directly splenic venules bypassing the spleen filtration function; (ii) the open-slow microcirculation, where blood goes through the filtration beds of the cords, facilitating the destruction of unhealthy RBCs and posterior erythrophagocytosis by specialized macrophages (mØ). In addition, blood in the open-slow microcirculation has a unidirectional passage through the IES before reaching the venous system. This further physical constraint represents a second stringent test for RBCs.[2,8]*

Figure 2.2 shows a chronological timeline of the evolution of the "splenon-on-a-chip concept", and the chapters were the experimental results will be further explained in detail. The first two versions were conceived to characterize hydrodynamic properties of blood cells, when flowing inwardly through a vascular-like network mimicking the splenon, at different conditions. Finally, a third version, aimed to facilitate biological studies of some diseases affecting the spleen, was engineered, using 3D printing tools. This initial prototype was designed taking advantage of the knowledge acquired from studies done with the previous versions. As a result, a plug-n-play and user-friendly platform was prototyped, which could, perhaps, be useful to perform different tests, in the future. The particularities of its complex 3D structure made stereolithography an attractive prototyping technique to guarantee cost/time effectiveness.
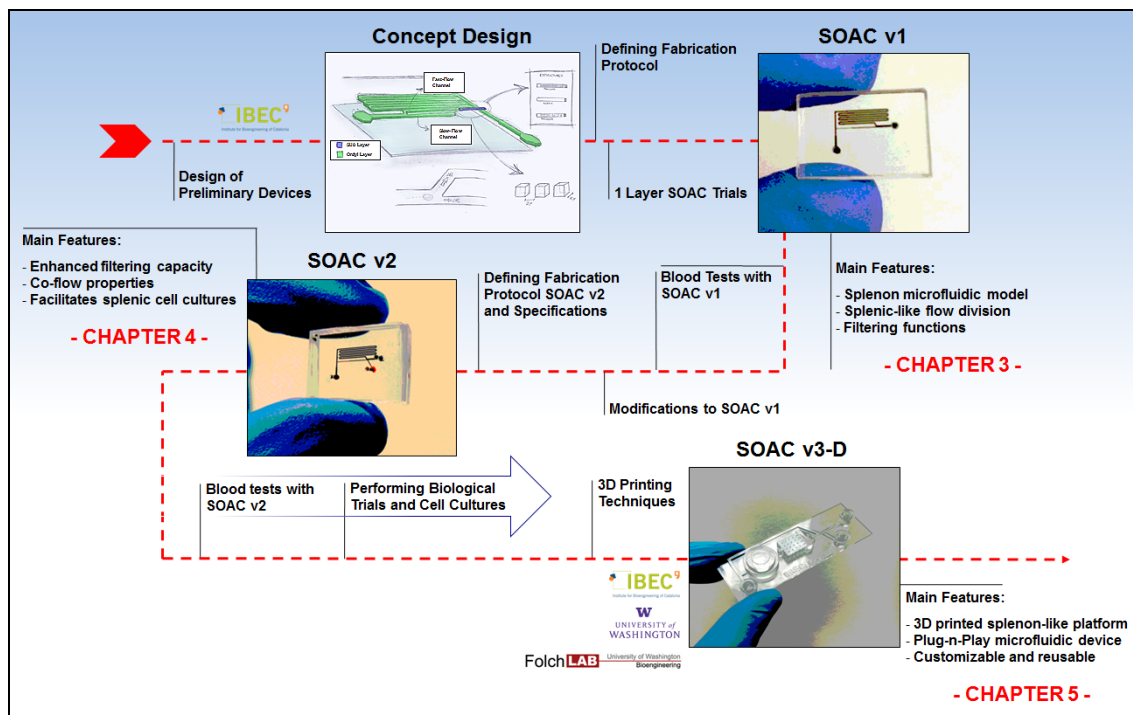
Figure 2.2. Splenon-on-a-chip development timeline. *Timeline showing the different Splenon-on-a-Chip (SOAC) concept prototypes and its main features.*

In this chapter will be detailed the different fabrication protocols, and the materials employed, to perform the experimental assays, using the following format:
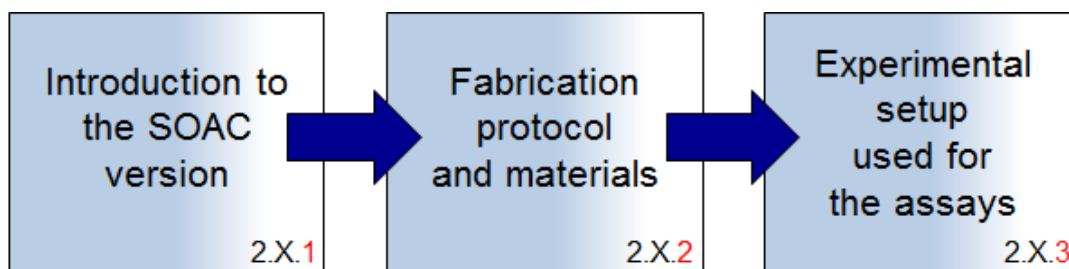
Figure 2.3. Scheme of the narrative (materials and methods) for the different splenon-on-a-chip platforms.

2.2. Splenon-on-a-chip version 1.

| Splenon-on-a-chip Version 1 | Splenon-on-a-chip Version 2 | Splenon-on-a-chip Version 3-D |

2.2.1. Introduction.

A two-layer microengineered device was designed to translate a simplified but accurate version of a human splenon (Figure 2.1).[8] This microfluidic device mimics the closed-fast and the open-slow circulations by means of two main channels, designed to provide a close physiological flow division. Moreover, in the slow-flow microchannel, blood flows through a pillar matrix resembling the reticular meshwork. At the end of the slow-flow channel, connection to the fast-flow channel is achieved through parallel 2 μm microconstrictions resembling the IES, where RBCs physically constraint before reaching the fast circulation ("venous system"), as it happens in physiological scenarios.[2] The electric circuit analogy was used to facilitate the device design (as explained in Chapter 1.1.7.5., Figure 2.4).[9]
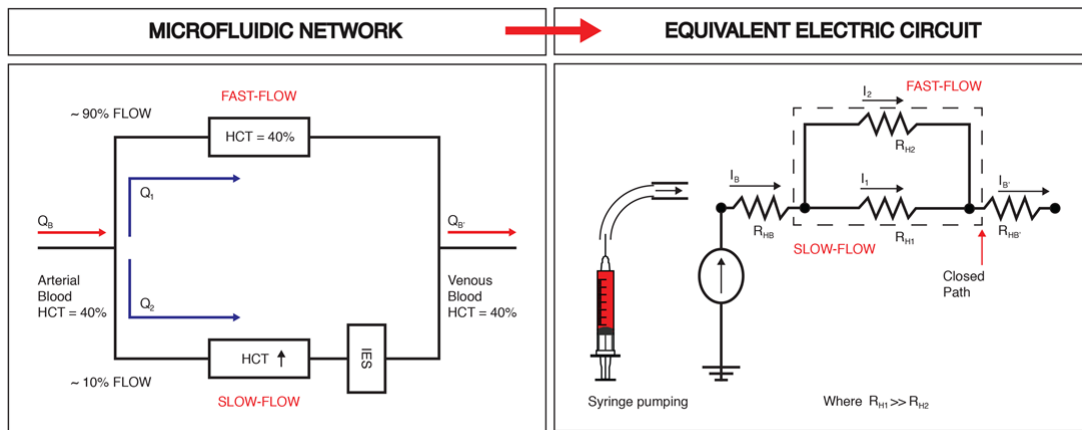
Figure 2.4. Electric circuit analogy used to design the microfluidic device. *Left panel: Diagram shows how the volume flow of arterial blood (Q_B) is divided into two different volume flows. Right panel: The equivalent electric circuit. Depending on which branch of the circuit, the resistance (R) and the current intensity (I) are different. The resistance in the open-slow microcirculation equivalent branch (R_{H1}) is much higher than the resistance in the closed-fast microcirculation equivalent branch (R_{H2}).*[8,9]
Abbreviations: Q, volume flow; HCT, haematocrit; I, current intensity; R, resistance.

The R_H calculations, complemented with COMSOL Multiphysics software simulations (COMSOL AB, Sweden), were used to set the dimensions of the secondary channel reproducing the fast-flow in the biological system. The microconstrictions and the pillars region were set to mimic the complex structure of the spleen in a simplified manner. The maximum number of slits simulating the IES was limited by the field of view of the microscopy equipment, since all of them should be visualized simultaneously in order to observe deformation scenarios of individual RBCs.

Fluid flow division between fast and slow-flow sections was meant to be kept near physiological values, of flow splitting into the slow-flow channel of the model.[1,2,4] A first approximation to the problem was done simulating aqueous media, and a range of values for the fast-flow channel length was estimated in order to try to closely achieve this physiological condition (Figure 2.5).
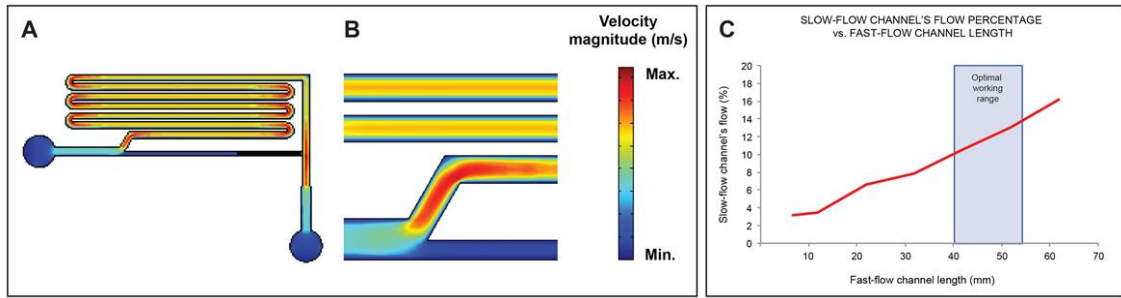
Figure 2.5. Comsol simulations of the microfluidic device to obtain a correct architecture. *Left panel: Diagrams show Comsol Multyphysics simulations showing (A) the velocity magnitude in the entire microfluidic device and (B) flow division at the bifurcation point (fast-flow channel versus slow-flow channel). This flow division is independent of the inlet flow rate so depends entirely on the architecture of the device. Right panel: graph representing the slow-flow channel's flow percentage, which is dependent on the fast-flow channel length. The study is addressed within the architecture and dimensions of the slow-flow channel.[8]*

However, because of the complex fluidic nature of blood,[3,4] further adjustments were performed experimentally. Preliminary assumptions were made in terms of having a Newtonian behavior of plasma in the microchannels.

Assessment of the calculations and the simulation results were, initially, obtained using water. Phosphate-buffered saline medium (PBS) plus fluorescent beads and blood were used later and dimensions for the fast-flow channel were fine-tuned in order to get, empirically, the desired flow division. To obtain a close spleen-like physiological behavior inside the device, the dimensional relations between the different elements of the platform were adjusted to similarly agree with reported measurements of human vessels in the red pulp.[2] Figure 2.6 shows the first version of the splenon-on-a-chip, with some specific dimensions. The microconstrictions act as the splenic IES, stretching mechanically the RBCs and reticulocytes (immature erythrocytes, RETs) in the planar configuration, while retaining or hinting the passage of non-healthy cells.
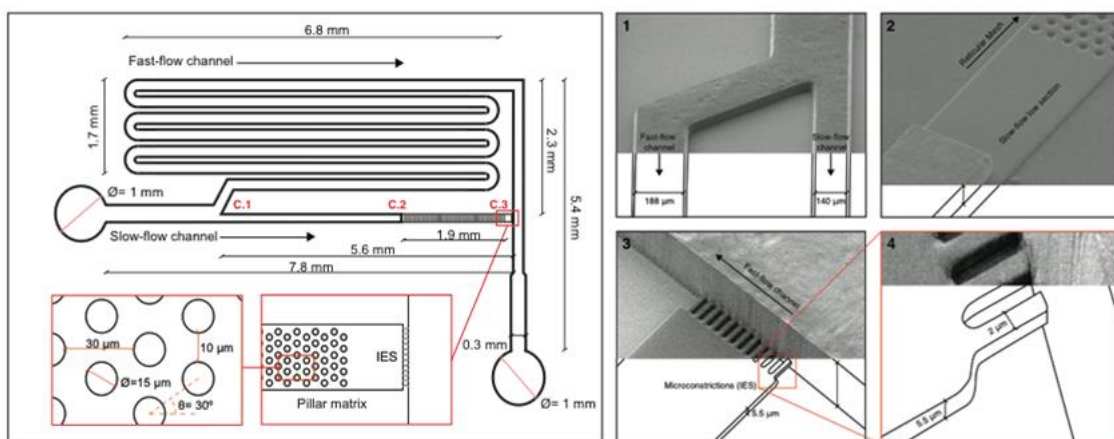
Figure 2.6. Microengineered model of the human splenon-on-a-chip. *Schematic representation and dimensions of the microfluidic device mimicking the human splenon. A pillar matrix in the slow-flow channel mimics the filtration beds of the red pulp before reaching the microconstrictions representing the IES. Details and measurements of the slow-flow channel: (1) flow division zone; (2) slow-flow channel; (3-4) microconstrictions representing the IES.[8]*

2.2.2. Fabrication protocol.

The fabrication of the splenon-on-a-chip version 1 consists of a multi-step procedure designed to obtain two different heights using three different photoresists by means of photolithographic and soft-lithographic techniques, customized for fabricating a multilayer platform. All procedures were carried out in the clean room facility of the Institute for BioEngineering of Catalonia (IBEC). All solvents and chemical were from Sigma-Aldrich Co. (USA), unless otherwise specified. SU-8 photoresists, and developer, were from MicroChem (Newton, MA, USA). Both Ordyl photoresist and developer were from Elga (Italy).

The master is fabricated over glass slides (Figure 2.7-A). A thoroughly cleaning protocol based on chemical baths and surface activation process is used for the slides. The process starts with three consecutive solvent baths of acetone, isopropanol and ethanol. Then, after dehydration, the glass surface is subjected to 10 W of O_2 plasma power for 10 minutes, in order to improve photoresist adhesion. Following the cleaning protocol, the first step to shape the master consists of patterning Ordyl SY alignment marks for a correct structuring of the bilayer device (Figure 2.7-[B-E]). The slide is then gyrated and following processes are performed on the plain side (Figure 2.7-F). This is done to avoid mask contact problems and resolution loses arising from Ordyl features height during the following microfabrication steps. Afterwards, the cleaning procedure is repeated, and a layer of SU-8 2000.5 is spun (500 nm). This layer will act as an interface between glass and further photoresist layers (Figure 2.7-[G, H]).

Later, in order to fabricate the first layer of this device (slow-flow channel), a 5.5 μm-high SU-8 10 negative photoresist is spun over the glass slide applying a three-step spinning protocol to obtain the desired SU-8 thickness (Figure 2.7-I). The slide is then soft-baked on a hot plate, before being exposed with a chrome-on-glass photomask to UV light (4 s, 24 mW cm^2, 345 nm) in a mask aligner (MJB4 aligner, SÜSS Microtec, Germany). After that, the slide is baked in the sequence of 65ºC for 1 minute and 95ºC for 3 minutes, left to cool for up to 1 hour, and finally developed using the SU-8 developer for 30 s (Figure 2.7-[J-M]).

For the second device layer (fast-flow channel), several Ordyl SY negative photoresist films are laminated on top of the last SU-8 layer, using a hot/cold laminator, in order to have a smooth attached film surface (Figure 2.7-N). Then, the slide is exposed through an acetate photomask to UV light (5 s, 24 mW cm^2, 345 nm) in the mask aligner, and subsequently placed on a hot plate at 65ºC for 3 minutes (Figure 2.7-[O,P]). The 3D master mould fabrication is finished by developing the Ordyl film using the Ordyl developer for 3 minutes (Figure 2.7-Q).

To replicate the master's microchannels, a PDMS pre-polymer mixture (curing agent-to-PDMS ratio of 1:11, Sylgard®184, Dow Corning) is placed in a desiccator and vacuum applied in order to remove bubbles. Then the mixture is poured on top of the SU-8/Ordyl master to fabricate a PDMS mould, heated up at 65ºC for 3 hours, and afterwards kept at room temperature for 24 hours. The casted PDMS is peeled off carefully and inlet and outlet holes are made using a Harris Uni-Core 1 mm puncher. After cleaning, both the glass and the PDMS structures are chemically modified in O_2 plasma and immediately pressed together to form a permanent bond.
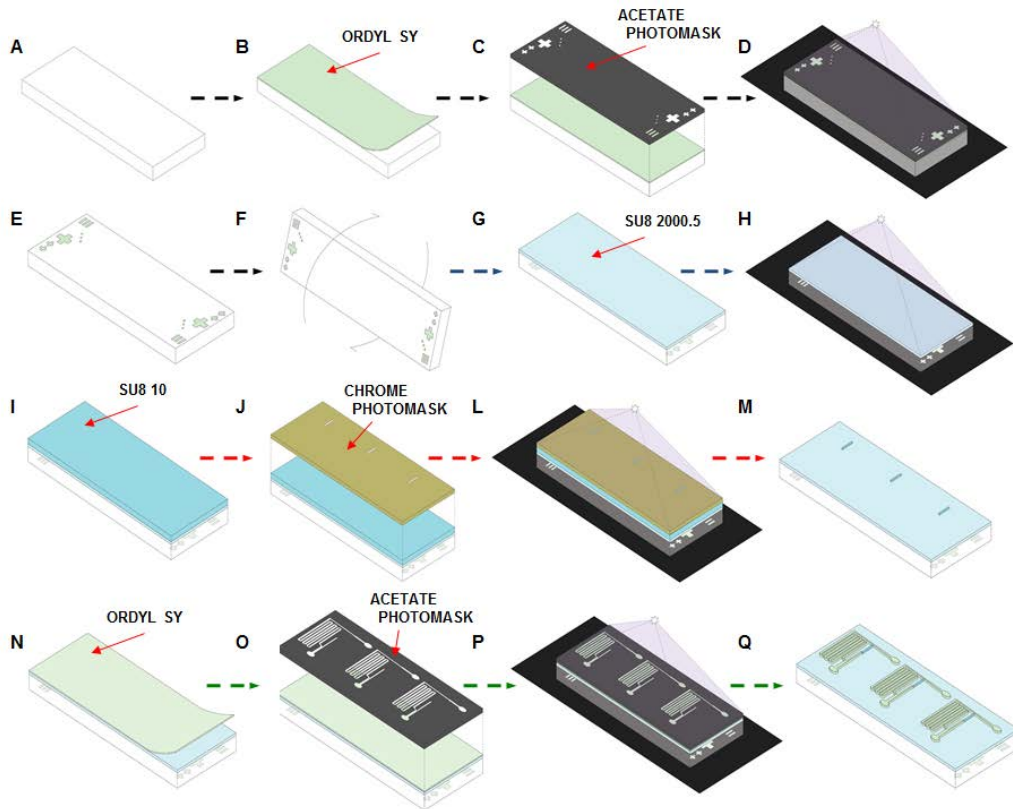
Figure 2.7. Schematic of the fabrication of the SU-8/Ordyl master. *The fabrication of the splenon-on-a-chip consists of a photolithographic multi-step procedure, as shown in this scheme.[8]*

It is relevant to highlight the importance of performing the protocol as detailed previously, since several errors can arise while fabricating, making unusable the master. One possible mistake is to construct firstly the higher layer than the lower one. Additionally, several problems regarding misalignments (Figure 2.8A) can occur, since the process is purely manual and the precision of the mask aligner does not ensure high exactitude. Further, if the UV exposure/post-bakes times are not correct, the structure could suffer several defects (Figure 2.8B). Finally, since Ordyl is a photofilm, manipulating it can be challenging (Figure 2.8C,D).
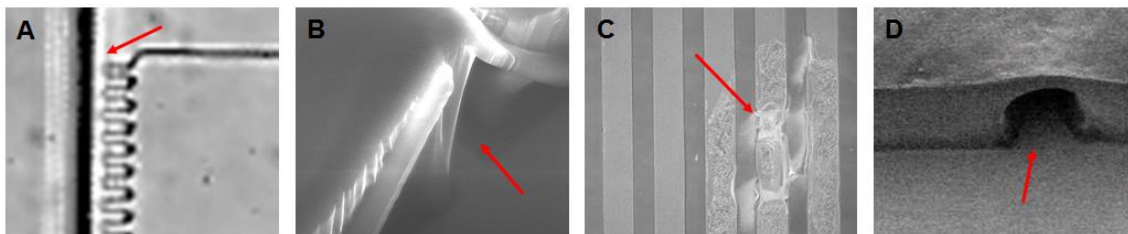
Figure 2.8 Problems arising in microfabrication process. *(A) Misalignments that happen when hard-contact is established in the mask aligner. (B) Defects when UV exposure/post-bake times are not appropriate. (C, D) Problems when laminating Ordyl. If the heat or pressure applied is not correct, it could be difficult to obtain the desired results.*

2.2.3. Biological materials and characterization procedure.

The experimental results obtained using the **splenon-on-a-chip version 1** will be presented in **Chapter 3.** Hereafter are listed the materials and setups used to perform the analysis.

2.2.3.1. Uninfected blood specimens.

The human RBCs were obtained from donors at the Blood and Tissue Bank (Barcelona), after written consent and in accordance with the ethics Committee protocols of the Blood and Tissue Bank. Upon receipt, RBCs were washed twice with incomplete Roswell Park Memorial Institute medium (RPMI) and then re-suspended at a 50% haematocrit, in the same medium. RBCs were immediately used (fresh RBCs) or maintained at 4°C for several weeks before the deformability measurements (old/aged-RBCs). For microfluidic experiments, aliquots of ~500 µl were injected into the devices.

2.2.3.2. Infected blood specimens.

Plasmodium yoelii (*P. yoelii*) non-lethal (17X) strain was obtained from the Malaria Research and Reference Reagent Resource Center (MR4), and the *P. yoelii*-GFP (Green Fluorescent Protein) transgenic line was generated as described elsewhere,[10] in collaboration with the Prof. Hernando del Portillo's Lab (ISGlobal/CRESIB, UB).[10] For mice infections, female BALB/c of 6-8 weeks of age (from Charles River Laboratories Inc., MA, USA) were infected by intraperitoneal injection of $5x10^5$ iRBCs obtained from the tail blood of donor mice at 5-10% parasitemia. Then, parasitemia was monitored using Giemsa staining of blood smears. The infected RETs (iRETs) and uninfected red cells were counted in different optical fields.

Blood from mice was collected in ethylenediamitetraacetic acid (EDTA) by intracardiac puncture of infected mice on day 11 post-infection, and then passed through a CF11 cellulose filter and washed with PBS, in order to remove leukocytes. Blood smears were done to check the efficiency of the CF11 column (Figure 2.9). Packed cells were re-suspended in RPMI at a 50% haematocrit and injected into the OCD. All studies involving mice were performed at the animal facilities of Hospital Clinic in Barcelona, in accordance with guidelines and protocols approved by the Ethics Committee for Animal Experimentation of the University of Barcelona (CEEA-UB).
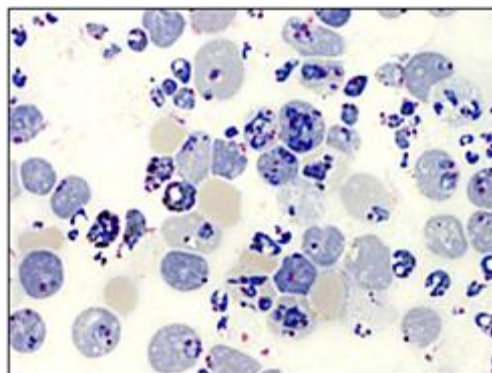
Figure 2.9. Plasmodium yoelii-infected reticulocytes. *BCB-Giemsa blood smear from a BALB/c mouse experimentally infected with P. yoelii reticulocyte-prone nonlethal 17X-GFP strain. Image was taken with Nikon Eclipse 50i 100x/1.30 oil. Courtesy of Prof. Hernando del Portillo's Group (ISGlobal/CRESIB, UB, Barcelona).[8]*

2.2.3.3. Experimental system operation.

The experimental setup consists of a 1 ml syringe (BD Plastipak, New Jersey, USA) connected through a needle with poly(tetrafluoroethylene) (PTFE) tubing (ChipShop, Jena, Germany) to the OCD. The syringe is actuated with a KDS 200 series pump (KD Scientific, Massachusetts, USA). Tubes were inserted into the access holes, which were slightly smaller than the outer diameter of the tubing to form a pressure seal between the tubing and the hole. A constant flow was then established on the OCD. Experiments with buffers and beads were carried out at room temperature, whereas experiments with cells were carried out at a physiological temperature of ~37⁰C. The setups used for experimental purposes can be seen in Figure 2.10.

Concerns regarding the possible formation of bubbles inside the OCD device were faced during the experimentation. Thus, a correct sample preparation through an exhaustive control of blood manipulation was included in the experimental protocol. Consequently, precautions were taken before each experiment while handling the blood samples with the syringe, eliminating possible bubbles, to the extent possible, both in the syringe and the tubing connected to the OCD.

2.2.3.4. Image capture and analysis.

Optical measurements for the microfluidic analyses were performed using an inverted optical microscope (Olympus IX71) with an integrated CCD Hamamatsu camera (Figure 2.10). Optical measurements of iRBCs were obtained using a laser scanning confocal microscope (TCS-SP5; Leica Microsystems). Several movies of 10-90 seconds were recorded of blood microcirculation in the splenon-on-a-chip. Bright field and fluorescence were acquired in two different channels (excitation/emission wavelength 488/505-580 for the GFP). Videos were analyzed using ImageJ software (Wayne Rasband, NIH). For its side, for colour photos/high-frame rate videos, a mobile phone was disposed in the microscope's eyepiece.
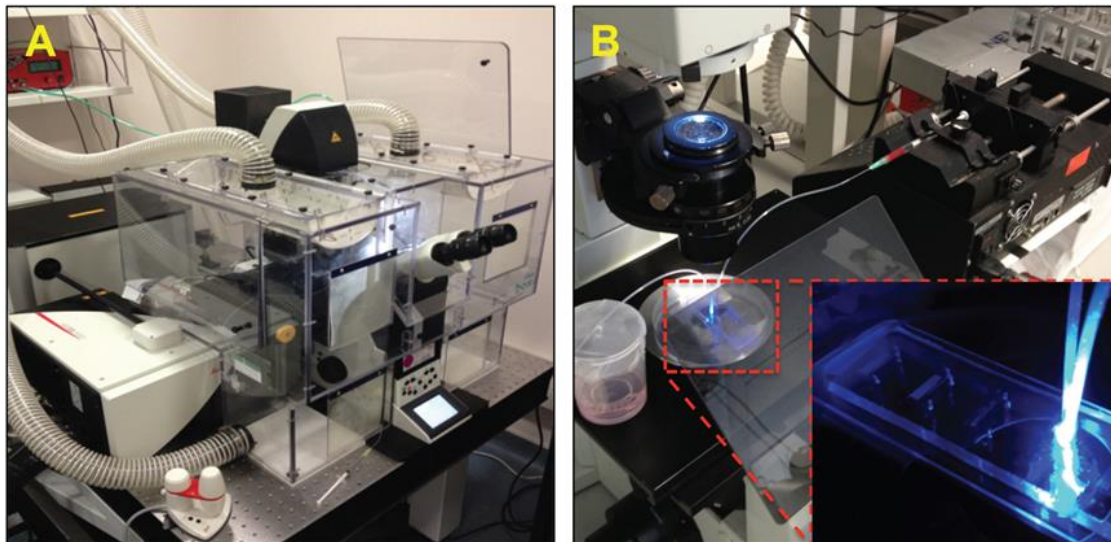
Figure 2.10. Experimental system operation. *(A) Laser scanning confocal microscope TCS-SP5 (Leica Microsystems) where in vivo imaging of the mouse spleen was obtained to determine the in vivo physiological blood flow rate. (B) Images for microfluidic analyses were taken with an inverted optical microscope (Olympus IX71) with an integrated CCD Hamamatsu camera.[8]*

2.2.3.5. Measurement of cell deformability.

Optical microscopy was used to obtain deformability measurements of individual cells in the slow compartment, as well as while passing through the slits, using ImageJ processing and analysis software. Three measures of each cell were obtained. Cell deformability was calculated measuring the elongation of blood cells (using high-speed/resolution microscopic videos) inside the slits in the X axis, the axis parallel to the flow direction. This technique could resemble what some authors refer to as "hydropipetting".[11] The deformation measurement ($D_{M\%}$) is, therefore, defined as the percentage of difference between the length in microns of a single cell in the slit (L_S) and the length in the pillar matrix zone (L_{RM}), as is shown below (Equation 9, Figure 2.11):

$$D_{M\%} = [(L_S - L_{RM})/ L_{RM}] \cdot 100 \qquad \text{(Eq. 9)}$$
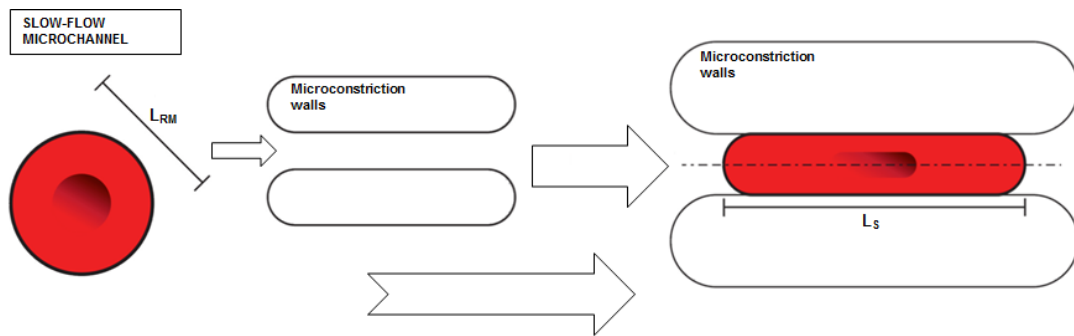
Figure 2.11. Measurement of cell deformability. *In order to calculate the deformability of cells, their diameter (L_{RM}) in the slow compartment, and the elongation (L_S) that they suffer as a consequence of passing through a microconstriction, is measured.*

2.2.3.6. Statistical analysis.

The median (M_{ed}) and the quartiles of the length and the deformation of the cells were analyzed using Microsoft Excel and IBM SPSS statistics program. Because statistical analysis entailed comparing two different cell populations, non-parametric Mann-Whitney *U* test was used.

2.2.3.7. *In vitro* haemolysis assay.

In order to calculate possible haemolysis of blood samples, an assay to measure cell breakage was performed using spectrophotometry as the analysis method.[12-14] Measurements were made before and after blood passage through a system.

So, 100 µl of different RBCs populations were added to 1000 µl of sterile PBS. After incubating at 37°C for 40 minutes, the samples were then centrifuged (1400 rpm, 10 minutes) at the same temperature. Then, the supernatant was transferred to a transparent wall cuvette. Absorbance of supernatants, which includes plasma and haemoglobin (from the broken RBCs), was then measured at an optical density (OD_{540}) of 540 nm. A blood sample in the presence of saponin was taken as positive control of haemolytic sample. The percent lysis difference ($H_{L\%}$) could be calculated using the following formula:

$$H_{L\%} = [(\text{Sample } OD_{540} - \text{Sample Before OCD } OD_{540})/ \text{Positive Control } OD_{540}] \cdot 100 \quad \text{(Eq. 10)}$$

2.3. Splenon-on-a-chip version 2.

Splenon-on-a-chip Version 1	**Splenon-on-a-chip Version 2**	Splenon-on-a-chip Version 3-D

2.3.1. Introduction.

The design/fabrication methods of this novel OCD is based on the previous version.[8] Compared with the former platform, it have been included two unique characteristics on this splenon-on-a-chip version 2: (*i*) the incorporation of a *Y*-junction/secondary inlet, devised to take advantage of laminar co-flow, and (*ii*) the fabrication of multiple layers in the slow-flow microchannel.

This platform mimics, in the same way as described previously, the closed-fast and the open-slow microcirculations by means of two main microfluidic channels. At the end of the slow-flow channel, however, connection to the fast one is achieved through narrower parallel ~1.5-1.8 µm wide microconstrictions.

The height of these microconstrictions (~4.8 µm) was studied and calculated empirically in order to try to reproduce the filtering functions achieved in the IES while preventing, to the extent possible, healthy RBCs clogging/lysis. For its side, the height of the pillar matrix zone (13.5 µm) was determined taking into account cells volume not to impede blood flow, and also to satisfy a physiological flow division. Figure 2.12 shows the specific dimensions of this OCD. The fast-flow channel dimensions were adjusted considering a supposed efficient diameter left by endothelial cells in the area of the section.
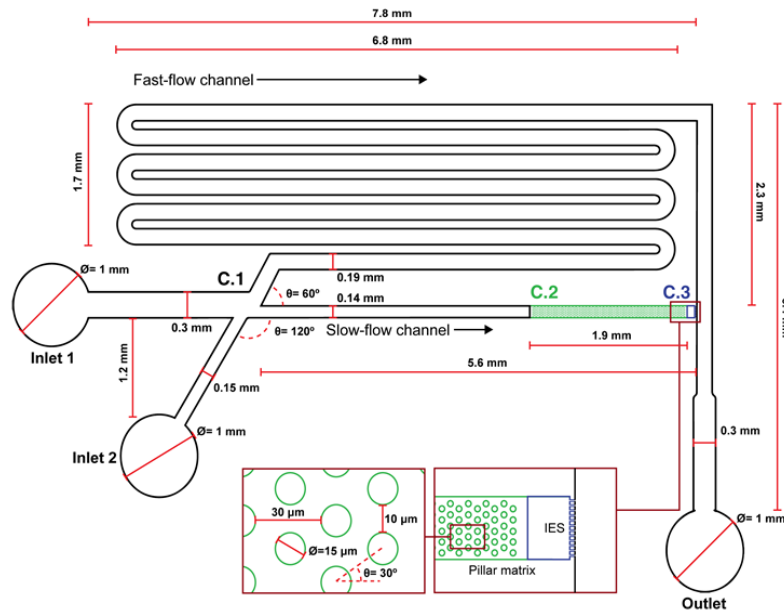
Figure 2.12. Microengineered model of the human splenon-on-a-chip version 2. *Schematic representation, and dimensions, of the second version of the splenon-on-a-chip concept. In different colours are shown the different layers (C.1, C.2 and C.3).*

2.3.2. Fabrication protocol.

The fabrication of the splenon-on-a-chip version 2 consists of a multi-step procedure designed to obtain three different heights using four different photoresists by means of photolithographic and soft-lithographic techniques, customized for fabricating a multilayer platform (Figure 2.13).

All fabrication works were carried out in the clean room facility of the Institute for BioEngineering of Catalonia (IBEC). All the solvents and chemical were obtained from Sigma-Aldrich Co. (USA) unless otherwise specified. SU-8 photoresists, and developer, were from MicroChem (Newton, MA). Ordyl photoresist, and developer, were from Elga (Italy).
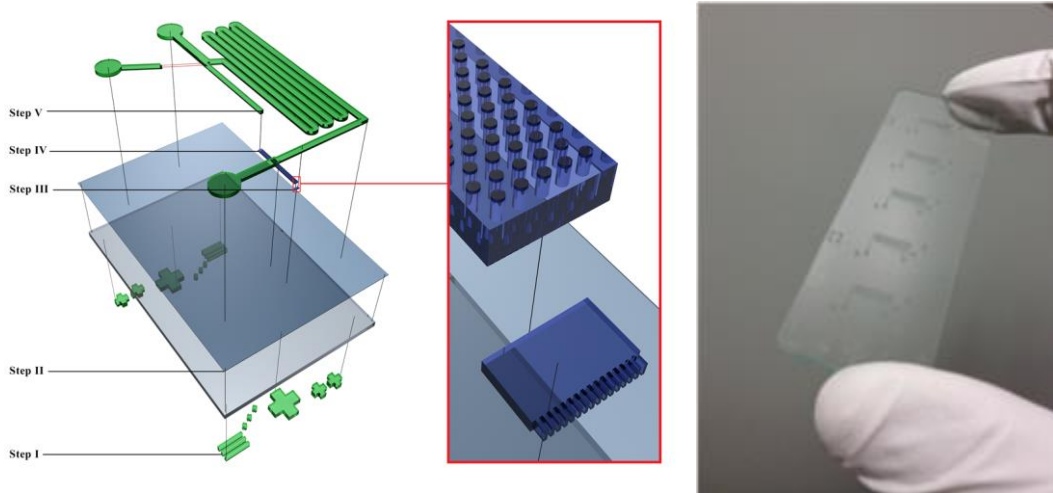
Figure 2.13. Schematic of the fabrication of the splenon-on-a-chip version 2. *Left Panel: scheme showing the different layers to construct the biomimetic microfluidic platform. Right panel: a photo of the SU-8/Ordyl master used to replicate with PDMS.*

The master is fabricated over glass slides. A thoroughly cleaning protocol based on chemical baths, and surface activation process, is used for the slides. The process starts with three consecutive solvent baths. Then, after dehydration, the glass surface is subjected to O_2 plasma power to improve photoresist adhesion.

Following the cleaning protocol, the first step consists on patterning Ordyl SY alignment marks for a correct structuring of the device in the XY axis (step I). The slide is then gyrated and following processes are performed on the plain side. The cleaning procedure is repeated and a layer of SU-8 2000.5 is spun (500 nm) over the slide. This layer will act as an interface between glass and further photoresist layers, improving layers adhesion and master durability (step II).

Later, in order to fabricate the first layer of the device (the constrictions simulating the IES), a ~4.8 µm-high SU-8 5 negative photoresist is spun over the glass slide applying a three-step spinning protocol to obtain the desired SU-8 thickness. The slide is then soft-baked before being exposed with a chrome-on-glass photomask to UV light (4 s, 24 mW cm^2, 345 nm) in a mask aligner (MJB4 aligner, SÜSS Microtec, Germany). After that, the slide is baked in the sequence of 65ºC for 1 minute and 95ºC for 3 minutes, left to cool for up to 1 hour, and finally developed using the SU-8 developer for 30 s (step III).

For the second layer, that corresponds to the pillar matrix constriction zone, a similar protocol is applied; since the desired height is, this time, ~13.5 µm, SU-8 10 photoresist is spun over the previous layer applying a three-step spinning protocol, exposed to UV light using a chrome-on-glass photomask (6 s, 24 mW cm^2, 345 nm) and developed for 2 minutes (step IV).

Several layers of Ordyl SY negative photoresist were used to shape the third layer (the fast-flow channel), that were laminated on top of the last SU-8 layer using a hot/cold laminator in order to have a smooth attached 60 µm-high film surface. Then, the slide is exposed through a chrome-on-glass photomask to UV light (5 s, 24 mW cm^2, 345 nm), in the mask aligner.

The fabrication of the master mold is finished by developing the film using the Ordyl developer for 3 minutes (step V). SEM images of a master can be found in Figure 2.14.

To obtain the final microfluidic device, PDMS is poured on top of the SU-8/Ordyl master and finally bonded to a glass slide, as described in the previous subchapter.
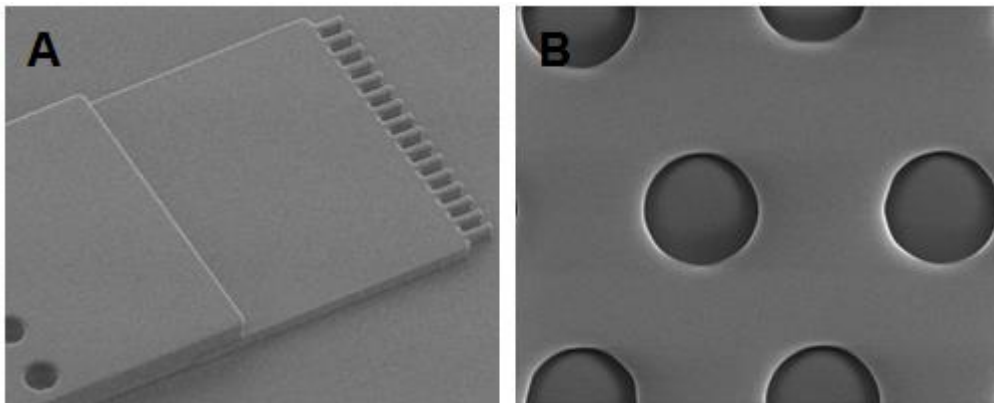
Figure 2.14. Details of the splenon-on-a-chip version 2 master. *(A) SEM image of the first and second layer. Also it can be appreciated a correct alignment of the layers of the device. (B) Pillar matrix details.*

2.3.3. Biological materials and characterization procedure.

The experimental results obtained using the **splenon-on-a-chip version 2** will be presented in **Chapter 4.** Hereafter are listed the materials and setups used to perform the analysis, using this OCD. The sections: "Uninfected blood specimens", "Measurement of cell deformability", "Image capture and analysis", "Statistical analysis" and "*In vitro* haemolysis assay" are common to the ones presented in subchapter 2.2.3. referred to the splenon-on-a-chip version 1.

2.3.3.1. Preparatory setup.

The preparatory setup (Figure 2.15A) could be used prior to experimentation for the purpose of biologically coat the OCD microchannels. It consists of (1-2) 1 ml syringes connected, through a needle with PTFE tubing, to the device. The syringe(s) is/are actuated by a neMESYS pumping station (Cetoni GmbH, Germany). Experiments with buffers and beads were carried out at room temperature, whereas experiments with blood specimens, cells and proteins were carried out at a physiological temperature of ~37ºC. Precautions were taken before each step to avoid, to the extent possible, the formation of bubbles inside the device.

2.3.3.2. Microscope stage culture chamber.

In vitro culture systems should ideally permit a correct adaptation of the cellular environment, by controlling, for instance, gas-exchange and sample temperature. In that sense, a precise control of those environmental conditions is imperative in order to maintain close physiological status (T=~37ºC, %CO_2=5%, %O_2=10%) for both the cell cultures and the human blood sample. These conditions will be hereinafter referred to as "physiological conditions".

For this purpose it was mounted and used a custom-made microscope stage incubator (Okolab, Italy) designed, and fabricated, to allow the accommodation of all the system components, plus being totally compatible with the laboratory (imaging) equipment previously available (shown in Figure 2.15A,B). Also, is able to maintain physiological conditions. This permits to have during all the experimentation the samples and the OCD at the desired ambient, therefore reproducing close organic situations. This may benefit cell cultures in a glass-PDMS chip and the creation of a hypoxic environment, interesting for applications evolving OCD technologies experimentation related to the human spleen. In this framework, the usage of PDMS as molding material has the advantage that it is permeable to gas, and transparent.

The chip holder consists of an "open" chamber, where the presented OCD can be inserted and directly observed through the microscope.

The system could remain fully closed when no external microfluidic connections are needed, so maintaining, to the extent possible, a configurable temperature, feature particularly important for preserving (*i*) the stability and survival of the biological samples and the (*ii*) foreseeability of the blood/samples dynamics (to the extent possible).
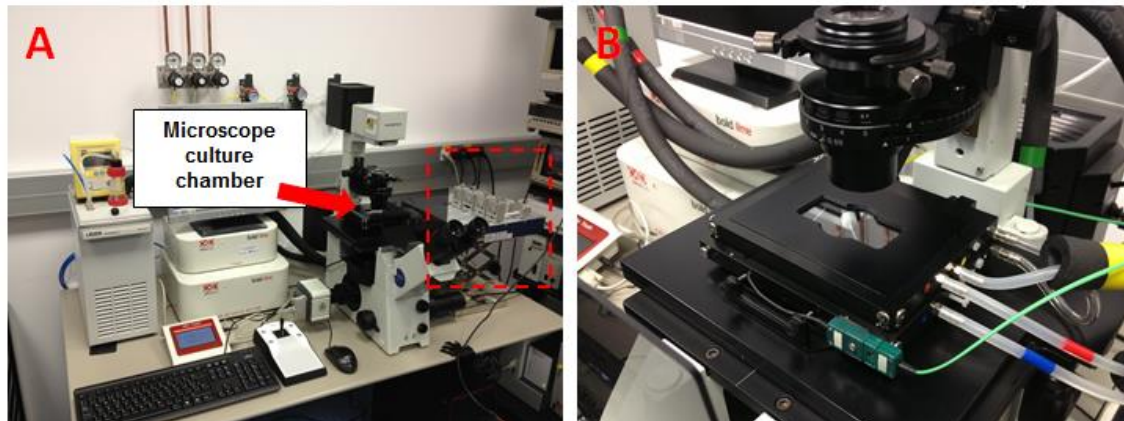
Figure 2.15. Experimental system. *(A) Shows the whole system, with an Okolab Bold Line temperature and gases unit, and a computer to control the image acquisition. Marked in red: the preparatory setup. (B) Represents a detail of the microscope stage culture chamber.*

2.3.3.3. Immunostaining on-chip and fluorescence imaging.

In order to evaluate a 3D endothelial lining in the fast-flow microchannel walls, the cells cultured inside the OCD were subjected to an immunostaining on-chip process for posterior fluorescence imaging.

Firstly, a formalin fixative solution was injected through the OCD microchannels at a flow rate of 10 µl min^{-1} and left 10 minutes inside the microfluidic device. The samples were subsequently permeabilized in 0.1 % Triton X-100/PBS for 10 minutes at room temperature. Afterwards, cell samples were blocked with 1% bovine serum albumin (BSA) in PBS for 1 hour. Then, primary antibody, diluted 1% in BSA/PBS, was injected and left for 1 hour at room temperature. F-Actin filaments were stained for 1 hour with phalloidin Alexa Fluor 568 diluted 0.1% (v/v) in BSA/PBS, followed by a 10 minutes wash with PBS. Nuclei were stained for 1 hour with Hoechst 33342. A final 10 minutes wash was performed with PBS.

2.3.3.4. Red blood cells detection using pattern recognition.

In this work, it could be used an approach to automatically count the number of RBCs in the IES section using a circular pattern recognition code written in MATLAB v.R2012b (The MathWorks, Natick, Ma, USA) optimized for this specific use.[15,16] Feature extraction was used to locate the RBCs based on their geometric features. This quantitative technique was able to approximately calculate the RBC count.[15,16]

Results suggested that the RBCs counting, in post-assay microscope images, exhibited a good precision.[16] The tested data (n=20) showed an estimation rate of 92.8%, when compared with manual counting (an example can be found in Figure 2.16).

Using this technique, it could be possible to (easily) estimate the number of RBCs in the section previous to the microconstrictions, in order to assess the density, and the accumulation of cells, in that region.
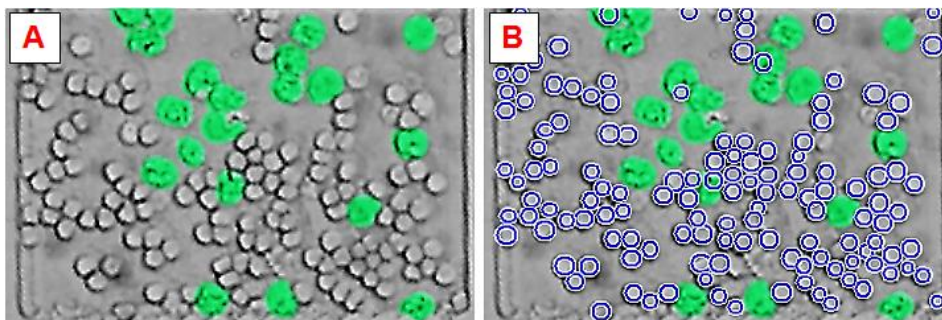
Figure 2.16. RBCs detection using Matlab. By using pattern recognition techniques it could be possible to detect and estimate the number of RBCs. Left Panel (A) shows an image of the IES section, with macrophages coloured in fake green. The Right Panel (B) shows the same image after applying the Matlab pattern recognition step. As may be observed, the finding of RBCs is highly successful. An average error value of 7.2% was calculated in the n=20 tests.

2.3.3.5. Microchannel coating process.

The coating process could be performed, if needed, using the preparatory setup and the custom microscope stage culture chamber described previously.

Sterile PBS can be introduced firstly to the platform in order to clean the microchannels. This process entails pumping the solution for ~15 minutes at a fixed flow rate of 15 µl min^{-1}.

Following the cleaning step, and with the purpose of coating separately the fast/slow-flow microfluidic channels, the solutions were introduced into the device using the different inlets that the device disposes. Laminar co-flow properties were used to direct the samples without mixing to the appropriate locations. Collagen type I (at a concentration of 0.4 mg ml^{-1}), inserted through the principal inlet (named inlet 1), will coat the fast-flow channel; as the slow-flow channel was meant to house macrophages, it will be coated with a fibronectin solution (at a concentration of 0.1 mg ml^{-1}), and therefore will be introduced through the secondary inlet (named inlet 2). If only one coating is needed, then the sample could be introduced, for instance, using inlet 1.

The coating solutions were injected at constant flow rates during ~1 hour through the device at 37ºC to form a thin coating, as uniform as possible. The devices were then left to rest overnight, with the solutions inside the microchannels, in a humidified cell culture incubator.

After the coating step, each device was washed for ~15 minutes with sterile PBS, at a constant flow rate of 30 µl min^{-1}, in order to remove any residual substance that might be harmful to cell cultures, and the excess of fibronectin/collagen. All the devices were subsequently stored in this solution at 4°C to prevent, to the extent possible, drying/evaporation of the coating layer.

Therefore, by taking profit of the properties of laminar flow inside the splenon-on-a-chip version 2 device, it could be possible to create a continuous coating layer along the different sections of the device. Then, this protocol could permit the building of a "fictitious ECM" in a homogeneous manner.

2.3.3.6. Human spleen macrophages.

The human spleen macrophages cell line (ATCC, CRL-9850), was grown in Iscove's modified Dulbecco's medium supplemented with 10% fetal calf serum, 0.05 mM 2-mercaptoethanol, 0.1/0.016 mM hypoxanthine and thymidine and 1% penicillin-streptavidin for 2 days. Cells were cultured in a T-75 cell culture flask (NUNC, Denmark) in a 5% CO_2 humidity incubator at 37°C.

2.3.3.7. Human splenic endothelial cells.

Human splenic endothelial cells (hSECs) (Sciencell™ Cat. Num. #5500) were cultured in growth medium consisting of Endothelial Cell Medium supplemented with 1% Endothelial Cell Growth Supplement, 1% Penicillin-Streptavidin and 5% fetal bovine serum.

Cells were allowed to proliferate in T-75 culture flasks coated with 0.1 mg ml^{-1} fibronectin until they reached 70-80% confluence in a 5% CO_2 humidity incubator, at 37°C. Experiments were performed using cells from passage 5-9. After approximately 2 days, cells were trypsinized with 0.25% of trypsin-EDTA (Gibco, USA).

2.3.3.8. Cell loading.

The utility of laminar co-flow to obtain localized functionalized regions in the biomimetic platform was investigated. As a proof of concept, first trials were done with NIH/3T3 fibroblast cell line, for example to direct the cells towards one of the channels, something challenging with just one inlet. The results attained supported the applicability of the methodology for this commitment, as can be seen in the example shown in Figure 2.17.
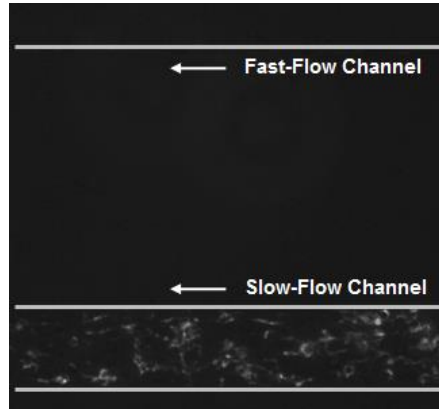
Figure 2.17. Usage of laminar co-flow to enhance cell culture applications inside the microfluidic device (trials with 3T3 Fibroblasts). *Capabilities of laminar co-flow in the biomimetic platform. With this approach it could be possible to direct the cells to a specific microchannel.*

When a macrophages and/or hSECs cell culture is needed, devices were previously sterilized, and afterwards filled with the correspondent complete cell media, and kept in a humidified cell culture incubator for ~5 hours, in order to allow the proteins in the media to diffuse into the OCD microchannel structure.

The cell suspensions could be loaded into the device using the preparatory setup and sterilized equipment, at specific concentrations. In the presence of hSECs in the channels, the devices were kept undisturbed, in the culture chamber, to permit those cells to attach to the surface. The usage of the laminar co-flow methodology could be useful to prevent the hSECs to enter, to the extent possible, into the slow-flow channel, as they could obstruct the constrictions simulating the IES, if grown.

The microscope stage chamber was used to maintain the temperature of the platform at ~37°C, and to have a correct gas exchange with the device when long periods of observation under the microscope were needed (in order to ensure, to the extent possible, a correct cell culture).

2.3.3.9. Experimental setup: autonomous closed-loop system.

The experimental setup consists, in first term, on a custom closed-loop system conformed by an autonomous pumping machinery. This fluidic system is composed by an (*i*) mp6 piezoelectric micropump (Bartels Mikrotechnik GmbH, Germany) and a (*ii*) home-made autonomous driving stage (Figure 2.18). This system could be used if a closed-loop approach is needed.
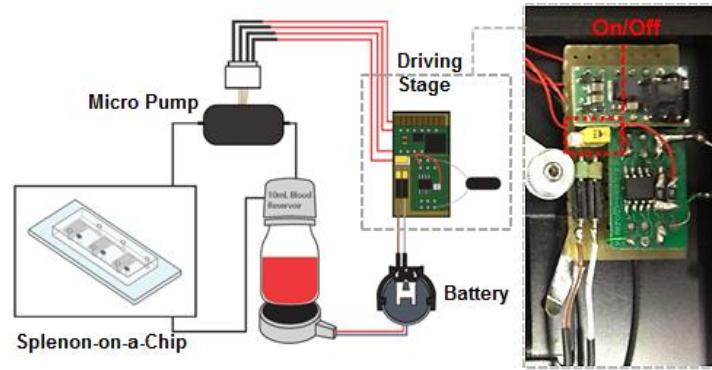
***Figure 2.18. Experimental setup using an autonomous closed-loop system**. Left Panel shows a scheme of the microfluidic closed-loop system with a detail of (Right Panel) the driving stage that activates the micropump. The driving stage can be switched on/off using an interrupter located in the front face. (With the help of Dra. del Moral).*

Due to the square signals generated, a pulsatile flow could be settled on the splenon-on-a-chip. It is believed that pulsatile flow better mimics the fluctuating flow of the blood stream in a human body. Thus, it could perhaps be possible to translate some rheological properties of the flow, by using this setup.[17]

This pumping system is connected to a battery holder in order to work totally autonomously with a 3V battery. This facilitates the usage of the entire system, inside the microscope stage culture chamber, without needing to be connected to the current.

There is also a small blood reservoir that acts as a blood tank, from where the micropump picks the sample. The tank is connected to a 3V coin vibration motor that acts as a customized micro-shaker. This permits to shake the blood/sample, preventing, to the extent possible, clogging or undesired sedimentation of the cells. For its side, the reservoir cap is made of PDMS in order to obtain a correct gas-exchange with the sample, and prevent tubing holes to provoke leakage.

The mp6 micropump, connected from one side to the blood reservoir, is responsible for infusing the blood/sample to the device. This means that the whole system could act as a "micro-human splenon-like platform" prototype as a proof of concept, working at close physiological conditions.

2.3.3.10. Experimental system operation using the closed-loop system.

Prior to experimentation, a pre-filtration device could be utilized for the purpose of removing the possible blood clots that could be previously in the blood sample (particularly in aged-samples).

The first step to start an experiment consists on fixing the ambient conditions of the microscope culture chamber, on the experimental system. Through a touch pad interface available (Okolab, Italy), these parameters can be easily manipulated. The experimental system should be washed with ethanol prior to use.

Straightaway, the splenon-on-a-chip OCD can be installed and connected through the adequate sterilized tubing to the autonomous closed-loop pumping station that will inject the sample to the microfluidic device. At this point, the driving station may be switched on.

Also, the preparatory setup could be used if a closed-loop approach is not needed.

Because this version of the splenon-on-a-chip have two inlets, the secondary one should be disabled during an assay; for achieving this, a PDMS cap covers the entrance and therefore no liquid exits through it.

The stage culture chamber should be closed during the experimentation, to maintain the desired conditions; only should be opened, for example, to replace the batteries that supply the driving stage and the vibration motor.

The process could be recorded by a capture and analysis software during the experiment. In the same way, temperature values and gasses percentages, inside the chamber, are also recorded in order to visualize and detect promptly any issue regarding the loose of stability in the system.

Concerns regarding the introduction of bubbles into the device were faced during the assays. Consequently, precautions were taken before each experiment. The Luer Lock adapter acted as a bubble stopper during the assay.

2.3.3.11. Flow cytometry erythrophagocytosis assays.

Mimicking, to some extent, the splenon immune response, by means of human macrophages, was interesting in order to evaluate the effectiveness to achieve close "physiological functions". In this regard, some RBCs phagocytosis (*i.e.* erythrophagocytosis, EP) tests were performed.

Briefly, different RBCs populations were "stained" with the PKH26 red fluorescent lipophilic dye (Sigma-Aldrich Co., USA).[18] For its part, macrophages were cultured as detailed previously, and then introduced in a blood reservoir, acting as "blood stream macrophages". So, macrophages were mixed with PKH26-labelled RBCs, at physiological conditions.

EP was measured by flow cytometry, after 1 hour, in order to estimate the percentage of splenic macrophages that could contain PKH26-labelled RBCs, and the mean fluorescence intensity. A total of ~$1 \cdot 10^4$ events were collected for each sample, and data was displayed in plots as red fluorescence *versus* side scatter dot plots. Those macrophages that supposedly phagocytized PKH26-labelled RBCs were therefore enclosed in the regions set for red fluorescence intensity, determined by cell size and fluorescence histograms. The negative control (macrophages cells alone) showed non-appreciable autofluorescence, and helped to define a fluorescent threshold. In addition, the phagocytosis of fluorescent latex microparticles by macrophages was analyzed, using the same methodology.

Precautions were taken in order to just take into account viable macrophages; dead cells were excluded, to the extent possible, from the quantification assay.

2.4. Splenon-on-a-chip version 3-D.

2.4.1. Introduction.

Splenon-on-a-chip Version 1	Splenon-on-a-chip Version 2	**Splenon-on-a-chip Version 3-D**

The majority of microfluidic devices are usually built in PDMS (see Chapter 1.1.6. for further information) due to the many favorable properties it offers for this particular field.[5,6] However, this polymer is normally not well suited for later translation into mass-fabrication procedures.[19,20]

For this reason, in collaboration with Prof. Folch Lab (University of Washington, UW, USA), new versions of the "splenon-on-a-chip concept" were designed and fabricated using a form of 3D printing named stereolithography. The idea was to create a prototype that could be user-friendly and plug-n-play format, where filtering tests could be performed using the setups already putted in place.[19,20]

However, nowadays it is challenging to print microchannels with the dimensions obtained using photolithography, due to XYZ resolution problematic. This fact was particularly critical due to the difficulty of fabricating the microconstrictions simulating the IES. For this reason, these devices could use commercial membranes with micrometer pore sizes. These membranes can be easily exchangeable, making those devices reusable (something that could be an advantage for many haematological clinical assays). Therefore, the aperture of the pores may also be customizable, depending on the study needs.

Also, the whole microfluidic device is included on the dimensions of a common glass slide, so it can be disposed effortless on a microscope holder (as the one presented). In addition, knowing the difficulties of connecting microfluidic tubing to a LOC, Luer Lock connectors were installed to facilitate this task. Their design also permits the injection of fluids *via* a syringe.

The channels dimensions were defined to have a section of around ~500 μm. It is necessary to highlight that the fabrication process entailed many problems due to the device small features, the complexity of the design and the complications of rinsing the uncured resin.

Associated to the device, the cap design is based on the idea of pressing the membrane to the bottom of the membrane holder and also of having the possibility to close the fluid motion when desired (only one portion of the cap has an open channel that allows liquid to pass through it).

In conclusion, four 3D printed devices were conceived (named splenon-on-a-chip version 3-D). Figure 2.19 represents the ones that have been tested. Version 1.0 is a "simpler" device, with just one inlet and one channel, and could perhaps be useful, in the future, to perform assays to evaluate the status or study some mechanical properties of blood cells or samples (acting like a filter-device). For its side, version 2.0 could be seen as a "3D printed evolution" of the previous splenon-on-a-chip platforms, since in it are disposed some structures corresponding to the main compartments of the human splenon, as detailed before, and reproduced in versions 1 and 2. The idea was to design a platform prototype, which could be produced using stereolithography. Figure 2.19 also highlights some of the sections included in those prototypes (for example, the membrane holder).
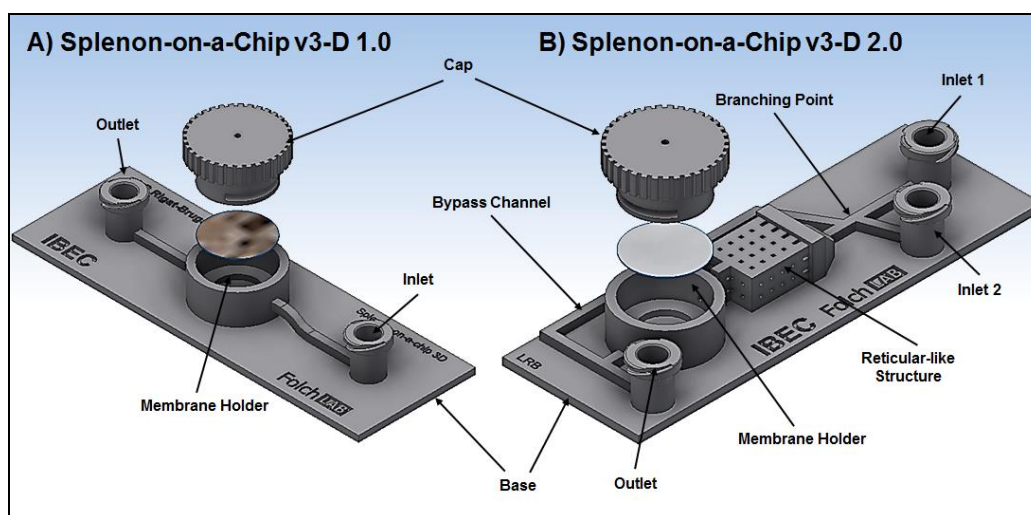
Figure 2.19. Splenon-on-a-chip version 3-D prototype models.

2.4.2. Fabrication protocol.

The devices CAD designs were engineered using Autodesk Inventor® (San Rafael, California), and finally saved using the *.stl* file format. The female Luer Lock connectors designs (original design by N. Felix, GrabCAD.com)[20] were merged with the inlet(s) and outlet microchannels.

The fabrication/building process of the devices was done by FineLine Prototyping, Inc. (Raleigh, North Carolina) on a Viper Stereolithography System (3D Systems, Rock Hill, South Carolina) in High-Resolution Mode (*i.e.* 100 µm XY resolution and 50 µm Z steps) using the "Substrate Build Style Option" process, in order to enhance the optical clarity. The resin selected for this purpose was the transparent-like Somos® WaterShed XC 11122 (DSM, Heerlen, Netherlands), due to its favorable mechanical properties and biocompatibility.[20]

2.4.3. Biological materials and characterization procedure.

The experimental results obtained using the **splenon-on-a-chip version 3-D** will be presented in **Chapter 5.** The materials and setups used to perform the tests (that are: "Uninfected blood specimens", "Image capture and analysis", "Microscope stage culture chamber", "Experimental setup: autonomous closed-loop system" and "Experimental system operation") are common to the ones that were presented in the subchapters 2.2.3. and/or 2.3.3., referred to the splenon-on-a-chip former versions.

2.5. Conclusions.

In this chapter it has been detailed the different designing strategies and methodologies used to built the distinct versions of the splenon-on-a-chip concept. The premise was to try to recreate, to the extent possible, some properties that make the splenon unique. Also, previously to the final first version, different "preliminary" devices were fabricated, such as cell-culture structures, or microdevices with constrictions.

By using a custom microfabrication protocol, employing several photoresists, in order to obtain multilayered devices (in an easy and cost-effective way), it was possible to model several novel

platforms that could have close splenon physiological measurements, and requirements (to the extent possible). This was partly feasible thanks to the use of Ordyl film resist to construct high-aspect-ratio devices, and the alignment marks.

To highlight, the development of the microconstrictions simulating the IES was challenging, as its dimensions are in the limit of the fabrication possibilities of the mask aligner. However, by refining the protocol it was finally possible. In the case of the 3D printed microfluidic devices, to overcome limitations regarding resolution, new versions prepared to employ porous membranes were designed, which fitted in the philosophy of creating a more "industrial" prototype that could be fabricated using non-expensive strategies.

2.6. References.

1. P.A. Buffet, I. Safeukui, G. Deplaine, V. Brousse, V. Prendki, M. Thellier, G.D. Turner and O. Mercereau-Puijalon, *Blood*, 2011, **117**, 381-392.
2. A.J. Bowdler, The Complete Spleen, Humana Press, 2nd edition, 2002.
3. N. Mohandas and P.G. Gallagher, *Blood*, 2008, **112**, 3939-3948.
4. I. Safeukui, J.M. Correas, V. Brousse, D. Hirt, G. Deplaine, S. Mule, M. Lesurtel, N. Goasguen, A. Sauvanet, A. Couvelard, S. Kerneis, H. Khun, I. Vigan-Womas, C. Ottone, T.J. Molina, J.M. Treluyer, O. Mercereau-Puijalon, G. Milon, P.H. David and P.A. Buffet, *Blood*, 2008, **112**, 2520-2528.
5. A. Mata, A.J. Fleischman and S. Roy, *Biomedical Microdevice*, 2005, **7**, 281-293.
6. J.C. McDonald and G.M. Whitesides, *Accounts of Chemical Research*, 2002, **35**, 491-499.
7. A.K. Au, W. Lee and A. Folch, *Lab Chip*, 2014, **14**, 1294.
8. L.G. Rigat-Brugarolas, A. Elizalde-Torrent, M. Bernabeu, M. de Niz, L. Martin-Jaular, C. Fernandez-Becerra, A. Homs-Corbera, J. Samitier and H.A. del Portillo, *Lab Chip*, 2014, **14**, 1715-1724.
9. K.W. Oh, K. Lee, B. Ahn and E.P. Furlani, *Lab Chip*, 2012, **12**, 515-545.
10. L. Martin-Jaular, M. Ferrer, M. Calvo, A. Rosanas-Urgell, S. Kalko, S. Graewe, G. Soria, N. Cortadellas, J. Ordi, A. Planas, J. Burns, V. Heussler and H.A. del Portillo, *Cell Microbiol.*, 2011, **13**, 109-122.
11. J.S. Dudani, D.R. Gossett, H.T. Tse and D. Di Carlo, *Lab Chip*, 2013, **13**, 3728-3734.
12. P.T. Cherian, X. Wu, M.M. Maddox, A.P. Singh, R.E. Lee and J.G. Hurdle, *Sci. Rep.*, 2014, **4**, 4721.
13. Q. Li, C. Dong, A. Deng, M. Katsumata, A. Nakadai, T. Kawada, S. Okada, C. Clayberger and A.M. Krensky, *Antimicrob Agents Chemother*, 2005, **49**, 388-397.
14. M. Arabski, A. Węgierek-Ciuk, G. Czerwonka, A. Lankoff and W. Kaca, *J Biomed Biothecnol*, 2012, **2012**, 286216.
15. T.J. Atherton and D.J. Kerbyson, *Image Vision Comput*, 1999, **11**, 795-803.
16. M. Maitra, R.K. Gupta and M. Mukherjee, *Int J Comput Appl T*, 2012, **16**, 18-22.
17. H.S. Son, K. Sun, Y.H. Fang, S.Y. Park, C.M. Hwang, S.M. Park, S.H. Lee, K.T. Kim and I.S. Lee, *Int J Artif Organs*, 2005, **28**, 609-625.
18. M.F. Veale, G. Healey and R.L. Sparrow, *Vox Sanguinis*, 2014, **106**, 219-226.
19. A. Urrios, C.A. Parra-Cabrera, N. Bhattacharjee, A.M. González-Suárez, L.G. Rigat-Brugarolas, U. Nallapatti, J. Samitier, C.A. DeForest, F. Posas, J.L. García-Cordero and A. Folch, *Lab Chip*, 2016, **16**, 2287-2294.
20. A.K. Au, W. Lee and A. Folch, *Lab Chip*, 2014, **14**, 1294-1301.

Chapter 3. A functional microengineered model of the splenon hydrodynamic properties

SUMMARY

With the aim of reproducing the filtering functions of a human splenon, on a chip, a microengineered OCD device model mimicking, to some extent, its hydrodynamic forces and its physical properties, was designed. In this first version of the human splenon-on-a-chip microfluidic device, the mechanical and physiological responses of the splenon have been mimicked and evaluated, to the extent possible. Experiments were performed using human RBCs and murine malaria-infected cells. To the best knowledge of the authors, this OCD resulted in the first functional model of the splenon. An innovative approach was set to explore alternative methods to study malaria and/or other haematological disorders, in order to could, ideally, help in facilitating some future functional studies of the human organ.

3.1. Introduction.

Through a complex organizational architecture, the spleen is perfectly adapted to selectively filter and eliminate old/senescent RBCs, as well as blood-borne infectious organisms, including the *Plasmodium* parasites.[1] Such complex architecture includes the splenic white pulp, red pulp, and the marginal zone, each of which is populated by specialized cells. The filtering capacity of the spleen is inherently linked to the complex vasculature of the organ, controlling events such as the (*i*) blood passage through a reticular meshwork in the red pulp, (*ii*) entry into the marginal sinuses or the marginal zone, (*iii*) drainage through perimarginal cavernous sinuses or capillary branches, or (*iv*) entry into the white pulp. The spleen's structure is thus implicitly related to its function as the only lymphoid organ responsible for blood surveillance.

In the current microcirculation model, based on washout experiments, ~90% of the blood-flow circulates through the spleen as closed-fast microcirculation, directly bypassing the spleen's filtration capacity. The remaining, however, circulates as open-slow microcirculation through the filtration beds of the cords, thus facilitating the recognition and destruction of non-healthy RBCs by macrophages.[1] Moreover, before reaching the venous system, *circa* ~10% of the blood in the open-slow compartment of sinusal spleens, such as the human spleen, must pass through the IES of the splenic sinusoids. This passage represents a test for functionality of RBCs, as less deformable cells could not traverse the IES.[2]

Infections by malaria parasites sometimes induce a dramatic splenic response, characterized by splenomegaly. At present, the understanding of human spleen pathology derives, mostly, from *post-mortem* examinations,[3] analyses of removed spleens, imaging of fixed spleen sections, animal models, cellular studies and/or novel medical imaging techniques.[4,5] Recently, an *ex vivo* model of the human spleen, able to maintain clearing and processing functions, was developed by P.A. Buffet *et al.*[6] Using this *ex vivo* system, a dual role on protection/pathology in malaria infections has been hypothesized.[7] However, despite the major advance this model represents for malaria and spleen studies, its use could remain limited due to the difficulties for adopting it as a routine tool in the laboratory.

Advances in bioengineering and microfluidics have made it possible to achieve the necessary technology to generate patterns of complex microstructures, allowing precise control of dynamic fluid flows of small volumes. In the area of malaria research, studies using microfluidic devices have been mainly utilized to measure the deformability of *Plasmodium*-parasitized iRBCs.[8-10] In the area of diagnostics, microfluidic devices have been proposed as promising tools for malaria detection, using separation principles based on the intrinsic properties of iRBCs.[11-13]

With the aim of studying the RBCs filtration in the spleen, as could be observed in the minimal structural functional red pulp unit, the splenon,[7] in this chapter it is presented the first version of a multilayered microengineered OCD model of the human splenon-on-a-chip.[14] With this device, engineered to mimic both the splenon closed-fast and open-slow microcirculations, the reticular meshwork and the IES (to the extent possible), it is intended to contribute to the advance in the knowledge of the spleen's function in malaria and/or, perhaps, other haematological disorders.

Initial studies, using the proposed model, focused on the malaria caused by *Plasmodium vivax* (*P. vivax)* parasite, a type of parasite that infects RETs, rather than RBCs. This fact makes its study and research very challenging, since RETs usually accounts for less than the 2% of total RBCs in circulation, situation that hampers any kind of systematic investigation of this form of malaria. For this purpose, a "*P. vivax*-like model" using *P. yoelii* will be explored.

3.2. Mimicking the hydrodynamic and haemorheological behavior of the splenon.

The aim was to reproduce, to some extent, the blood circulatory patterns of the splenon, *in vitro.* For this purpose, a complex microfluidic network was defined (details in Chapter 2.2.).

3.2.1. Device fabrication.

In this chapter it is going to be used the splenon-on-a-chip version 1 microfluidic device. The fabrication methodology is described in Chapter 2.2.2.; a brief description is included here. All procedures were carried out in the clean room facility of the IBEC.

The construction of the OCD master consists on a multi-step procedure designed to obtain two different heights using three different photoresists, by means of photolithographic techniques, customized for fabricating a multilayer platform. The final device is obtained by soft lithography, using PDMS as molding material (Figure 3.1).[14]
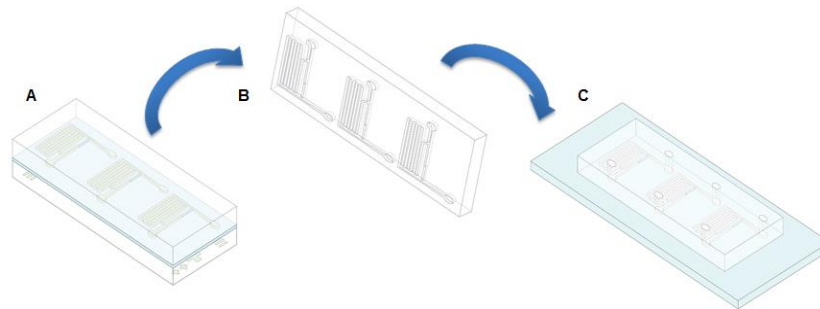
Figure 3.1. Splenon-on-a-chip version 1 replication process and final platform. (A) Master replication process using PDMS. (B) The PDMS stamp is peeled off carefully and finally (C) bonded to a glass slide to obtain the splenon-on-a-chip biomimetic platform.[14]

3.2.2. Proof of concept: flow dynamics measured using microbeads.

The hydrodynamic behavior of the OCD microfluidic device was initially tested using fluorescent microbeads (Polysciences, Inc., Warrington, PA) of different diameters, diluted in PBS. These preliminary assays focused on the "critical" sections of the OCD, to confirm that flow motion and division in these devices could be similar to that of the splenon on a proportional scale (Figure 3.2A). Also, it was pivotal to examine the behaviour of the pillar matrix section, to confirm that it could act like a particle "retention mechanism", not as a deterministic lateral displacement step (Figure 3.2B). Once these trials were completed, adaptations on the device structure were done in order to work with a non-Newtonian physiological fluid like human blood.
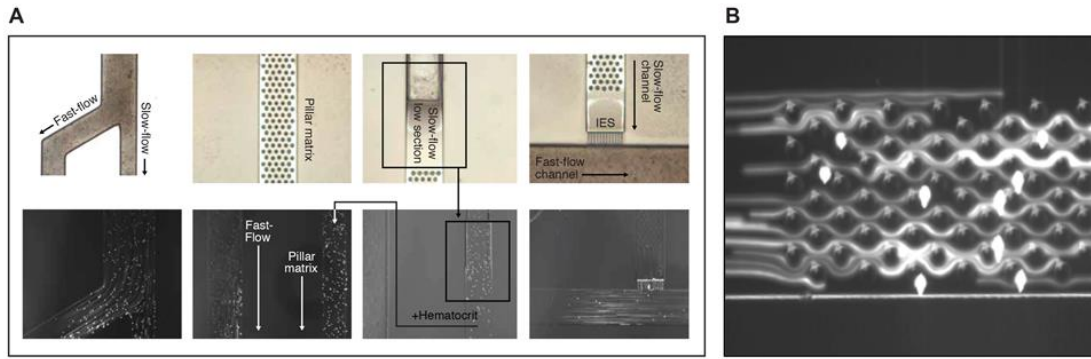
Figure 3.2. Microfluidic device initial validation. *(A) Testing the microfluidic device "critical" sections with different fluorescent microbeads. (B) Pillar matrix constriction zone evaluation.*[14]

3.2.3. Physiological flow division.

Recent data has showed and confirmed a splenic dual microcirculation, with approximately 90% of the blood input flowing through a closed/fast-flow compartment (please see Chapter 1.3.2. for further details).[1,15] Thus, hydrodynamic studies were performed in order to translate this organ's flow behavior inside the splenon-on-a-chip, calculating the R_H of the different OCD branches. Of significance, microfluidic analyses confirmed that the final design, and architecture, imposed to this microfluidic device mimicked the two-compartment blood circulation of the human splenon, and with the channel representing the slow-flow accounting for ~10% of the flow (Figure 3.3).
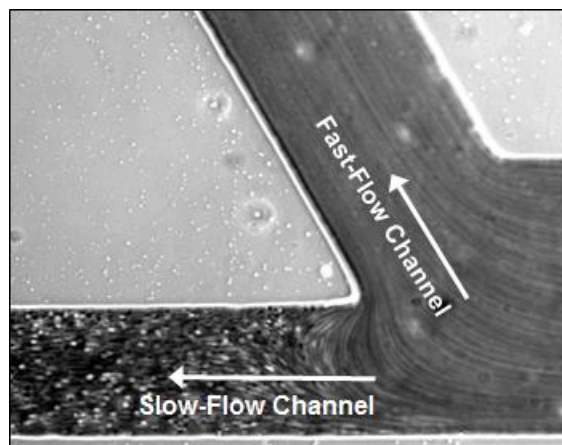
Figure 3.3. Blood flow division inside the microfluidic device. *Image showing that the ~90% of the blood flow goes through the fast-flow channel whereas the remaining ~10% goes through the slow-flow channel.*[14]

3.2.4. Physiological flow rate.

Reproducing, to the extent possible, the splenon flow rate could be an important step to be able to translate physiological scenarios, with respect to the possible cell-environment interactions.

3.2.4.1. Physiological flow rate *in vivo*.

The physiological flow rate imposed in the OCD device was obtained in collaboration with Prof. Hernando del Portillo's Lab (ISGlobal/CRESIB), after analyses of intravital images of the spleen of Balb/c mice injected with (fluorescein isothiocyanate)-labelled RBCs, in order to quantify the

velocity of the cells in the small vessels just before reaching the open circulation in the red pulp, as described elsewhere.[16] Intravital microscopy of spleen vessels was performed (n=10), and a velocity of ~740 µm s^{-1} was estimated.

3.2.4.2. Physiological flow rate *in vitro*.

Different flow rates, using human blood, were tested and studied using diverse OCD version 1 structures (changing, for example, the height of the fast-flow channel) and a value ranging from ~1-5 µl min^{-1} (depending on the blood sample) could be able to translate similar velocities in the slow-flow channel (before the constriction section) as the ones obtained through *in vivo* imaging of the spleen of mice. Therefore, in this biomimetic device, it has been achieved an architecture such that this velocity could be in the 120-760 µm s^{-1} range, that is, to some extent, comparable to physiological status, depending, also, on the channel position of the RBCs. Furthermore, the structure of this OCD device ensures, in principle, negligible haemolysis, at those flow rates.

3.2.5. Mimicking the reticular meshwork in the slow-flow channel.

3.2.5.1. The reticular meshwork of the red pulp.

The slow-flow compartment only "holds" a small portion of the blood flow. Its reticular meshwork consists on a "reticular-like system" of reticular cells, generating slow flow pathways through the spleen. The RBCs motion through this structure is also dependent on their deformability, adding another selective behavior to this organ. Further, a progressive increase in haematocrit value could also be observed in this section of the splenic red pulp, situated before the IES.[1]

3.2.5.2. Different strategies to mimic the reticular meshwork.

In order to reproduce, to the extent possible, this complex reticular structure, different solutions were tested inside the device, like for example: using magnetic/non-magnetic microparticles (of different diameters, Figure 3.4A and B, respectively) or *in situ* polymerization (Figure 3.4C).
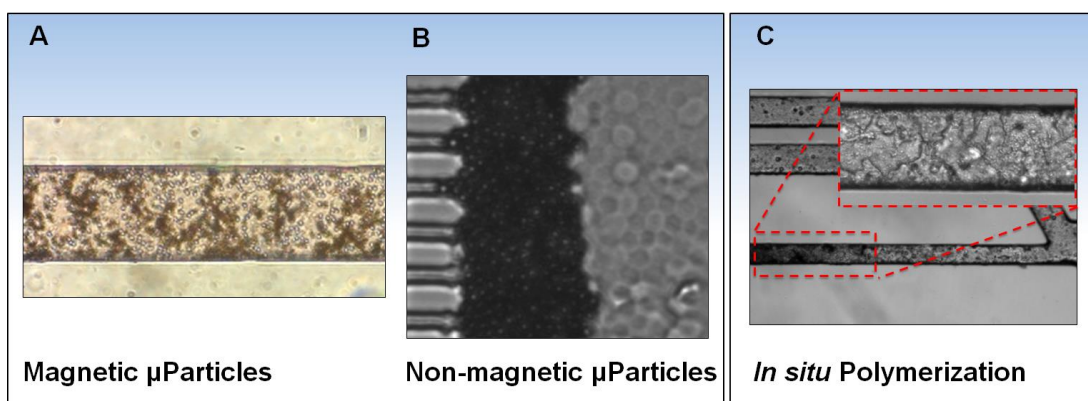
Figure 3.4. Different strategies to mimic the reticular meshwork. (A) Usage of magnetic microparticles that, with the help of a magnet, they could be directed towards the slow-flow channel. (B) Different diameter microbeads were injected into the splenon-on-a-chip and retained on the IES. However the interstices left were very small to permit the passage of the vast majority of RBCs. (C) In situ polymerization using pHEMA.

The particle solution was conceived to resemble the rambling physiological system, through the interbead interstices. For its side, polymerizing pHEMA could allow the creation of pores in the hydrogel structure, depending on the amount of water used in the solution.

However, it was difficult to create a homogeneous disposition with predictable behavior and, the most important, capable of giving reliable and reproducible results (more complicated due to working with "whole" blood rather than with diluted samples). This is why another strategy was explored, using structures created by photolithographic techniques.

3.2.5.3. Pillar matrix approach.

Finally, to try to mimic the reticular meshwork, a pillar matrix constriction section was designed and constructed in the slow compartment, to further lower the flow rate value and making viable to increase the cell density in that channel. Further, this structure is the major contributor to rise the R_H in the slow-flow channel, indispensable to achieve the objective: to be able to reproduce close physiological flow divisions. This approach ensures that the OCD device will have always the same constrictions simulating, to the extent possible, the reticular meshwork.

To highlight, designing such an array of posts is not straightforward, since a vast quantity of organizations and architectures will tend to generate a deterministic lateral displacement effect, where a specific arrangement of those pillars within a microchannel could predictably modify the trajectory of the cells.[17]

In that sense, it was important to define a pillar disposal that could be able to increase the R_H in that channel (without lateral displacement, in order to maintain a RBC in the same or adjoining streamlines, not introducing artefacts deviating from the desired behavior), helping to decrease the velocity, and enhancing the options of increasing the haematocrit, but ensuring no clogging or breakage of the RBCs. In addition, the distance between the posts had to be large enough to permit cell cultures. So, there was a compromise between the dimension and the separations of the pillars.

Another design consideration to be aware of is the pillar shape. In this regard, it was decided to design, model and fabricate circular-shaped pillars. Circular posts have seen to increase the R_H in a more efficient way when compared, for instance, to other geometrical figures.[17]

Therefore, as a result, thanks to the designed pillar matrix, it is possible to increase the RBCs density until the equilibrium (an example in Figure 3.5), although this effect is dependent on the haematocrit of the sample and intrinsic physical properties. However, as noted before, the major contribution of this matrix is to ensure a high R_H.
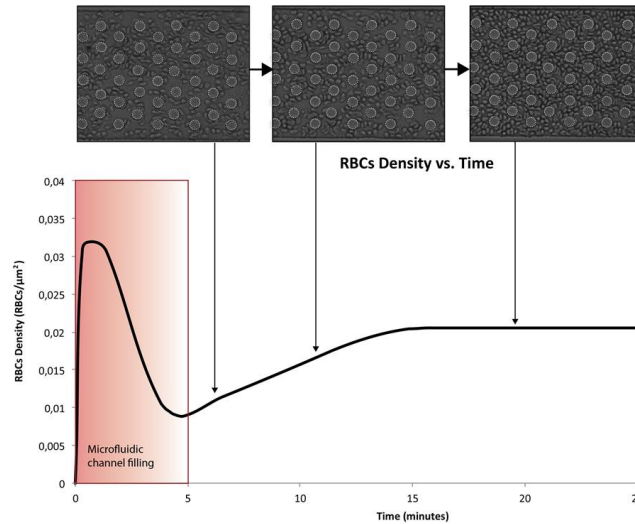
Figure 3.5. RBCs density versus Time in the pillar matrix section of the slow-flow channel. *Upper panel. An example of a Time-series images of the pillar matrix in the slow-flow channel showing an increase of RBCs density. Lower panel. In this experimental example, after the initial minutes required for the OCD channel filling, the graphic shows an increase of RBCs per μm^2.[14]*

3.2.6. Deformability of studied cells.

In this subchapter there will be used some of the methodologies described in Chapter 2.2.3.

The height of part of the slow-flow channel (the constriction section) was established in 5.5 µm in order to stretch the RBCs in the microconstrictions simulating the IES (with a width≈2 µm) in the planar configuration, while retaining or hinting the passage of unhealthy cells. So, following the validation of the platform hydrodynamics, deformability tests of fresh and aged human RBCs were performed (Figure 3.6A).
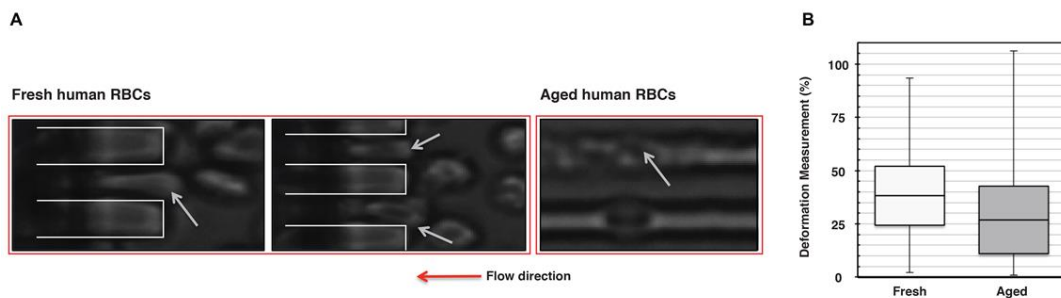
Figure 3.6. Deformability of fresh and aged-RBCs inside the slow-flow channel of the OCD. *(A) Transit of fresh and aged-RBCs through the microconstrictions mimicking the IES, in the slow-flow channel. White squares represent physical borders of the microconstrictions. (B) Median and the quartiles of the deformation percentage of fresh and aged-RBCs populations. Data was analyzed using Mann-Whitney U test (p=0.001).[14]*

Using the Mann-Whitney *U* test (with n=130 for each population), it was observed a statistically significant difference between the deformation percentage of old (M_{ed}=26.9%) and fresh RBCs (M_{ed}=38.3%) passing through the constrictions mimicking the IES (*p*=0.001, Figure 3.6B). This is consistent with the expectation that old RBCs are significantly less deformable than younger RBCs.[2,9,18]

Having made these observations with human RBCs samples, deformability measurements were then performed, in collaboration with Prof. del Portillo's Lab, with blood cells from BALB/c mice infected with *P. yoelii* 17X, constitutively expressing GFP, to facilitate image acquisition (Figure 3.7A). It was decided to use this transgenic line because it has a tropism for RETs, known to be highly deformable upon infection with RET-prone malarial parasites,[19] hence acting, to a certain extent, as a model of *P. vivax* malaria. *P. yoelii*-infected RETs could be easily detected in phase contrast images before, during, and after passage through the microconstrictions.

Measurements of iRBCs and RBCs inside and outside the slits revealed a statistically significant difference in the deformation percentage of infected cells (M_{ed}=34.3% and 19.1%, each) using the Mann-Whitney *U* test (n=130, *p*=0.006, in Figure 3.7B). Moreover, it was observed that the length of infected and non-infected cells, both in the slits (M_{ed}=9.06 μm and 7.62 μm) and in the pillar matrix zone (M_{ed}=6.74 μm and 6.4 μm), showed statistically significant differences using the Mann-Whitney *U* test, with a value of $p<0.0001$ and $p=0.002$, respectively, thus indicating a larger dimension of iRBCs on average.
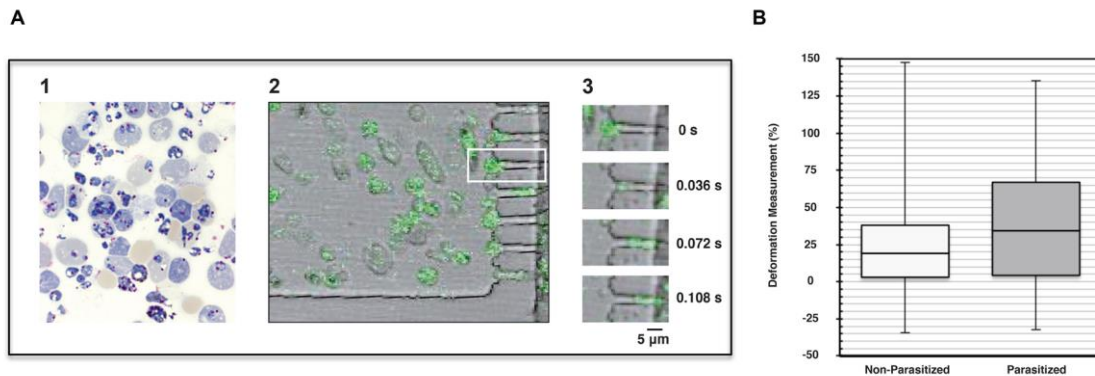
Figure 3.7. Deformability of parasitized and non-parasitized blood cells inside the slow-flow channel of the OCD. *(A) Transit of blood from P. yoelii non-lethal strain (17X-GFP) infected mice through the microconstrictions in the slow-flow channel. (1) BCB-Giemsa blood smear from a BALB/c mouse experimentally infected with the 17X-GFP strain. (2) CCD-image showing P. yoelii-GFP-infected RETs in the slow-flow channel and passing through the microconstrictions. (3) Time lapse-series show the passage of an infected RET (green) going through a microconstriction. (B) Graph showing the median and the quartiles of the deformation percentage of parasitized and non-parasitized cells. Data was analyzed using Mann-Whitney U test (p=0.006).[14]*

3.3. Discussion.

The minimal functional unit of the red pulp, able to maintain filtering functions has been termed, as stated, the splenon.[7] In this chapter are presented the (preliminary) experimental results of the first version of the novel multilayered microfluidic device of the human splenon-on-a-chip,[14] device that aims to help in the studies of the role of the organ in some haematological disorders.

The rheological properties of RBCs during haematological disorders have been examined using various different techniques.[20,21] Of particular relevance are the studies on RBCs deformability upon malarial infections, as several attempts have been made to try to associate the changes in cells deformability with pathology.[22-27]

Microfluidic devices have brought into these studies the possibility of performing individual cell deformability measurements, in real-time.[9] Sophisticated devices and/or imaging quantification approaches have recently demonstrated that the geometry of the cell could play a key role in its passage through the spleen.[28]

However, unlike any previous spleen-like device, this splenon-on-a-chip version incorporates two compartments (with physiological-like flow divisions) and two physical barriers representing the reticular meshwork and the IES, where cells stretch in a unidirectional manner. Thus, cells in the suspension are likely deformed by a combination of several hydrodynamic forces. Mainly because of these reasons, cell deformability was calculated measuring the elongation of blood cells.[29] It is believed this procedure to be the most accurate and precise possible to obtain the measurements required by this system, where multiple cells pass through the same slit, under different hydrodynamic forces, in a very short period of time.

To demonstrate the validity of such methodology, it was shown that old RBCs are normally less deformable than freshly drawn RBCs, which is consistent with previous studies.[2,9] Moreover, to better capture and quantify the deformability and passage of iRBCs through the constrictions, using this method, peripheral blood of BALB/c mice, experimentally infected with the *P. yoelii* 17X-GFP strain, was used. This strain has a tropism for RETs and constitutively expresses GFP throughout the intraerythrocytic developmental cycle, therefore facilitating image acquisition and quantification. These results indicated that iRETs were significantly more deformable than non-infected RETs. This is in agreement with the higher deformability of iRETs reported for *P. vivax*, a human malarial parasite with RET tropism.[19]

A potential limitation of this first device version is the slit size, as it seems that slits in the human spleen could be smaller.[30] However, an *in vivo* imaging of the dynamic passage of *Plasmodium* parasites in the rat sinusal spleen demonstrated that IES remain closed for long periods of time, that around 15% are open in any one particular 5 minutes period, and that the size of those IES vary from wide open (allowing the passage of RBCs without any physical constraint) to scarcely open, where RBCs need to squeeze to reach the venous flow.[30]

3.4. Conclusions.

Many successful microfluidic devices have been developed in the area of OCD technology, but the fabrication of the presented functional biomimetic model represents the first step in the long-term goal of constructing a fully functional 3D model of the human spleen, since no other OCD platform mimicked before the hydrodynamic behavior of the splenon, to the best knowledge of the authors.

The preliminary properties of this microfluidic device reproducing, to some extent, the blood flow patterns and the filtering functions of the human splenon were shown. To validate the use of this platform, several experiments were carried out with different types of blood cells. Initial results suggested that this OCD could be able to reproduce some physiological status, while also being capable to distinguish some RBC populations by means of deformation/mechanical properties.

3.5. References.

1. A.J. Bowdler, The Complete Spleen, Humana Press, 2nd edition, 2002.
2. N. Mohandas and P.G. Gallagher, *Blood*, 2008, **112**, 3939-3948.
3. B.S. Wilkins, *British journal of haematology*, 2002, **117**, 265-274.
4. C.R. Engwerda, L. Beattie and F.H. Amante, *Trends in parasitology*, 2005, **21**, 75-80.
5. H.A. Del Portillo, M. Ferrer, T. Brugat, L. Martin-Jaular, J. Langhorne and M.V. Lacerda, *Cellular microbiology*, 2012, **14**, 343-355.
6. P.A. Buffet, G. Milon, V. Brousse, J.M. Correas, B. Dousset, A. Couvelard, R. Kianmanesh, O. Farges, A. Sauvanet, F. Paye, M.N. Ungeheuer, C. Ottone, H. Khun, L. Fiette, G. Guigon, M. Huerre, O. Mercereau-Puijalon and P.H. David, *Blood*, 2006, **107**, 3745-3752.
7. P.A. Buffet, I. Safeukui, G. Deplaine, V. Brousse, V. Prendki, M. Thellier, G.D. Turner and O. Mercereau-Puijalon, *Blood*, 2011, **117**, 381-392.
8. Q. Guo, S.J. Reiling, P. Rohrbach and H. Ma, *Lab Chip*, 2012, **12**, 1143-1150.
9. J.P. Shelby, J. White, K. Ganesan, P.K. Rathod and D.T. Chiu, *Proceedings of the National Academy of Sciences of the United States of America*, 2003, **100**, 14618-14622.
10. S. Handayani, D.T. Chiu, E. Tjitra, J.S. Kuo, D. Lampah, E. Kenangalem, L. Renia, G. Snounou, R.N. Price, N.M. Anstey and B. Russell, *The Journal of infectious diseases*, 2009, **199**, 445-450.
11. P. Gascoyne, C. Mahidol, M. Ruchirawat, J. Satayavivad, P. Watcharasit and F. Becker, *Lab Chip*, 2002, **2**, 70-75.
12. P.A. Zimmerman, J.M. Thomson, H. Fujioka, W.E. Collins and M. Zborowski, *The American journal of tropical medicine and hygiene*, 2006, **74**, 568-572.
13. H. Bow, I.V. Pivkin, M. Diez-Silva, S.J. Goldfless, M. Dao, J.C. Niles, S. Suresh and J. Han, *Lab Chip*, 2011, **11**, 1065-1073.
14. L.G. Rigat-Brugarolas, A. Elizalde-Torrent, M. Bernabeu, M. de Niz, L. Martin-Jaular, C. Fernandez-Becerra, A. Homs-Corbera, J. Samitier and H.A. del Portillo, *Lab Chip*, 2014, **14**, 1715-1724.
15. I. Safeukui, J.M. Correas, V. Brousse, D. Hirt, G. Deplaine, S. Mule, M. Lesurtel, N. Goasguen, A. Sauvanet, A. Couvelard, S. Kerneis, H. Khun, I. Vigan-Womas, C. Ottone, T.J. Molina, J.M. Treluyer, O. Mercereau-Puijalon, G. Milon, P.H. David and P.A. Buffet, *Blood*, 2008, **112**, 2520-2528.
16. M. Ferrer, L. Martin-Jaular, M. Calvo and H.A. Del Portillo, *Journal of visualized experiments: JoVE*, 2012, DOI: 10.3791/36093609 [pii].
17. J. McGrath, M. Jimenez and H. Bridle, *Lab Chip*, 2014, **14**, 4139-4158.
18. B.M. Cooke, N. Mohandas and R.L. Coppel, *Advances in parasitology*, 2001, **50**, 1-86.
19. R. Suwanarusk, B.M. Cooke, A.M. Dondorp, K. Silamut, J. Sattabongkot, N.J. White and R. Udomsangpetch, *The Journal of infectious diseases*, 2004, **189**, 190-194.
20. M. Antia, T. Herricks and P.K. Rathod, *Cellular microbiology*, 2008, **10**, 1968-1974.

21. J. Stuart and G.B. Nash, *Blood reviews*, 1990, **4**, 141-147.
22. G.B. Nash, E. O'Brien, E.C. Gordon-Smith and J.A. Dormandy, *Blood*, 1989, **74**, 855-861.
23. L.H. Miller, S. Usami and S. Chien, *The Journal of clinical investigation*, 1971, **50**, 1451-1455.
24. A.M. Dondorp, P.A. Kager, J. Vreeken and N.J. White, *Parasitol Today*, 2000, **16**, 228-232.
25. S. Suresh, J. Spatz, J.P. Mills, A. Micoulet, M. Dao, C.T. Lim, M. Beil and T. Seufferlein, *Acta biomaterialia*, 2005, **1**, 15-30.
26. J. Sleep, D. Wilson, R. Simmons and W. Gratzer, *Biophysical journal*, 1999, **77**, 3085-3095.
27. J.P. Mills, M. Diez-Silva, D.J. Quinn, M. Dao, M.J. Lang, K.S. Tan, C.T. Lim, G. Milon, P.H. David, O. Mercereau-Puijalon, S. Bonnefoy and S. Suresh, *Proceedings of the National Academy of Sciences of the United States of America*, 2007, **104**, 9213-9217.
28. T. Herricks, K.B. Seydel, G. Turner, M. Molyneux, R. Heyderman, T. Taylor and P.K. Rathod, *Lab Chip*, 2011, **11**, 2994-3000.
29. J.S. Dudani, D.R. Gossett, H.T. Tse and D. Di Carlo, *Lab Chip*, 2013, **13**, 3728-3734.
30. C. Lavazec, G. Deplaine, I. Safeukui, S. Perrot, G. Milon, O. Mercereau-Puijalon, P.H. David and P. Buffet, *Methods Mol Biol*, 2013, **923**, 291-297.

Chapter 4. Mimicking splenic functions and vascular scenarios *in vitro.*

SUMMARY

Continuing with the previous work, aiming to improve the capabilities and possible limitations of the first splenon-on-a-chip design, a more "organic-like" OCD will be presented.

The device can incorporate a 3D coating, and human spleen cells. This enhanced splenon-on-a-chip, that will be named "version 2", exploits laminar co-flow properties and could be completed with an autonomous closed-loop pumping system. The overall prototype aims to facilitate, in the future, some experimental assays.

As a proof of concept, several physiological scenarios were, to the extent possible, reproduced and studied, such as (i) some blood-tissue interactions, by incorporating an endothelial lining, supported by a collagen network, or (ii) certain aspects of the splenic immune response.

4.1. Introduction.

In the previous chapter it was presented our first OCD platform[1] that could mimic some physical and hydrodynamic properties of the splenon.[1-3] Although this microfluidic device could translate several organ-level scenarios, it failed to introduce part of the cellular microenvironment, limiting its applicability to reproduce, to some extent, some disease/physiological processes.

The spleen, and more concretely its red pulp, has a unique vessel organization. For instance, arterial blood that arrives into the cords "forms an open blood system", lacking from endothelial revetment (the slow-flow compartment).[3,4] The combination of specific anatomical features, and cellular components, located in this particular section, such as (*i*) the reticular meshwork, (*ii*) the IES and (*iii*) highly active macrophages, supports the fact that this organ is a crucial site for the important blood-filtering process in the human body.[2,3,4]

In this chapter it will be detailed an enhanced splenon-on-a-chip platform, named "version 2" (a continuation of the preceding device), taking into account the previous physiological features,[3,4] suggesting that could be used to create an interesting healthy/disease model that could perhaps have, in the future, the potential to prioritize some preclinical animal-based assays.

In this regard, and in the framework of human spleen diseases, the pathological enlargement or obstruction of this organ could be a common response to an infection or a blood disorder, drug induced[5] or not. Thus, cell deformation and retention in the red pulp may be a critical process for diverse inflammatory phenomena. It was reasoned that it could be possible to replicate splenon obstruction events by testing several RBCs populations, and study their biomechanical behavior when interacting with the restrictive microconstrictions simulating the IES.

Moreover, another goal is to demonstrate the practicality of the OCD for some structure-function studies.[6] In this regard, this device could take advantage of laminar co-flow phenomenon (CFP), by using the additional secondary inlet, in order to properly coat or culture, with human splenic cells, the different sections of the novel OCD, when needed. LOC devices using CFP have been used in applications such as *in situ* functionalization,[7] selective treatments of different types of cells[8] or for particle exchanging along fluid streams.[9] However, this strategy of CFP employment could also be useful to differentiate the "cellular architecture" of the device fluidic compartments.

To further complete the platform, an autonomous closed-loop pumping station was introduced, which could be integrated with the OCD. The whole system was designed to fit on a microscope stage culture chamber, as the one presented in Chapter 2.3.3.2.

Several (non-autonomous) closed-loop circuit approaches had been previously developed, such as *ex vivo* perfusion systems[10] or microfluidic culture devices.[11] Our approach, however, permits to represent blood flowing through a splenon-like microfluidic device, at physiological conditions, by means of a micropump activated by a home-made driving stage, thus ensuring portability in a cost-effective manner.

4.2. Splenon-on-a-chip version 2.

An OCD able, to some extent, to (*i*) reproduce the filtering functions of the human splenon and to (*ii*) translate the hydrodynamic properties and physiological events previously described, was engineered; this was possible thanks to the use of human splenic cells and the development of a renewed microfluidic structure. Blood can be pumped through the OCD channels by means of the autonomous pumping system.

4.2.1. Device fabrication.

The methodology is described in detail in Chapter 2.3.2. All works were carried out in the clean room facility of the IBEC.

The fabrication of this second version of the biomimetic platform master consists on a multi-step procedure, designed to obtain three different heights using four different photoresists, *via* using custom photolithographic techniques.

The fabrication steps (principally) require spinning, curing and developing several SU-8s family photoresists over glass slides, for building the slow-flow channel. The fabrication of the master 3D mold is finished by laminating, and developing, Ordyl films, to shape the fast-flow channel.[1] The master is then replicated in PDMS in order to obtain the final device (Figure 4.1).
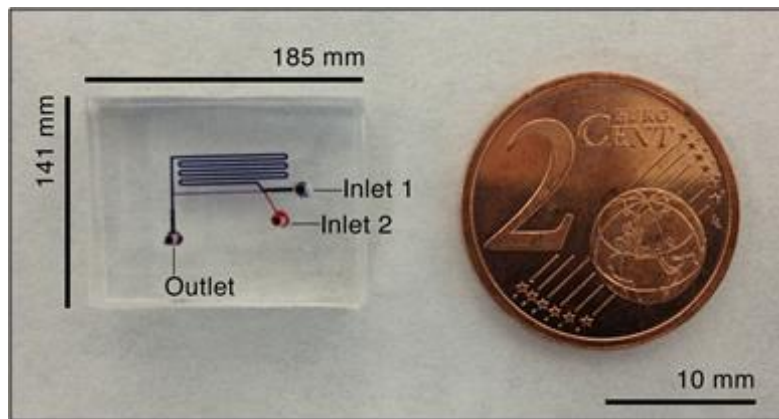
Figure 4.1. Splenon-on-a-chip version 2. *Representation showing a microfluidic platform example, fabricated in PDMS, with some measurements, and a comparison with a 2 cent euro coin. Also it is shown the disposal of the inlets/outlet.*

4.2.2. Autonomous closed-loop system and microfluidic studies.

Using the pumping machinery (a scheme can be found in Figure 4.2A; for further details please see Chapter 2.3.3.9.), the blood circulation patterns were studied, inside the device, in order to verify the similarity to the splenon flow behavior. More specifically, it was desired to translate, to the OCD, close physiological hydrodynamic properties in order to extrapolate the results, to the extent possible, to real scenarios. First, microfluidic analyses confirmed that the architecture of this OCD mimicked the two-compartment splenic circulation (Figure 4.2B). In addition, using this system, it could be possible to infuse similar physiologically-related slow-flow channel velocities, with a pulsatile flow.
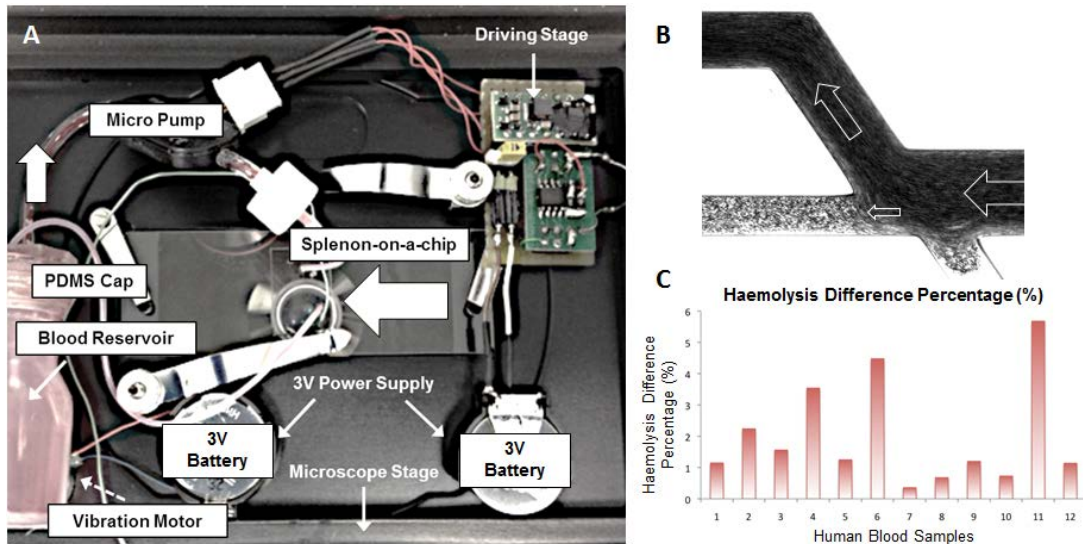
Figure 4.2. Autonomous pumping station and splenon-on-a-chip version 2 hydrodynamic studies.
(A) Microfluidic device with an autonomous closed-loop system. (B) Microfluidic analyses confirmed that the device, when infusing human blood, mimicked the two-compartment splenon microcirculation pattern. In this case, the secondary inlet is disabled so, as can be observed, blood does not flow in that channel. (C) Haemolysis assays performed in healthy human blood samples.

In order to characterize its performance, and calculate possible lysis of the RBC samples during its passage through the micropump or the entire system, an assay to calculate cell breakage was performed, using spectrophotometry as the analysis method (for more information please see Chapter 2.2.3.7.). After calculating the absorbance (at 540nm) of the different tested blood samples, results suggested that there was no relevant lysis throughout the distinct trials (Figure 4.2C). In these tests, a lysis difference mean value of 2% was estimated when just pumping the samples through the closed-loop system and a mean value of 3.36% when using, also, an OCD platform.

4.2.3. Constriction device for calculating slits measurements.

One of the new features of the splenon-on-a-chip version 2 platform is that the blood filtering properties could be enhanced due to the multilayered structure of its slow-flow microchannel. To accomplish this task, the dimensions of those constrictions simulating the splenon IES were re-calculated empirically, in order to better differentiate some distinct RBCs populations depending on their deformability or mechanical properties, to the extent possible.

Based on the methodology used previously to calculate RBCs deformability in the slits (detailed information can be found in Chapter 2.2.3.5.-6.), a simple microfluidic device was designed and fabricated for this commitment. This constriction device, shown in Figure 4.3A, was fabricated using SU-8s photoresists. After replicating with PDMS, different trials were performed using the devices with human blood samples, studying the elongation of the RBCs when passing through the different slits (Figure 4.3B, upper panel. RBC shape recovery in the lower panel, suggesting that this structure should not affect, in principle, cell integrity). The deformation measurements, calculated in these trials, can be seen in the graph of Figure 4.3C.

Because the splenon-on-a-chip is going to be operated during long lapses of time, a height of ~4.8 μm was finally established in the slits, in order to prevent, to the extent possible, clogging of healthy RBCs and/or undesired haemolysis.
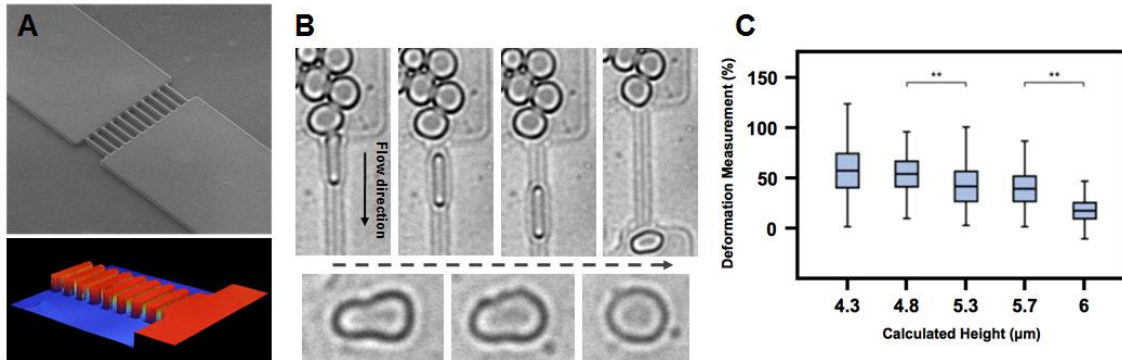
Figure 4.3. Constriction device operation and calculation of height dimensions. (A) Constriction device images using SEM (upper) and an interferometer (lower). (B) A RBC passing through a slit of the constriction device. Also it is shown the shape recovery of a healthy RBC. (C) Deformability tests (** represents p<0.001, n=100). Data was analyzed using Mann-Whitney U test.

As detailed previously, there are several geometric factors that may influence RBC deformability in flow.[12] In the presented case, as the dimension of the constrictions gets lower, greater is the deformation that the RBCs have to achieve in order to pass through the simulated IES, as the efficient diameter of the slits significantly reduces. This also increases the R_H and consequently the pressure applied to the blood cells, and its velocity. Reducing the height under the threshold of RBCs rheological possibilities could perhaps induce (*i*) a cell lysis, due to mechanical stress, and/or the (*ii*) retention of healthy cells.

Several authors have reviewed different techniques for the study of RBCs deformability. In this regard, haemorheological methods that individually analyze RBCs have been widely used in the field of microfluidics.[12] One of the first works in this subject was presented by J.P. Shelby *et al.*[13] In its microfluidic single-cell capillary device, microchannels with different widths were tested in the framework of malaria disease evaluating, for instance, the capillary blockage of *Plasmodium falciparum* (*P. falciparum)* iRBCs. Similar microfluidic approach was later used by T. Herricks *et al.*,[14] that studied the minimum cylindrical diameter (MCD) of both RBCs and iRBCs in a device with multiple channel constrictions. The conclusion was that *P. falciparum* iRBCs showed higher MCD.[14] For its side, in the works of P. Preira and colleagues, or the one presented by J. Picot *et al.*, microfluidic gradual filter devices were developed.[15,16] In the last mentioned, the fabrication of 2 to 5 μm-wide microchannels was achieved in order to mimic the splenic red pulp IES; in this structure, trophozoite stage *P. falciparum* iRBCs presented a higher entrapment in the narrower constrictions in comparison with ring stage iRBCs.[16] This gradual filter approach was also used in the device proposed by J.P. Brody *et al.* to study the RBCs elastic properties.[17]

Other works, using funnel-like microconstrictions, characterized the deformability of RBCs and iRBCs as an interesting tools for malaria detection, and could even act as "microcytometers", to mechanically characterize iRBCs in blood samples.[18,19] The approach presented here, however, was useful to estimate one optimal height to draw a distinction, to the extent possible, between healthy and non-healthy RBCs, in the proposed system, as a proof of concept.

4.2.4. Characterization of fluid dynamics for co-flow mechanism usage.

The architecture of the device, and the input flow rates used, ensures low *Re* in the platform. As a consequence of that, when utilizing the laminar co-flow mechanism (that is, to infuse samples through both inlets at the same time), transport between both input streams occurs *via* diffusion. Thus, under these microscale laminar flow conditions, several liquid streams are able to interact with each other, while flowing, without mixing before the branching point.[7,8]

The fluid dynamics of the OCD was firstly characterized using COMSOL Multiphysics software, based on the Navier-Stokes equation, and experimentally by modifying the input flows of both inlets, in order to properly use laminar co-flow when needed.

In this regard, the inlets flow rate values represents a parameter of foremost importance.[7,8] For instance, the frontier between both fluids can be displaced, when needed, just by controlling the flow rate ratio of inlets 1 and 2 (Q1 *versus* Q2, respectively), and employ the laminar CFP for hydrodynamic focusing.[7,8] It is important to highlight that, even at low tested flow rates, diffusion does not occur before the branching point, since the disposal of the secondary inlet 2 has been determined to face this drawback (therefore avoiding problems due to mixing phenomenon).[7,8]
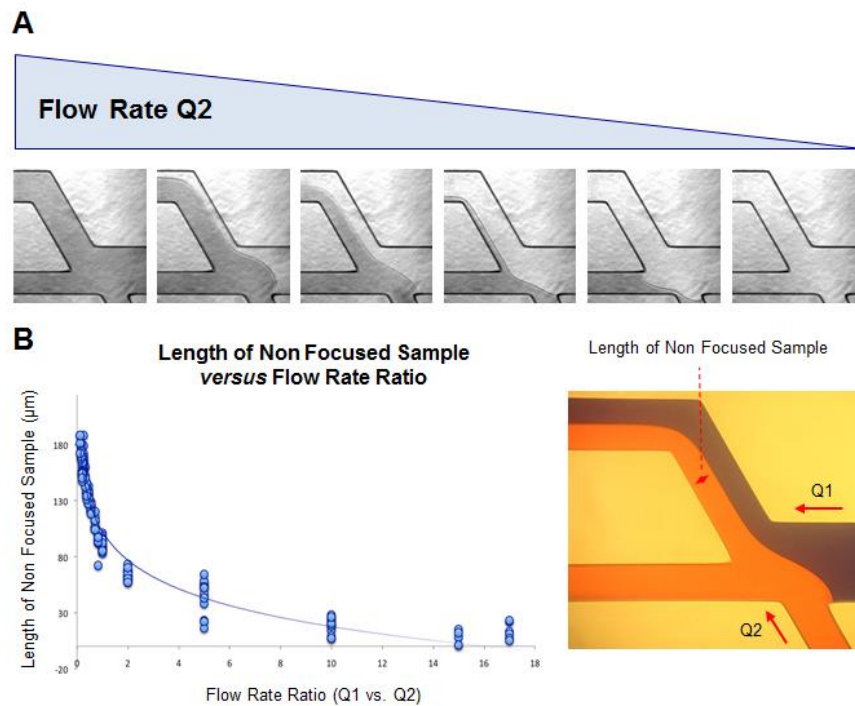
Figure 4.4. Characterization of fluid dynamics using the co-flow mechanism. *(A) Different samples entering through both inlets at different flow rate ratios. (B) Graph plotting the length of non-focused sample in the slow-flow channel versus different flow rate ratios (Q1 versus Q2), infusing collagen and fibronectin in different microdevices.*

For the characterization of fluid dynamics, the flow rate of the principal inlet (inlet 1) was fixed, using syringe pumps, whereas a progressive scanning of values was given to the secondary inlet, in order to accordingly define the most suitable ratio to control channel occupation (Figure 4.4A).[8]

After preliminary trials, a characterization using collagen and fibronectin samples was realized. This helped to direct each one to the respective channels in the coating process (Figure 4.4B). A clear difference between the samples could be visualized by, for instance, optical inspection, and the location of the interface position was, therefore, possible to follow.

From the data obtained and presented in Figure 4.4B a ratio value of ~16 was found that could represent one optimal fluid separation scenario (slow- *versus* fast-flow channel). A ratio value of 1 could be fixed in order to study the effect of a drug in a treated sample *versus* the control one, in the fast channel (using this ratio, this compartment may be "equally" divided by two samples).

4.2.5. 3D protein coating on-chip.

Despite the many advantages that PDMS offers as a molding material,[1,20,21] the number of cell types that may be cultured on top of it could remain limited. Untreated bare PDMS is, normally, not fully suitable for a straightforward cell culture. Coating this polymer with proteins capable of attaching to PDMS' surface was seen, after studies, as a possible solution to this issue (please see Chapter 2.3.3.5. for more information).

In this framework, several protein coatings were deeply tested. In order to better accommodate human macrophages in the slow-flow compartment, a fibronectin coating was seen that could offer an adequate scenario (some trials in Figure 4.5A).
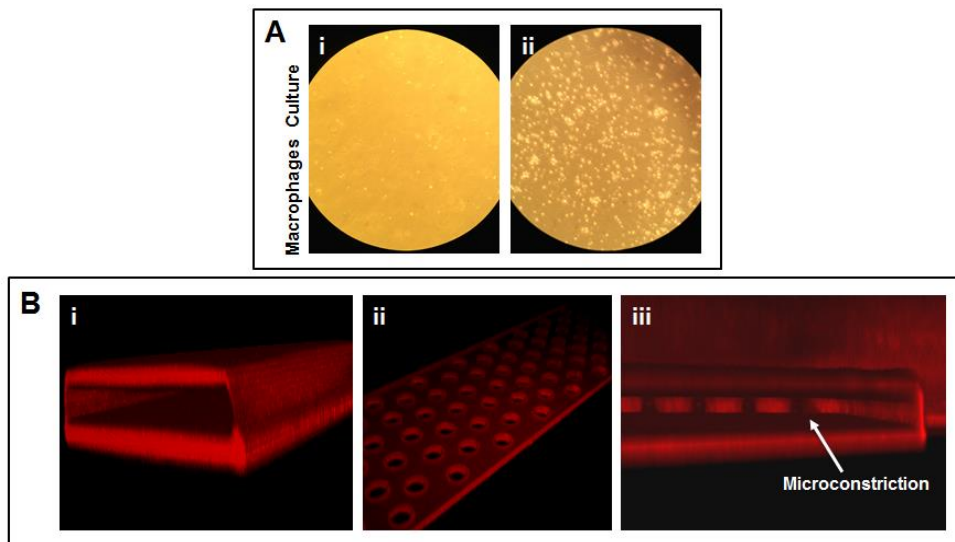
Figure 4.5. Cell culture trials and 3D coating verification. *(A) Macrophages culture trials (i) with bare PDMS and with (ii) fibronectin. (B) Tests done with several protocols made it possible to finally obtain a 3D protein coating in the device structure. It is shown (i) the fast-flow channel, (ii) the pillar matrix constriction section and finally (iii) the IES section connecting to the fast-flow channel (arrow pointing a microconstriction).*

On its side, to deal with a correct culture of hSECs in the fast-flow microchannel, and to better recreate the blood vessel activity, a solution consisting on collagen type I was selected to be introduced into the microfluidic system. It was important to separate the coatings in the different channels in order to prevent blockage of the constrictions simulating the IES, due to the high collagen density.

To make sure that it could be possible to obtain a 3D coating, trials were made to test the final coating protocol, using Streptavidin (Texas-red conjugated) protein. As could be observed in the test of Figure 4.5B, the coverage and homogeneity of the protein deposition was successful in all the channels. Thus, proteins could perhaps be physically adsorbed to the internal walls of the microchannels, and therefore could provide a "natural environment" for cells, both in the glass substrate and in the PDMS surface.

4.2.6. Splenon cellular environment.

After the verification of the coating protocol, the next step entailed culturing the human spleen cells inside the microfluidic device. It should be noted that culturing cells (more challenging in human types) within microchannels it is not something straightforward.

The ultimate aim was to mimic, to some extent, part of the cellular environment of the different sections of the human splenon,[3,4] at close physiological conditions (as shown in the scheme of Figure 4.6A).
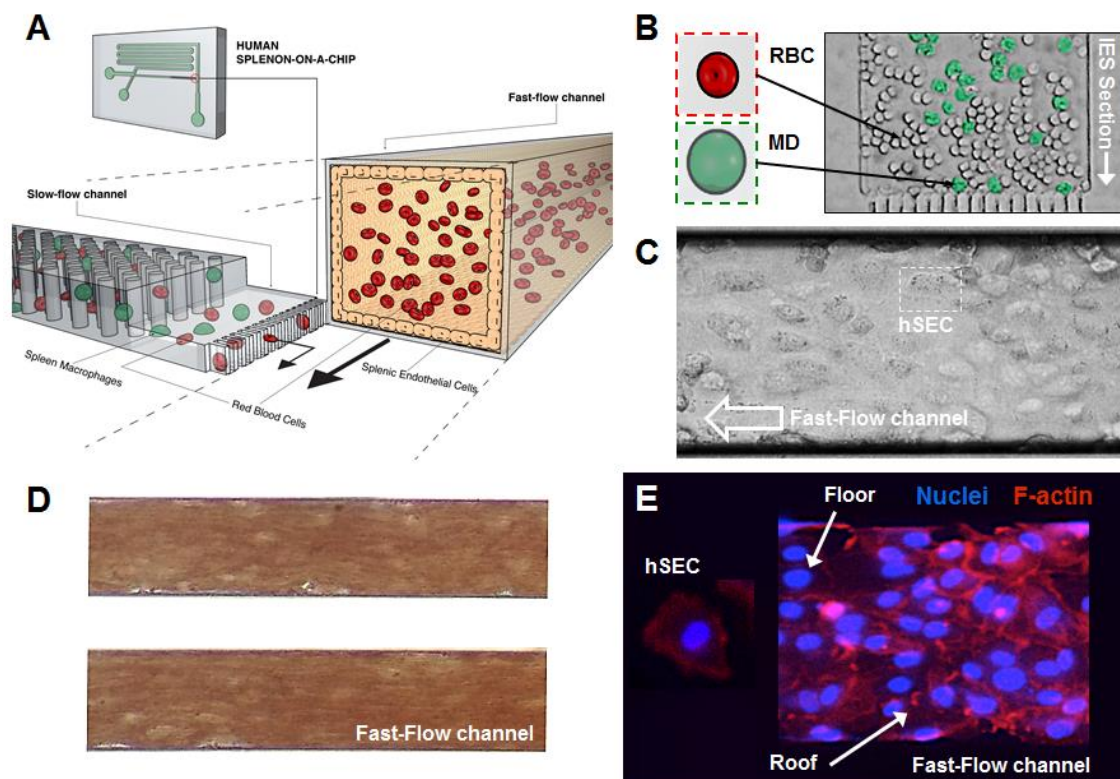
***Figure 4.6. Cell culturing in the splenon-on-a-chip version 2 device**. (A) Scheme of the biomimetic platform. (B) Some macrophages cultured in the slow-flow channel represented in fake green. RBCs are flowing aside. (C) hSECs cultured in the fast-flow channel. (D) A colour-photo of blood flowing within a hSECs network. (E) Immunostaining to show a 3D-hSECs structure in the fast-flow channel.*

It was possible to culture human macrophages along the slow-flow microchannel (Figure 4.6B). However, since these cells tended to adhere and stay immobile in the surface, after few hours, finally it was preferably not to culture them in order to be able to observe possible phagocytosis events. As it will be shown later, flowing macrophages could likely incline to remain in the slow-flow compartment, due to the constrictions located in that section.

For its side, hSECs culture was achieved in the fast-flow channel (Figure 4.6C). No appreciable disengagement of those cells was observed during experimentation when flowing blood through the device (Figure 4.6D shows an example of RBCs flowing inside a "hSECs cover"). In order to evaluate a possible hSECs 3D cell structure, an immunostaining on-chip was performed (please see Chapter 2.3.3.3. for more information), and suggested that could perhaps be possible, with a correct coating and experimental conditions, to obtain a "vein-like architecture" (Figure 4.6E).

In this regard, achieving a correct coating is indispensable, and essential, to obtain a viable cell culture inside the device. Likewise, maintaining adequate experimental conditions (such as gas exchange and/or close physiological temperature, to name but a few) is also crucial for cells to grow in the channels. Appearance of bubbles inside the OCD could also represent a menace for cell survival.

4.3. Reproducing splenic functions using the splenon-on-a-chip version 2.

4.3.1. Red pulp immune response.

RBCs (with a lifespan of ~120 days) constantly interact with macrophages in the blood stream, particularly in the liver and the spleen, situation of paramount importance for the maintenance of RBCs homeostasis.[22]

However, the process in which macrophages in the splenic red pulp are able to "sense" different cells and removing, for instance, aged-RBCs, is even nowadays not fully well understood.[22] It is known that unhealthy old RBCs, parasitized or affected by any hereditary disease that modifies their structure, could be taken away by splenic macrophages, especially in the open circulation (as detailed in Chapter 1.3.).[22]

In this regard, in order to evaluate if the platform could be capable of mimicking, to some extent, this "immune" response, some EP assays were performed. So, flow cytometry techniques were used to test the possible ability to "perceive" differences between several samples (please see Chapter 2.3.3.11. for more details). Also, "residential" macrophages were inspected visually, to asses if there was any mechanism regarding RBCs removal in the slow-flow compartment.

On this subject, in Figure 4.7A can be observed a macrophage, inside the splenon-on-a-chip (in the IES limit), phagocytizing an aged-RBC that was not able to cross to the fast-flow channel. Results suggest that immune cells could perhaps be able to detect and remove from circulation non-healthy RBCs, as they seem to do in a real human system.[2,22] Also, trials with (fluorescent) microbeads were performed, and phagocytosis of the spheres was intuited (Figure 4.7B).
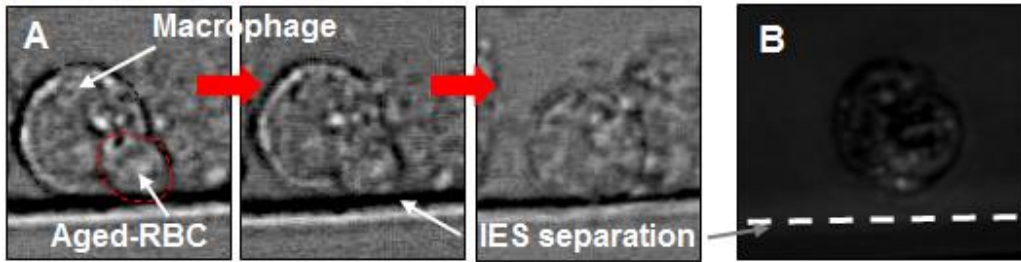
Figure 4.7. Macrophages interaction with cells and particles. *(A) Sequence of images showing a macrophage, in the limit between the IES and pillar matrix sections, phagocytizing a RBC. (B) A macrophage with fluorescent microbeads.*

Flow cytometry trials could suggest that the tested macrophages could be able, presumably, to phagocytize RBCs, to a greater or lesser extent, depending on the storage time of these RBCs. Representative flow cytometry plots are shown in Figure 4.8. Anyway, as a proof of concept, the results suggest that the macrophages were able to initiate EP processes. However, further tests should be done in order to fully understand the macrophages interaction with (different) RBCs.

In these assays, macrophages in the presence of "young" RBCs displayed a mean EP of 27.7% (an example can be seen in Figure 4.8A). When the blood specimens were >10 weeks aged-samples, an enhanced positive staining could be observed, up to an EP of 83% (Figure 4.8B). In both cases, R1 or R2 regions of the set data defined two distinct populations of negatively or positively stained macrophages, respectively. Additionally, trials with fluorescent microbeads, with a dimension of roughly ~1 µm, were also performed. As could be seen in the example of Figure 4.8C, in this case the EP was of ~99%, indicating that the tested macrophages seemed to be very active against those small elements.
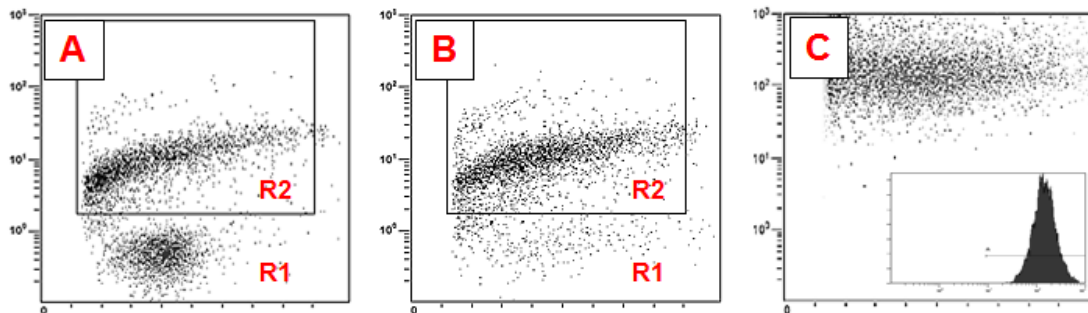
Figure 4.8. Erythrophagocytosis assays. *Proof of concept trials. (A) EP of "young" RBCs populations. (B) EP of "old" RBCs populations. In this case, practically all the macrophages are displayed in region R2, suggesting high EP. (C) EP of fluorescent microbeads; a histogram is also shown (in the lower right corner).*

4.3.2. Macrophage interaction with the slow-flow channel.

When flowing macrophages through the OCD (with the closed-loop system), it could be possible to observe that these cells tended to stay, after infusing the sample during ~1 hour, on the slow-flow channel (an example is shown in Figure 4.9A), whereas in the fast-flow channel it could be seen them flowing without any impediment (as expected). This fact could seem to be manifestly related to the architecture imposed to the slow-flow microchannel.

Macrophages could be retained either because of the IES, the height change in the IES section, or due to the pillars (Figures 4.9A,B), so they could concentrate in the desired "locations".[2,3,4,22]
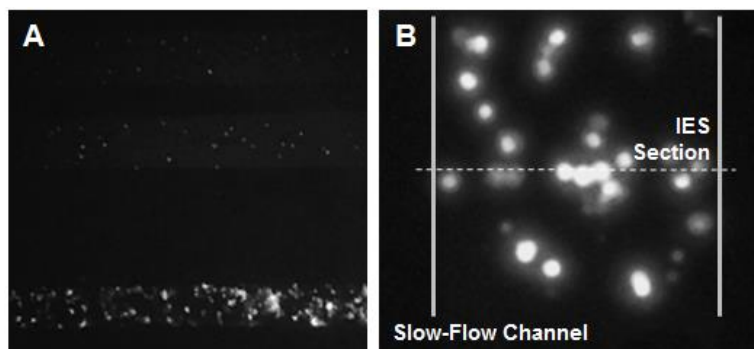
Figure 4.9. Macrophages in the slow-flow channel. (A) Macrophages flowing inside the splenon-on-a-chip platform could be retained in the slow-flow constriction section. (B) Those macrophages could be stopped in the IES section.

As a proof of concept, these results could suggest that, just by flowing blood samples inwardly through this OCD, the macrophages could be likely "housed" in the compartment arranged for their purpose. This fact could indicate that the OCD device could be able to reproduce, to some extent, some physiological conditions, thanks to its intrinsic microfluidic structure.

A preliminary hypothesis could suggest that the macrophages could also be located in the open system of a human red pulp, apart from possible (bio)chemical or physical signals/mechanisms, due to the structure of the IES and the reticular meshwork, therefore facilitating their housing in that specific area.[2,3,4,22]

4.3.3. Studying nanoparticles distribution inside the splenon-on-a-chip.

The analysis and/or study of nanoparticles (bio)hazard could be probably, nowadays, one of the major research preoccupations in the field of toxicology.[28]

Several types of inorganic nanoparticles, with different features, are being developed for a wide variety of different applications[28] (ranging from imaging for diagnostic purposes to photothermal therapy).[23-28]

After their *in vivo* administration, the circulatory system could distribute them to the organs, with absence of apparent control. Thus, a precise characterization of their accumulation in preclinical models could be interesting before studies in humans.[28]

In the framework of the spleen, due to having a reticuloendothelial system and containing a vast number of macrophages, nanoparticles could be accumulated in its structure.[28] For instance, H.L. Herd *et al.* described that macrophages may have a key role in nanoparticles processing.[29] They appreciated that mice spleens could show a slight rise in the number of inflammatory cells, due to the residence of those elements in the organ.[29]

They also observed that, in the particular case of the spleen (and also in the liver), there was an uptake of nanoparticles by macrophages.[29] For their part, X.D. Zhang and colleagues[30] showed that, for example, 30 nm gold nanoparticles accumulated in mice spleens.[28,30] Besides, other studies stated that there was a larger detection of a wide diameter range of gold nanoparticles in a spleen in comparison with some other organs (in animal models).[28,31,32]

However, studying this kind of phenomena in the human spleen is something challenging. For that matter, spherical gold nanoparticles (red-coloured), with a diameter lower than 90 nm, were produced, using the Turkevich *et al.* method (briefly, entailing a reaction of chloroauric acid and a sodium citrate solution, to finally form the tested nanospheres).[30,33] The aim was to test those nanoparticles inside the splenon-on-a-chip, as a preliminary proof of concept assay.

When injecting the nanoparticles on their own through the device, no accumulation was founded throughout the platform (as expected, since the dimensions of the constrictions are much larger than those of the gold spheres).

However, when performing trials with also blood samples and macrophages, different situations took place. Analyzing the slow channel, it could be possible to find certain agglomerations in the zone mimicking the reticular meshwork, as can be observed in Figure 4.10A, pointed with white arrows. In this figure's right panel, an example of a device with cell debris can be seen, and gold nanoparticles were stacked in their contour, something that could happen in a reticular structure as the one existing in the human red pulp, since it is where the velocity is supposed to be lower, and the labyrinthine architecture could perhaps facilitate nanoparticle retention.

Also, it could be possible to intuit a macrophages phagocytosis activity (in the slow-flow channel too), as could be observed in Figure 4.10B.
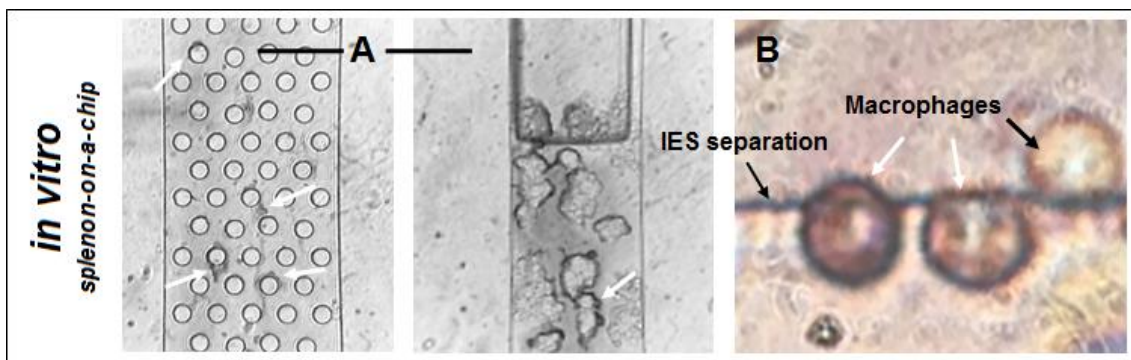
Figure 4.10. Nanoparticles accumulation in the slow-flow channel of the splenon-on-a-chip. *(A) Gold nanoparticles retention in the slow-flow channel. (B) Pointed with white arrows: human macrophages that could have phagocytized gold nanoparticles; pointed with black arrow: a macrophage that does not seem to have phagocytized gold nanoparticles (differences in terms of colour).*

4.3.4. Blood-splenic endothelium interactions.

The microvasculature acts as a mediator in the interaction between blood and the environment, playing an important role in several cardiovascular diseases.[34]

In this framework, this splenon-on-a-chip could also provide a dynamic platform for the study of several vascular structures and functions. The intention was to have the possibility to present either *(i)* a "pro-thrombotic state" of the fast-flow microchannel, thanks to the collagen coating, simulating, hence, an inflammatory scenario,[35] or a *(ii)* "non-thrombotic" one, when cultured with hSECs. This versatility in configurations could lead to study several haematological situations.

So, in this context, several tests could be done in the framework of platelet-oriented studies. For instance, in a collagen-coated microchannel, with no hSECs culture (scheme in Figure 4.11A),[35] platelets (a component of blood whose one main function is to stop the bleeding process), when injected to the system, could be able to adhere to the device channel walls; in a lapse of ~10 minutes, platelets could form a large aggregate, covering the surface (as shown in the example of Figure 4.11B). These results suggest that could be possible to use the device to study, to the extent possible, in the future, some mechanisms related to platelet aggregation phenomena.[34]
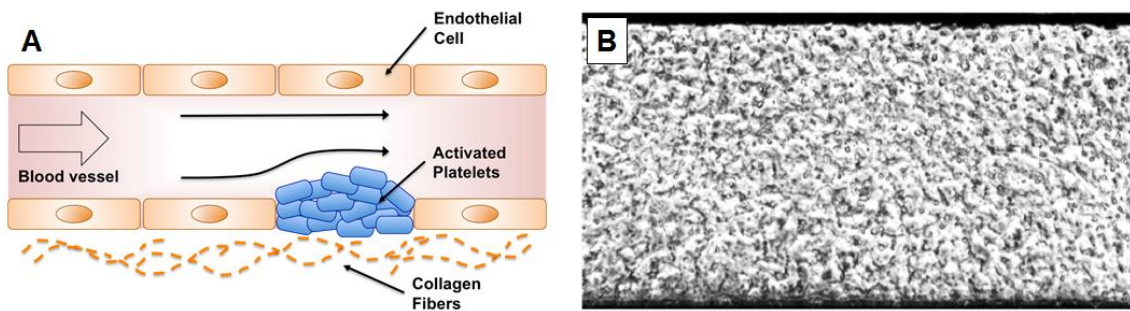
Figure 4.11. Platelet adhesion in the collagen-coated channel of the splenon-on-a-chip. *(A) Scheme of a pro-thrombotic state, leading to platelet aggregation (in physiological conditions).[35] (Figure adapted from Reference 35). (B) In a collagen-coated channel, platelets infused to the system could adhere to the surface.*

Also, it was possible, when flowing human RBCs inside the device, to visualize, in real time, *in vitro* thrombus formation (the final consequence of blood coagulation, as shown in Figure 4.12A example).
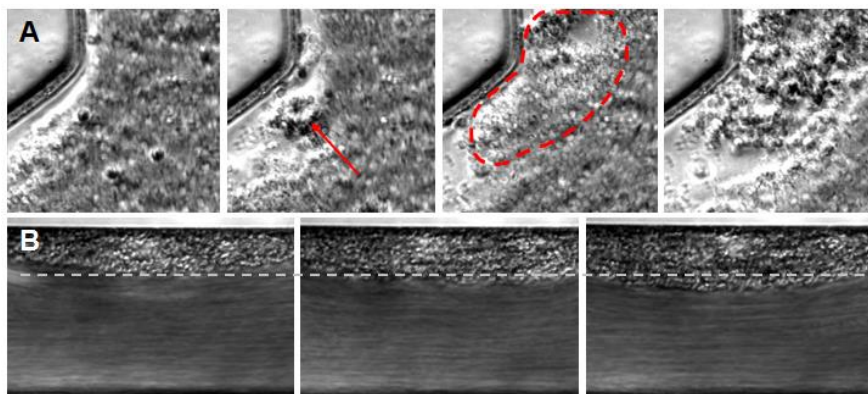
Figure 4.12. In vitro thrombus formation inside the splenon-on-a-chip. *(A) Sequence of images presenting a thrombus forming inside the OCD. (B) Thrombus increasing its volume, with the passage of time.*

The possibility to replicate, to some extent, this pathological scenario could be of great interest for the biotechnological and/or pharmaceutical industry. Besides, it could be possible to follow the growth of a thrombus, with the passage of time, in the device microchannels, working at physiological conditions (Figure 4.12B).

4.3.5. Laminar co-flow usability for future testing.

Taking advantage of laminar CFP, using the additional inlet 2, a drug-treated sample could flow simultaneously with a control sample in the same channel, thus helping to better appreciate the mechanism of action of the chemical(s). To test the efficiency of this mechanism, first trials were made using Trypsin/EDTA, and cellular medium. In Figure 4.13 it is shown cell portion substrate release of a cultured hSEC by using this product, when flowing over part of its section.[36]
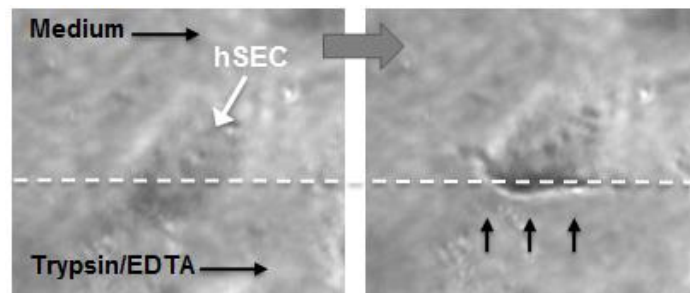
Figure 4.13. Detachment of a hSEC after treatment with Trypsin/EDTA. As a proof of concept, when infusing Trypsin/EDTA through one inlet, and cellular medium through the other, the part of a cell subjected to the chemical showed a detachment of the surface, whereas the other part was maintained adhered to the microchannel.

Having made these preliminary trials, verifying the utility of the co-flow mechanism, experiments with human blood were then executed, at physiological conditions. Hence, if infusing two whole blood samples, with and without Heparin Sodium (HpS), through the different OCD inlets (as an example), opposite results could befall inside the platform (proof of concept in Figure 4.14). To highlight, the HpS solution may be used to treat and/or prevent the formation of thrombus in the circulatory system.
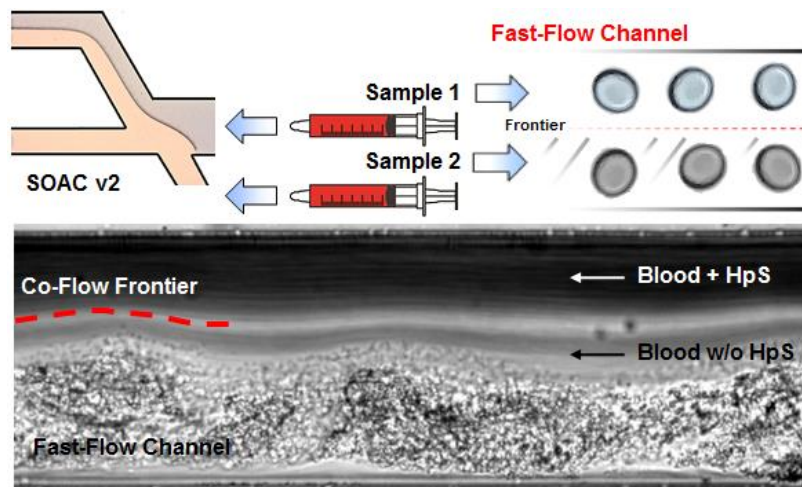
Figure 4.14. Co-flow mechanism usage for future testing trials (proof of concept). Assay made with human blood, were it could be appreciated how the sample not treated with HpS formed a clot in the fast-flow channel.

In this experimental assay (Figure 4.14), the drug-treated sample did not seem to adhere to the collagen-coated surface. For its side, the sample with no HpS solution formed blood clots in the fast-flow compartment, and substantial differences can be straightforward observed in the same channel. These preliminary results suggest that this OCD could, perhaps, be used to deepen in the study of some vascular diseases, such as portal vein thrombosis (that could lead to a spleen volume augmentation),[37] and could also become, in the future, an interesting screening device, partly thanks to the possibility that offers to employ laminar CFP.

4.3.6. Mimicking splenon obstruction conditions on-a-chip.

As a pathological model, the "sensitivity" of this version of the splenon-on-a-chip (using the new architecture, with the re-calculated slit dimensions) was examined using several RBCs samples treated with small amounts (<0.6%) of glutaraldehyde (GTA), a fixative agent that ("artificially") reduces this cell deformability.[38,39] When flowing GTA-RBCs through the device (Figure 4.15A), they were not able to pass through the IES-like constrictions, so, with the passage of time, the clogged slow-flow channel mimicked an "obstructive scenario" (Figure 4.15B). An obstruction of the slow-flow channel will induce all the flow to go to the fast-flow compartment (Figure 4.15C).

So, as demonstrated, it could be possible to see, using this device, the both sides of the coin: RBCs that are able to pass "easily" through the slits, and GTA-RBCs that, due to their increased rigidity, are stopped in the slow-flow channel. Therefore, these preliminary results suggest that there could be other intermediate scenarios, where these cells could have difficulties to traverse the constrictions. Hence, different trials with, for instance, aged-RBCs and blood samples in the presence of Chloroquine (CQ), were tested as a proof of concept.
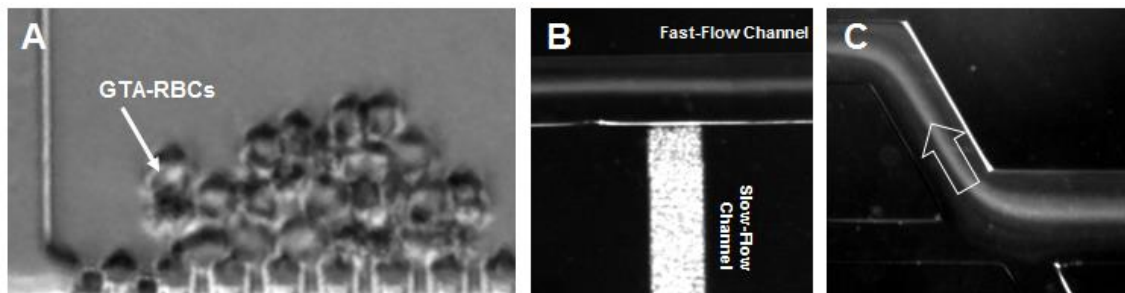
Figure 4.15. Obstruction model using GTA-RBCs. *(A) GTA-RBCs unable to pass through the microconstrictions, inducing an (B) obstruction in the slow-flow channel. (C) An obstruction of the slow-flow channel will induce the flow to go to the fast-flow compartment.*

Using this new architecture, a "splenomegaly-approach" (Figure 4.16A) could be addressed. By counting the number of RBCs in the IES section (Figure 4.16B), at different time lapses and with different cell populations (for further information about the RBCs detection protocol, please see Chapter 2.3.3.4.), a graph may be plotted (example in Figure 4.16B), representing the maximum RBC density (R_D) *versus* Time. If the blood sample is not very "healthy", the value of R_D is going to be, in principle, higher than when flowing fresh RBCs. When working with some aged-RBCs samples, it could be possible to observe an obstructive scenario (as can be seen in the example of Figure 4.16C), with the passage of time.
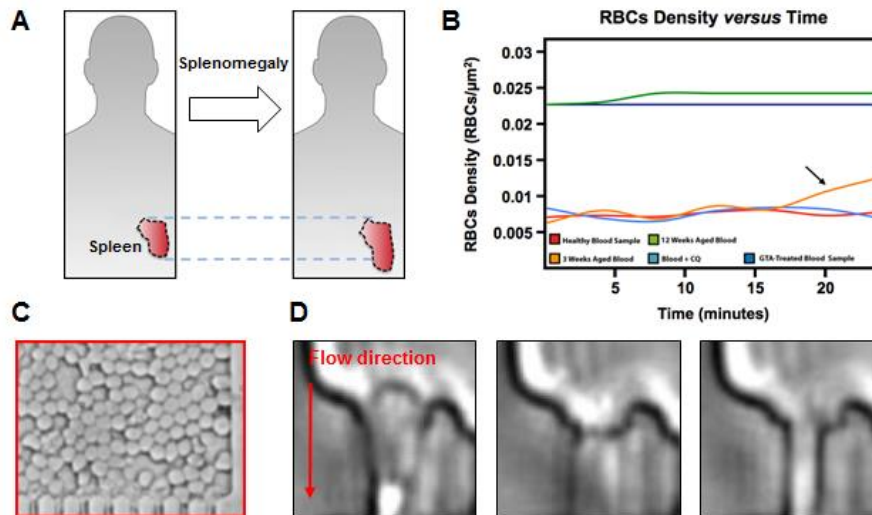
Figure 4.16. Trials with different RBCs populations to study cell retention in the IES section. *(A) Illustration of a splenomegaly, where the spleen is enlarged in the pathological situation, represented in the right image. (Figure adapted from ADAM, Inc.). (B) Graph showing RBCs density versus Time, once reached the equilibrium. (C) Example of an aged-blood sample flowing through a device. (D) A sequence where it can be seen a non-fresh RBC having difficulties to pass through a constriction.*

An "extreme" result could be represented by the 12 weeks aged-sample example, where RBCs were rigid enough to collapse the microconstrictions. In the case of a 3 weeks aged-sample, an abnormal accumulation of RBCs in the slow-flow compartment could be perceived (pointed with a black arrow, Figure 4.16B), but without clogging the OCD (in Figure 4.16D can be seen a non-fresh RBC having difficulties to pass through a constriction).

In this framework, one of the additional objectives was to try to replicate, to the extent possible, *in vivo* splenic filtering results using the splenon-on-a-chip. So, the idea was to assess if it could be possible to evaluate drug collateral toxic effects in the reference of splenic diseases. One of the drugs tested was CQ, a 4-aminoquinoline utilized in several autoimmune diseases. Also, it is used for the treatment of malaria.[40] In order to evaluate if this drug could provoke a significant alteration to not only the iRBCs, but also to RBCs stiffness, some blood specimens were treated with that drug at clinical relevant dosage.[40] As could be observed in Figure 4.16B no statistically significant differences in terms of the R_D could be noticed, a preliminary result that, as a proof of concept, could perhaps be in agreement with S. Huang *et al.*[40] animal experimental result (that did not observe significant changes in the size of mice spleen after CQ treatment).[40]

In some timeframes could be appreciated an oscillatory behaviour of the R_D in the IES section. This fact could correlate with a fluctuation in the fluidic pressure (and R_H) in the channel, due to a congestion-decongestion process in the constrictions. When several slits are blocked by cells, a difference in pressure could likely take place, until they will be dislodged from the constriction, unless they are too rigid to pass through.

Staying on this subject, when the slow-flow channel gets obstructed, to some extent, as can be observed in the GTA-model (in Figure 4.15C), the flow will direct to the fast-flow compartment, increasing, therefore, the hydraulic pressure in that channel. This result may perhaps reproduce what could happen, for example, in a portal hypertension scenario, that could cause the splenic enlargement.[37] In situations of occlusions of the organ vascular supply, such as those mimicked in the OCD, subsequent tissue necrosis could take place.

4.3.7. Microjets testing on the splenon-on-a-chip.

In collaboration with Prof. Samuel Sanchez's Smart Nano-Bio-Devices Lab (IBEC, Barcelona), several developed autonomous microjets[41,42] were evaluated inside this splenon-on-a-chip. The aim was to test the applicability of this innovative technology to reduce blood clots in an efficient way (for example, by carrying, in the future, drug(s) in its surface).[42] As demonstrated, using this OCD it is feasible to "generate" thrombus *in vitro*, so the device could represent an ideal testing ground for that matter. Also, it could be interesting to study how those microjets might behave in a complex environment, such as the proposed OCD, at different experimental conditions.[42]
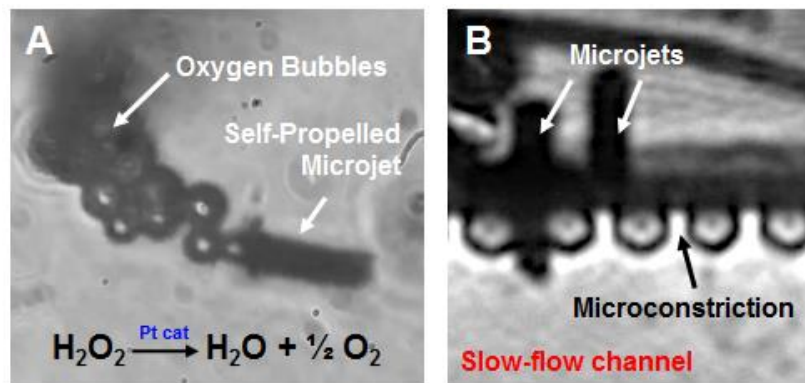
Figure 4.17. Usage of microjets inside the splenon-on-a-chip. *(A) An image of a self-propelled microjet and the oxygen bubble trail "used" to travel along the media.[42] (B) Microjets in the microconstrictions of the splenon-on-a-chip. The tested microjets are courtesy of Prof. Samuel Sanchez's Lab.*

The tested microjets controlled motion is inherently linked to their tubular structure, that consists on multimaterial rolled-up microtubes, but being the inner layer a platinum (Pt) catalyst. This last structural particularity propitiates, and initiates, the breakdown of the hydrogen peroxide (H_2O_2) "fuel", allowing them to travel along the liquid media (Figure 4.17A). When these microjets are immersed in a H_2O_2 solution, as it enters inside the tube, it is decomposed into water and also oxygen, which is accumulated into the inner hollow chamber, propelling the microjet by a stream of bubbles.[41,42] Figure 4.17A shows a microjet, with a dimension of scarcely ~1.5 μm width and around 10 μm long, using the mentioned principle.

Due to the ferro-magnetic layer covering the outer part of their structure, the dynamics of these microjets may be controlled by means of a magnetic field, making viable to direct them towards a nearby location (to some extent).[41,42]

Using this last characteristic, it was possible to help direct the microjets to specific sites of the splenon-on-a-chip (as a proof of concept). In the case presented in Figure 4.17B, it can be seen several microjets trying to enter, and pass through, the constrictions. These preliminary trials suggest that the splenon-on-a-chip could provide an interesting architecture for testing those newfangled devices: for instance, if a microjet is not sufficiently small, it could get blocked in the constrictions, suggesting that in a human spleen could perhaps occur a similar scenario. Tests with more biocompatible versions of these microjets are foreseen.

4.4. Discussion.

In this chapter, an enhanced version of the splenon-on-a-chip prototype was presented. As new features, this platform incorporates, firstly, a secondary inlet 2, devised to take advantage of laminar CFP; also, in order to enhance the filtering properties of the OCD, a multilayered slow-flow channel was fabricated. The new height of the constrictions was calculated experimentally, aiming to better "differentiate" some distinct RBCs populations, depending on their mechanical properties, to the extent possible.

For that matter, it was possible to reproduce, to the extent possible, obstruction/splenomegaly-like scenarios. As a pathological model, GTA-RBCs were tested, and the results suggested the fact that the designed slits could be able to filter some cells lacking deformability. In this regard, some flowing aged-RBCs, or rigid cells, were likely retained in the slow-flow channel, if unable to pass through the constrictions.

One of the principal aims of this study was, to the extent possible, to mimic, additionally, part of the most representative cellular environment of the splenon.[2,3,5,37] For this commitment, different human splenic cells were tested with this OCD version.

To evaluate, and study, some blood-endothelium interactions, a collagen solution was coated in the channels, offering the possibility, to some extent, to perform platelet-adhesion testing. In this regard, and taking advantage of laminar CFP, it was possible to test HpS.

Further, the splenic immune response was mimicked to the extent possible. In that sense, it was feasible, as a proof of concept, using human macrophages, to observe, and characterize, some EP events.

Finally, the platform could be completed with an autonomous closed-loop pumping system, that permits to incorporate the entire OCD inside a microscope incubator, to perform experiments at close physiological conditions.

4.5. Conclusions.

OCD mimicking, to some extent, some physical and biological properties of the splenon, is reported.

This second version of the splenon-on-a-chip, that is able to take advantage of laminar CFP, could perhaps help, someday, to have a better understanding of some spleen's functions.

Also, the presented device could be connected to an autonomous closed-loop pumping system (if needed), that could act as a "micro splenon-like prototype", where future assays with different chemicals could be conducted. This pumping machinery could be also useful, not only for these needs but, perhaps, to be used for distinct research applications.

To validate the use and the effectiveness of this OCD as a human physiological model, different experiments were carried out, using human spleen cells. Further, blood-tissue interface assays were also faced, suggesting the potential of this device to perform, to the extent possible, future tests related to the haematological field.

4.6. References.

1. L.G. Rigat-Brugarolas, A. Elizalde-Torrent, M. Bernabeu, M. de Niz, L. Martin-Jaular, C. Fernandez-Becerra, A. Homs-Corbera, J. Samitier and H.A. del Portillo, *Lab Chip*, 2014, **14**, 1715-1724.
2. P.A. Buffet, I. Safeukui, G. Deplaine, V. Brousse, V. Prendki, M. Thellier, G.D. Turner and O. Mercereau-Puijalon, *Blood*, 2011, **117**, 381-392.
3. A.J. Bowdler, The Complete Spleen, Humana Press, 2nd edition, 2002.
4. R.E. Mebius and G. Kraal, *Nat. Rev. Immunol.*, 2005, **5**, 606-616.
5. A. Petroianu, *Expert Opin. Drug. Saf.*, 2007, **6**, 199-206.
6. J.W. Song and L.L. Munn, *Proc. Natl. Acad. Sci. U. S. A.* , 2011, **108**, 15342-15347.
7. C.A. Parra-Cabrera, C. Sporer, I. Rodriguez-Villareal, R. Rodriguez-Trujillo, A. Homs-Corbera and J. Samitier, *Lab Chip*, 2012, **20**, 4143-4150.
8. A. Benavente-Babace, D. Gallego-Perez, D.J. Hansford, S. Arana, E. Perez-Lorenzo and M. Mujica, *Biosens Bioelectron*, 2014, **61**, 298-305.
9. D.R. Gossett, H.T.K. Tse, J.S. Dudani, K. Goda, T.A. Woods, S.W. Graves and D. Di Carlo, *Small*, 2012, **8**, 2757-2764.
10. P.A. Buffet, G. Milon, V. Brousse, J. M. Correas, B. Dousset, A. Couvelard, R. Kianmanesh, O. Farges, A. Sauvanet, F. Paye, M. N. Ungeheuer, C. Ottone, H. Khun, L. Fiette, G. Guigon, M. Huerre, O. Mercereau-Puijalon and P. H. David, *Blood*, 2006, **107**, 3745-3752.
11. T. Herricks, K.B. Seydel, G. Turner, M. Molyneux, R. Heyderman, T. Taylor and P.K. Rathod, *Lab Chip*, 2011, **11**, 2994-3000.
12. J. Stuart and G.B. Nash, *Blood Reviews*, 1990, **4**, 141.147.
13. J.P. Shelby, J. White, K. Ganesan, P.K. Rathod and D.T. Chiu, *Proceedings of the National Academy of Sciences of the United States of America*, 2003, **100**, 14618-14622.
14. T. Herricks, M. Antia and P.K. Rathod, *Cellular Microbiology*, 2009, **11**, 1340-1353.
15. P. Preira, V. Grandné, J.M. Forel, S. Gabriele, M. Camara and O. Theodoly, *Lab Chip*, 2013, **13**, 161-170.
16. J. Picot, P.A. Ndour, S.D. Lefevre, W. El Nemer, H. Tawfik, J. Galimand, L. Da Costa, J.A. Ribeil, M. de Montalembert, V. Brousse, B. La Pioufle, P. Buffet, C. Le Van Kim and O. Français, *Am. J. Hematol.*, 2015, **90**, 339-345.
17. J.P. Brody, Y. Han, R.H. Austin and M. Bitensky, *Biophysical Journal*, 1995, **68**, 2224-2232.
18. Q. Guo, S.J. Reiling, P. Rohrbach and H. Ma, *Lab Chip*, 2012, **12**, 1143-1150.
19. H. Bow, I.V. Pivkin, M. Diez-Silva, S.J. Goldfless, M. Dao, J.C. Niles, S. Suresh and J. Han, *Lab Chip*, 2011, **11**, 1065-1073.
20. A. Mata, A.J. Fleischman and S. Roy, *Biomedical Microdevice*, 2005, **7**, 281-293.
21. J.C. McDonald and G.M. Whitesides, *Accounts of Chemical Research*, 2002, **35**, 491-499.

22. D.Z. de Back, E.B. Kostova, M. van Kraaij, T.K. van den Berg and R. van Bruggen, *Frontiers in Physiology*, 2014, **5**, 1-11.

23. H.C. Huang, S. Barua, G. Sharma, S.K. Dey and K. Rege, *Journal of Controlled Release*, 2011, **44**, 344-357.

24. J.V. Jokerst and S.S. Gambhir, *Accounts of Chemical Research*, 2011, **44**, 1050-1060.

25. S.H. Radwan and H.M. Azzazy, *Expert Review of Molecular Diagnostics*, 2009, **9**, 511-524.

26. J.K.S. Park, J. Tae, B. Choi, Y.S. Kim, C. Moon, S.H. Kim, H.S. Lee, J. Kim, J. Park, J.H. Lee, J. E. Lee, J.W. Joh and S. Kim, *Nanomedicine*, 2010, **6**, 263-276.

27. X. Huang, I.H. El-Sayed, W. Qian and M.A. El-Sayed, *Journal of the American Chemical Society*, 2006, **128**, 2115-2120.

28. M. Varna, P. Ratajczak, I. Ferreira, C. Leboeuf, G. Bousquet and A. Janin, *Journal of Biomaterials and Nanobiotechnology*, 2012, **3**, 269-279.

29. H.L. Herd, K.T. Bartlett, J.A. Gustafson, L.D. McGill and H. Ghandehari, *Biomaterials*, 2015, **53**, 574-582.

30. X.D. Zhang, D. Wu, X. Shen, P.X. Liu, N. Yang, B. Zhao, H. Zhang, Y.M. Sun, L.A. Zhang and F.Y. Fan, *International Journal of Nanomedicine*, 2011, **6**, 2071-2081.

31. W.H. De Jong, W.I. Hagens, P. Krystek, M.C. Burger, A.J. Sips and R.E. Geertsma, *Biomaterials*, 2008, **29**, 1912-1919.

32. G. Sonavane, K. Tomoda and K. Makino, *Colloids Surf. B Biointerfaces*, 2008, **66**, 274-280.

33. J. Turkevich, P. Stevenson and J. Hillier, *Discuss. Faraday Soc.*, 1951, **11**, 55-60.

34. Y. Zheng, J. Chen, M. Craven, N.W. Choi, S. Totorica, A. Diaz-Santana, P. Kermani, B. Hempstead, C. Fischbach-Teschl, J.A. López and A.D. Stroock, *Proceedings of the National Academy of Sciences of the United States of America*, 2012, **109**, 9342-9347.

35. L. Brass, *Nature Medicine*, 2009, **15**, 607-608.

36. S. Takayama, J.C. McDonald, E. Ostuni, M.N. Liang, P.J.A. Kenis, R.F. Ismagilov and G.M. Whitesides, *Proceedings of the National Academy of Sciences of the United States of America*, 1999, **96**, 5545-5548.

37. A. Petroianu, The Spleen, Bentham eBooks, 2011.

38. A.M. Forsyth, J. Wan, W.D. Ristenpart and H.A. Stone, *Microvascular Research*, 2010, **80**, 37-43.

39. M.E. Myrand-Lapierre, X.Deng, R.R. Ang, K. Matthews, A.T. Santoso and H. Ma, *Lab Chip*, 2015, **15**, 159-167.

40. S. Huang, A. Amaladoss, M. Liu, H. Chen, R. Zhang, P.R. Preiser, M. Dao and J. Han, *Infect. Immun.*, 2014, **82**, 2532-2541.

41. S. Sanchez, A.A. Solovev, S.M. Harazim, C. Deneke, Y.F. Mei and O.G. Schimdt, *The Chemical Record*, 2011, **11**, 367-370.

42. S. Sanchez, L. Soler and J. Katuri, *Angew. Chem. Int. Ed.*, 2015, **54**, 1414-1444.

Chapter 5. Usage of 3D printing techniques to build a splenon-like microfluidic platform

SUMMARY

In this chapter, a novel platform based on the previously described OCD devices will be proposed: a splenon-like filtration unit prototype fabricated using stereolithography.

PDMS techniques, although proven (very) efficient for conceptual testing in research laboratories, are not readily translated into mass-fabrication methodologies, and are difficult to be used for complex 3D architectures. On the other hand, strategies closer to large volume manufacturing tend to be too expensive for prototyping. The idea, then, was to solve these issues while gaining deeper understanding on 3D printing, in order to improve on certain aspects of the splenon-on-a-chip device.

The possibility to create a microfluidic device that could be "mass-produced", user-friendly and plug-n-play ready was perceived as interesting in order to, ideally, help to overcome, in the future, some of the difficulties that are inherently linked to splenic pathological and physiological studies.

5.1. Introduction.

Microfluidic devices are generally built by milling, hot embossing, molding or soft lithography or multiple-layers bonding using polymers, being PDMS the most commonly used (as detailed in Chapter 1.1.6.).[1-3] PDMS is, importantly, elastomeric, a property that is key for producing some particular fluidic components.[1,4-7] But, despite some interesting features (such as the possibility to replicate micron-resolution structures),[6,8,9] PDMS mold fabrication requires a time-consuming manual procedure.[1,8,9] Also, in order to be cost-effective, alternative molded devices have to be produced on a large scale and, habitually, are difficult to be customized straightforwardly,[1,8] thus making them not fully suitable for rapid prototyping.[1]

This methodology, though being widely used, may lack some of the flexibility required by startup companies or for massive clinical tests, where materials closer to the ones available for volume production procedures need to be tested.[1] Is then in this scenario where 3D printing presents its credentials (to help to overcome, to some extent, those challenges), providing alternative tools to, perhaps, advance in the studies of different fields.[1]

From an historical perspective, the concept of this 3D technique was first described by C. Hull.[10] It was in the 1980s when he obtained the patent for stereolithography and when he founded 3D Systems, and developed the *.stl file format.[10] With his work, together with the (*i*) development, and posterior patenting, of the Fused Deposition Modeling technology, and (*ii*) the first patented apparatus termed "3D printer" (in 1993), 3D printing was ready to revolutionize manufacturing.[10] From that moment, this technology has found industrial applications on a wide variety of issues.

3D printing,[1,11] referring to a number of processes that encompass layer-by-layer or (also known as) additive manufacturing techniques, allows synthesizing solid 3D objects but under a precise computer control. It has recently achieved the maturity to even construct complex micro devices at high resolution and fast building times, with the capacity of simplifying the fabrication process to few steps.[1,10-13] Apart from microfluidics,[1,11,12,14] this kind of technology has become, likewise, a promising fabrication tool for a broad range of applications, even in the biomedical field.[1,10-14]

With respect to a research context, there are several distinct 3D printing methods available;[10,11] some of them, like Stereolithography (very relevant to microfluidic device fabrication), are highly consolidated, while others, like Bioprinting, are in the process of developing.[10,11,15,16] The factors to determine the machine or technique of choice are, mainly: (*i*) resolution, (*ii*) building time, (*iii*) material selection and properties (such as, for example, transparency or mechanical properties), (*iv*) build size and/or (*v*) price.[10,11,16]

3D printing techniques that are able to fabricate microfluidic devices normally use photopolymer resins as working materials, due to the characteristics needed for this kind of platforms.[1,10,11,16] Stereolithography,[1] Digital Micromirror Device-based Projections printing, Inkjet printing or Two-photon polymerization are some of the most used methodologies in this framework.[10,11,12,14,16,17]

Stereolithography technology,[1,12,14,17] for its part, allows for the fabrication of 3D structures using photopolymerization (starting from a photosensitive resin precursor on a vat) by means of either

a digital light projector (DLP, as shown in the scheme of Figure 5.1A) or a laser.[1,18,19] Due to its interesting advantages, has become an attractive way to fabricate complex microfluidic devices, because of its minimal-labor process and decreasing costs,[20] partly thanks to the low usage of liquid medium.[1] This procedure have seen to be one of the most appropriate for producing low-cost microfluidic devices, in comparison with other mentioned methods.[20]

Using this technique, channels defining microfluidic devices may be fabricated by polymerizing its walls and draining, afterwards, the uncured resin of the internal structure.[1,20,21] The design of these devices may be done entirely using CAD softwares (such as Autodesk Inventor®), which could be compatible to finite-element modeling.[1,12,20] This fact allows the designing of (complex) "plug-n-play" devices, such as the one presented in Figure 5.1B.[1,12,20]
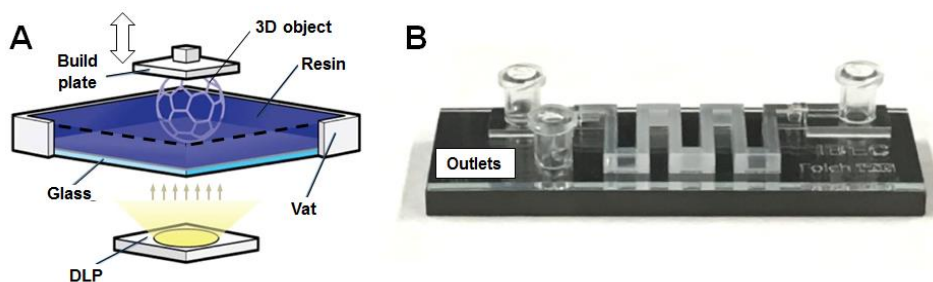
Figure 5.1. Stereolithography setup and a 3D printed device. *(A) DLP stereolithography setup. (Figure adapted from Reference 1). (B) Particle separator device, fabricated using stereolithography, that could take profit of gravitational and/or magnetic properties to supposedly direct different elements to different outlets (by L.G. Rigat-Brugarolas et al.).*

Although in recent years there has been a breakthrough in the field of microfluidics, the uptake rate in basic research has not seemed to follow the same trend. Surely there are several factors that affect this but, probably, the conventional time-consuming processes for manufacturing the chips have, maybe, highlighted this result.[11]

Within this framework, and taking profit of stereolithography as building process, and its intrinsic properties (interesting for microfluidic device fabrication), a novel "industrial-like" version of the splenon-like prototype, aiming to facilitate clinical assays (particularly in a medical or biological environment), will be presented. This filtering unit prototype has been conceived, and designed, to try to overcome several restrictions of the previous versions of the splenon-on-a-chip, having the possibility of "fast mass-production", ease of use or simple-customization. So, in this regard, rather than "operating" with PDMS microconstrictions (simulating the splenon IES)[22] this version of the splenon-on-a-chip works with (exchangeable) porous membrane filters.

The idea, however, is not to replace or avoid using the first OCDs models, devices that could be used to perform blood assays and/or to study some biological hypotheses (as described), but to address the problem associated to the difficulty of performing "splenon-oriented" studies from different points of view (to the extent possible), and with the possibility of perhaps having a large number of replicas in a short time.

5.2. Splenon-on-a-chip version 3-D.

5.2.1. Device fabrication using stereolithography.

In collaboration with Prof. Folch Lab (University of Washington, UW, USA), different strategies were targeted in order to fabricate the 3D transparent filtering platforms designed and presented in Chapter 2.4., using stereolithography. The first trials involved testing the poly(ethylene glycol) diacrylate (PEG-DA)-250 as building material, using different photoinitiators.[1] PEG-DA has been used, previously, to fabricate microfluidic devices, but mainly using photolithography.[1,23] P.N. Nge *et al.* made an exhaustive evaluation of various favorable properties of PEG-DA, compared to other polymers.[24] This is why it was thought the PEG-DA-250 (that can be cheap, transparent and biocompatible) to be an excellent choice for this commitment (taking into account that some other available stereolithographic resins usually do not have all those favorable properties).[1]

In this regard, using an Ilios 3D-Printer (Ilios3D, Larnaca, Cyprus), a fabrication procedure was tested and reported, obtained in collaboration with Prof. Folch Lab, for transparent PEG-DA-250 resin 3D printing, as described elsewhere (A. Urrios *et al.*, more information in Reference 1).[1]

Although this approach provides now a major step in "laboratory" 3D printing, the need of high-throughput fabrication, at that moment, resulted in testing another photocurable resin, that could permit high resolution while remaining transparent enough, as could be possible with PEG-DA,[1] to fabricate the novel splenon-on-a-chip prototype. One resin that offers this kind of properties is the so-called Somos® WaterShed XC 11122.

It is for this reason that the devices were finally built by Fineline Prototyping, Inc. (Raleigh, North Carolina), that has the expertise, and commonly uses the Somos® WaterShed XC 11122 resin, as detailed in Chapter 2.4.2. Mail-order microfluidics have been reported to have "interesting" advantages, particularly in the sense of providing a simple route for the obtainment of complex transparent microdevices, with high XYZ resolutions.[20] Albeit this attractive feature, it was even difficult to fabricate the designed splenon-on-a-chip versions due to their architecture. Figure 5.2 shows some differences when fabricating these devices with different techniques.
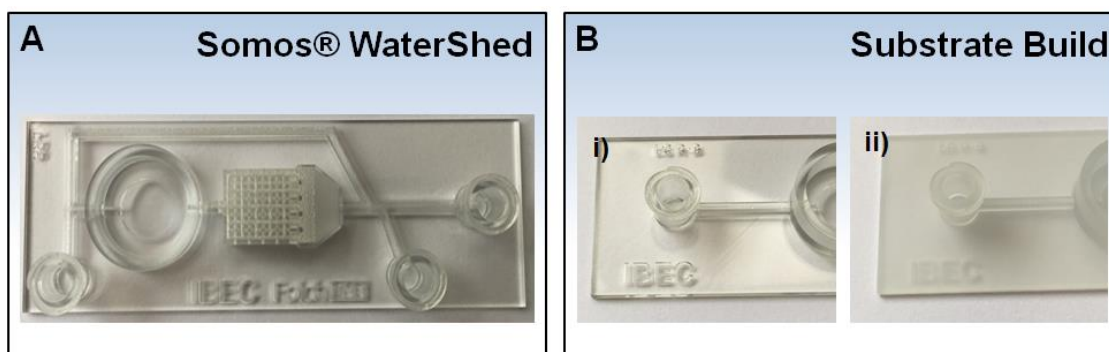

Figure 5.2. Studies with different techniques. *(A) A device fabricated with the Somos® WaterShed XC 11122 resin. (B) A Fineline Prototyping, Inc. proprietary process called "Substrate Build Style" could also be selected to fabricate the device: (i) device fabricated with or (ii) without this build option.*

5.2.2. Splenon-on-a-chip versions 3-D.

Eventually, several prototypes, shown in Chapter 2.4., were fabricated, and finally tested. These devices will be referred to as: splenon-on-a-chip "version 3-D 1.0" and "version 3-D 2.0" (Figure 5.3, left and right panel, respectively). The first platform represents a "simpler" version, whereas the last mentioned corresponds to a more "accurate" splenon-like concept, since it incorporates, in a simplified manner, the compartments simulating the splenon dual microcirculation.[9,22]

Figure 5.3A,B presents some details and planes of the first version, a "filter-like" device with one inlet and one outlet. The disposal of these connections is not random, since the fluid entrance must connect with the upper face of the membrane (Figure 5.3Aii), that has to be positioned on the membrane holder, designed for this purpose. This section is common to the second version (Figure 5.3C,D, details and planes, respectively), although this one has channels representing distinct microcirculations, and a "reticular-like" structure, that pretends to resemble the reticular meshwork (Figure 5.3Cii).[9,22] The microfluidic device may be positioned on a microscope holder (Figure 5.3E); thanks to the fact that it has two inlets, it is able to take advantage of laminar CFP (Figure 5.3F). Also, blood samples may flow through a device without evident difficulties (Figure 5.3G represents the "open circulation"[9,22] and 5.3H the branching point of the channels).
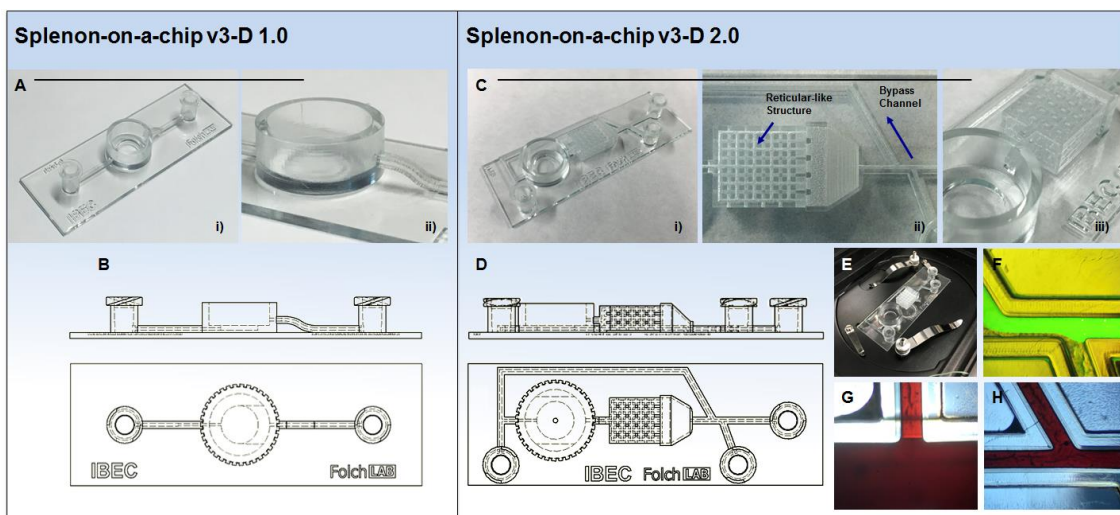

Figure 5.3. Splenon-on-a-chip 3D preliminary prototypes. (A) Images of the first 3D printed device. (B) Planes of the device. (C) Images of the second 3D printed device. (D) Planes of this version. (E) A 3D device disposed on a chamber. (F) Fluorescence image showing CFP. (G) The "open circulation" achieved in the device. (H) The branching point.

5.2.3. Microfluidic connectors.

The female Luer Lock connectors (Figure 5.4A), built into these splenon-on-a-chip versions, are one of the most important elements of the prototypes. Makes it possible, using Luer adapters, to (easily) interface the tubing with the devices in a reversibly way (Figure 5.4B). Also, its structure permits (*i*) syringes to be disposed directly (as shown in Figure 5.4C) and (*ii*) the connection of a broad range of (commercial) components to the inlet(s) and/or outlet, helping to "customize" the device when needed (Figure 5.4D).[20] Thanks to this feature, this version ensures a user-friendly status, since the disposal of these adapters is simple, and should entail no problematic in terms

of possible sample leakage. This amicable connectivity is, possibly, one of the strengths of this 3D microfluidic device version.
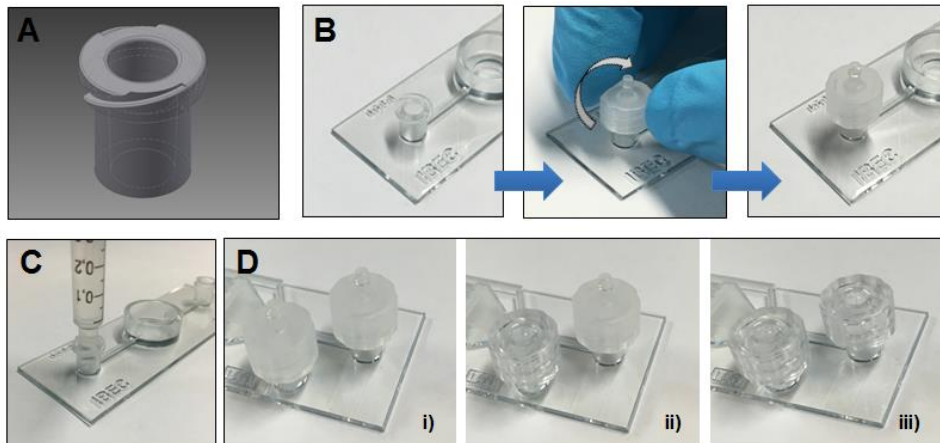

Figure 5.4. Device connectivity. *(A) Female Luer Lock design visualized using Autodesk Inventor®. (Original design by N. Felix, GrabCAD.com).[20] (B) The disposal of Luer adapters is simple and reversible. (C) The structure of the connectors allows, in addition, the disposal of syringes. (D) Different components may be disposed in the device to have, for example (i) two inlets opened, (ii) one inlet opened and one closed or (iii) both inlets closed.*

5.2.4. Membrane characterization.

As one key feature of this splenon-on-a-chip, it could be possible to filter the blood samples, this time, by using porous membrane filters, allowing the 3D platforms to be partly customizable and reusable, virtue perhaps not usually available in common microfluidic devices.

In first instance, membranes with a pore size of ~5 μm were selected for this commitment. This decision was based, in part, on the featured pores, that had, sometimes, apertures similar to the ones presented in the previous versions. This is of particular relevance, since replicating "close" splenon IES dimensions was required in order to try to replicate, to the extent possible, some physiological scenarios. After the characterization using Atomic Force Microscopy (AFM, Figure 5.5A), it could be possible to define that its Young's modulus was high enough to suggest that unhealthy samples could perhaps not be able to pass easily through the apertures (~870 MPa, Figure 5.5B).
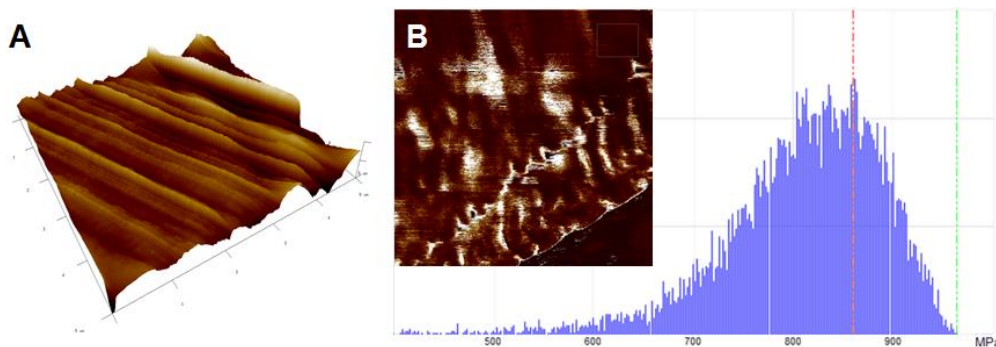
Figure 5.5. Membrane characterization. *(A) AFM relief image. (B) Mechanical properties characterization of a membrane, using AFM techniques.*
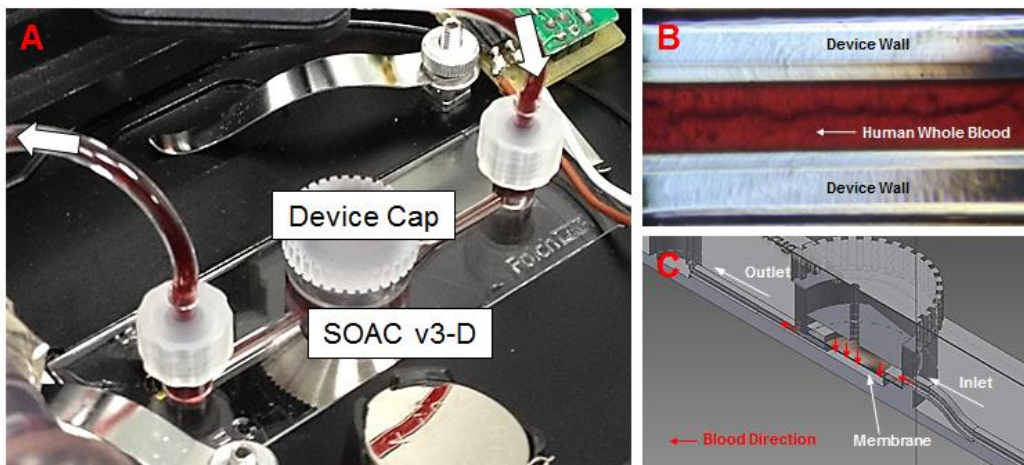
5.2.5. Operating principle of the system.

One of the premises while designing these microfluidic devices was that their operability had to be as simplest as possible. Thanks to the connectivity presented before, these platforms allow a wide range of tubes and fittings to be incorporated to the inlets/outlets. A proper connection to the autonomous closed-loop pumping machinery was interesting for the study. Also, the distinct version prototypes could be placed effortless in the microscope culture chamber (Figure 5.6A).

The selection of the building material was, obviously, a factor of paramount importance; in this sense, the Somos® WaterShed resin was transparent enough to permit the visualization, *via* an inverted microscope, of different samples flowing inside the devices (example in Figure 5.6B).

Once the platform and the pumping system are correctly linked, the next step entails disposing a cap and a membrane, before starting an experiment. As it was described in Chapter 2.4., the basic operating principle of the device is that a membrane has to be disposed in the membrane holder, and the cap, designed for this particular device (with the correct dimensions to prevent, to the extent possible, a sample leakage), should press, and hold, the membrane along its outer diameter, leaving the internal part to supposedly filter the samples.

The scheme found in Figure 5.6C represents the intended blood direction/motion, starting in the inlet, passing through the "membrane holder section" and, finally, getting out of the device.

Figure 5.6. Operating principle of the splenon-on-a-chip version 3-D. *(A) A microfluidic device disposed in the microscope culture chamber and connected to the autonomous closed-loop system. (B) Blood flowing inside the device. (C) Scheme representing the intended blood direction/motion inside the device.*

5.3. Blood studies using the 3D microfluidic device prototype.

The capacity to perform tests to evaluate the state of a blood sample, in a simple manner, could perhaps be, in the future, an interesting method to: (*i*) verify the health of a person, (*ii*) be used as therapeutic monitoring or to (*iii*) prove the viability of a blood sample.

In this regard, in order to preliminarily test the usability of the 3D printed microfluidic platforms to characterize, to some extent, blood status, trials were done using human samples, as a proof of concept. By disposing a membrane in a device (in this case, the "simpler" version 1.0, as shown in Figure 5.7A), blood was pumped through it, and afterwards the membrane was collected for further analysis.

Most representative and preliminary results/images of the post-assay membranes are shown in Figure 5.7Bi. In these cases, as could be observed, as the tested blood sample is "more aged", differences in terms of membrane appearance could perhaps get more evident once the sample has passed through it. These membranes were weighed on a bascule (Figure 5.7Bii), and it was possible to notice that an increase in weight could be measured (from $7.7 \cdot 10^{-6}$ kg to $8.9 \cdot 10^{-6}$ kg, control and aged blood sample, respectively).
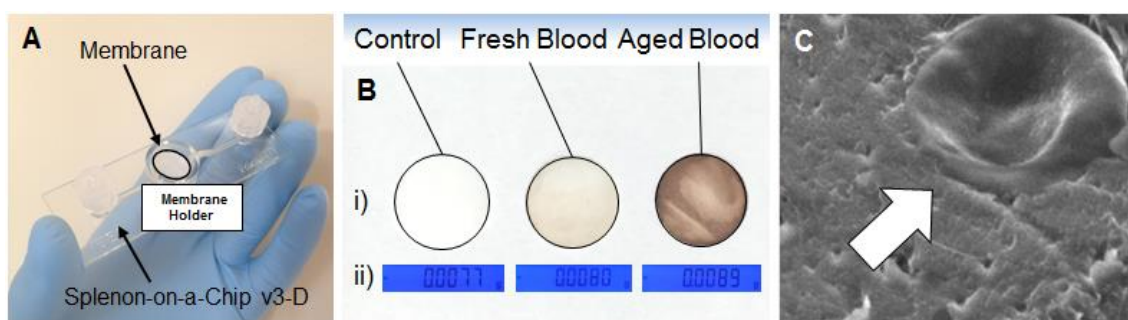
Figure 5.7. Blood studies performed using the splenon-on-a-chip version 3-D (proof of concept). (A) Splenon-on-a-chip version 3-D with a membrane disposed inside the holder. (B) (i) Assays with different blood samples; (ii) shows the weights of the different membranes. (C) SEM image of a cell in a membrane.

Obviously, this methodology to "estimate or assess" the deformability of RBCs or the status of different blood samples could differ from the 2D strategy used in the previous splenon-on-a-chip versions (more information in Chapter 2.2.3.5.). In the case of these 3D printed devices, it would not be possible to measure/observe the elongation of the RBCs while crossing the constrictions, something interesting for the evaluation of some pathological settings. Even so, both techniques may be complementary.

In any case, an advantage of utilizing a "porous membrane approach" could be that, rather than having a low number of constrictions (simulating the IES), in this case the number of apertures could be several times greater than when using a conventional PDMS-constructed device, and could perhaps offer a more detailed approach of what could be likely to happen in the splenon. Also, as shown in Figure 5.7C, blood samples could be inspected once a membrane has been collected, allowing to analyze those cells that have been not able to pass through the structure. Studies with different membranes and samples are envisioned.
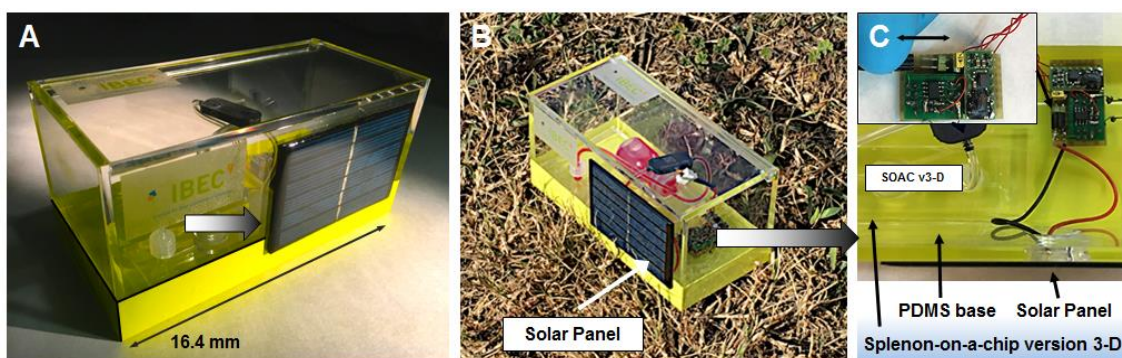
5.4. Autonomous filtering unit solar platform prototype.

A not inconsiderable proportion of people in the world have no access to electricity. This means that, for example, some families, in developing countries, have to spend part of their income on basic energy services.

Being aware of this (important) global problem, and taking into account the specifications shown with respect to the autonomous pumping system (designed to work with the devices), one of the project final aims was to design the first phase of what could be a future "splenon-like filter unit" prototype that could, using these devices, perhaps facilitate, in the future, some haematological tests taking profit of solar photovoltaic technology.

This preliminary prototype, presented in Figure 5.8A, could operate with a solar panel located in its casing (measures [length/width/height] ≈ 164 mm x 80 mm x 80 mm). This way, the pumping machinery (placed in the interior) can work totally autonomously using solar energy. Thus, some future testing could be done without needing to be connected to the current (Figure 5.8B shows an example, as a proof of concept, of a water with color additive test carried outdoor).


Figure 5.8. Autonomous filtering unit solar platform first prototype. (A) Image of the prototype showing the solar panel. (B) A water test carried outdoor. (C) Detail of the interior of the prototype.

Figure 5.8C presents some details of the interior of this first prototype. It is important to note that the driving stage can easily switch its source of energy, by changing the connector disposed for that purpose (upper box of Figure 5.8C). Inside can be found a custom base, designed to locate the splenon-on-a-chip 3D printed version and the blood reservoir, having also an inferior layer to place a micro-shaker.

5.5. Discussion and conclusions.

3D printing techniques that are able to synthesize transparent objects, and microfluidic devices, at acceptable resolution have gained importance in the last years.[10,11,16] This fabrication process could also efficiently accelerate the creation of complex platforms.[1,11] So, the "mass-fabrication" of user-friendly and plug-n-play apparatus, in an easy way, could be seen as an important point to advance studies in the field of, for instance, haematology.

For that matter, in this part of the work it has been presented several devices, fabricated using stereolithography, with the intent of representing, to the extent possible, another study point of view in the framework of splenic research. The final aim was to fabricate an "industrial" splenon-like filtering prototype that could provide a promising approach to conduct future blood-oriented tests in a simple way (a comparison with the previous versions in shown in Figure 5.9). One of the particularities of these 3D platforms is that they work with porous membrane filters.
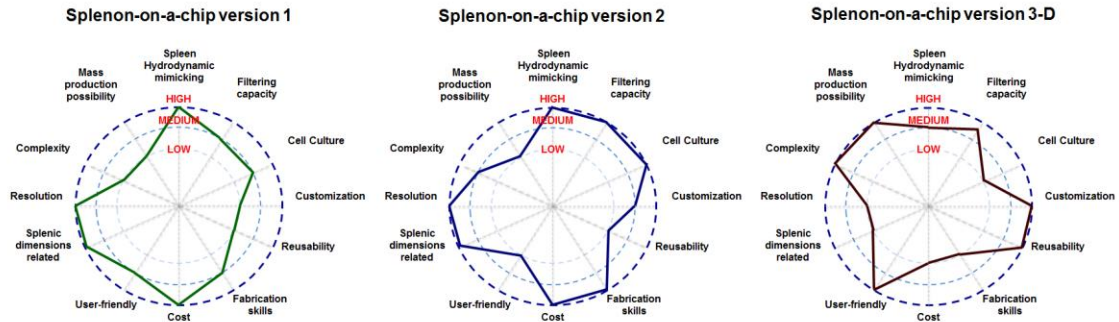
Figure 5.9. Comparison between the different splenon-on-a-chip versions. *Radar charts illustrating the tradeoffs for each version of the splenon-on-a-chip. The different categories are common between them.*

The preliminary results suggested that a membrane, after a trial, could perhaps be able to show or present some visual differences depending on the status of the samples. Although more trials (with distinct membranes and samples) should be done in order to fully characterize the system and the methodology and, therefore, determine its robustness, those initial trials represents the initial touchstone of this proof of concept strategy.

A preliminary prototype, the proof of concept of an "autonomous filtering unit solar platform" was designed, that could be able to help, in the future, to conduct studies in an innovative way. As it can operate without needing to be connected to the current, it may be useful to undertake some future tests in any location.

Therefore, 3D printed devices, such as the ones shown, could become, in the future, interesting platforms, manufactured at any part, without the need of big infrastructures (just employing a 3D printer).[1,12,14]

5.6. References.

1. A. Urrios, C.A. Parra-Cabrera, N. Bhattacharjee, A.M. González-Suárez, L.G. Rigat-Brugarolas, U. Nallapatti, J. Samitier, C.A. DeForest, F. Posas, J.L. García-Cordero and A. Folch, *Lab Chip*, 2016, **16**, 2287-2294.
2. A. Mata, A.J. Fleischman and S. Roy, *Biomedical Microdevice*, 2005, **7**, 281-293.
3. J.C. McDonald and G.M. Whitesides, *Accounts of Chemical Research*, 2002, **35**, 491-499.
4. T.K. Kim, J.K. Kim JK and O.C. Jeong, *Microelectronic Engineering*, 2011, **88**, 1982-1985.
5. T. Thorsen, S.J. Maerkl and S.R. Quake, *Science, 2002,* **298**, 580-584.
6. G.M. Whitesides, *Nature,* 2006*,* **442**, 368-373.
7. E.K. Sackmann, A.L. Fulton and D.J. Beebe, *Nature*, 2014, **507**, 181-189.
8. A. Folch, Introduction to BioMEMS, CRC Press, 2013.
9. L.G. Rigat-Brugarolas, A. Elizalde-Torrent, M. Bernabeu, M. de Niz, L. Martin-Jaular, C. Fernandez-Becerra, A. Homs-Corbera, J. Samitier and H.A. del Portillo, *Lab Chip*, 2014, **14**, 1715-1724.
10. C. Gross, J.L. Erkal, S.Y. Lockwood, C. Chen and D.M. Spence, *Anal. Chem.*, 2014, **86**, 3240-3253.
11. C.M.B. Ho, S.H. Ng, K.H.H. Li and Y.J. Yoon, *Lab Chip*, 2015, **15**, 3627-3637.
12. A.K. Au, N. Bhattacharjee, L.F. Horowitz, T.C. Chang and A. Folch, *Lab Chip*, 2015, **15**, 1934-1941.
13. J.R. Tumbleston, D. Shirvanyants, N. Ermoshkin, R. Janusziewicz, A.R. Johnson, D. Kelly, K. Chen, R. Pinschmidt, J.P. Rolland, A. Ermoshkin, E.T. Samulski and J.M. DeSimone, *Science*, 2015, **347**, 1349-1352.
14. W. Lee, D. Kwon, W. Choi, G.Y. Jung, A.K. Au, A. Folch and S. Jeon, *Sci. Rep.*, 2015, **5**, 7717.
15. S.V. Murphy and A. Atala, *Nature Biotechnology*, 2014, **32**, 773-785.
16. N. Bhattacharjee, A. Urrios, S. Kang and A. Folch, *Lab Chip*, 2016, DOI: 10.1039/c6lc00163g.
17. I. Shallan, P. Smejkal, M. Corban, R.M. Guijt and M.C. Breadmore, *Anal. Chem.*, 2014, **86**, 3124-3130.
18. A. Waldbaur, H. Rapp, K. Lange and B.E. Rapp, *Anal. Meth.*, 2011, **3**, 2681-2716.
19. P.J. Bártolo, Stereolithography: Materials, Processes and Applications, Springer, 2011.
20. A.K. Au, W. Lee and A. Folch, *Lab Chip*, 2014, **14**, 1294-1301.
21. H.W. Kang, I.H. Lee and D.W. Cho, *J. Manufacturing Sci. & Eng.*, 2004, **126**, 766-771.
22. A.J. Bowdler, The Complete Spleen, Humana Press, 2nd edition, 2002.
23. Y.K. Cheung, B.M. Gillette, M. Zhong, S. Ramcharan and S.K. Sia, *Lab Chip*, 2007, **7**, 574-579.
24. P.N. Nge, C.I. Rogers and A.T. Woolley, *Chemical Reviews*, 2013, **113**, 2550-2583.

Chapter 6. General conclusions

6. General conclusions.

6.1. Conclusions.

In this work, different OCD biomimetic devices mimicking, to the extent possible, some splenon properties have been designed, fabricated and tested with the aim of facilitating future functional studies of the spleen in relation to some haematological disorders.

In order to construct the microfluidic devices, novel fabrication protocols (detailed in **Chapter 2**), based on photolithographic techniques, had to be defined to finally obtain multilayered devices, in a cost-effective manner. The premise was to replicate, to the extent possible, the architecture of the human splenon.

Furthermore:

Developing and using the **first splenon-on-a-chip version**, that was presented in **Chapter 3**, it could be possible to mimic, to a certain extent, close splenon blood flow patterns and the organ filtering functions. Unlike any other previous spleen-like device, this platform incorporates two compartments with a close splenon-like flow division, and two physical barriers representing the reticular meshwork and the IES. To validate the use of this platform, several experiments were carried out with different types of blood samples. As a proof of concept, it was shown that, when traversing the constrictions, old RBCs were usually less deformable than fresh RBCs. Posterior analysis allowed studying the passage, and deformability, of infected cells through the IES-like slits, using blood of BALB/c mice experimentally infected with *P. yoelii*. The results showed that, statistically, iRETs were more deformable than uninfected cells. Therefore, these results could suggest that this OCD device prototype could be capable of reproducing, to the extent possible, some physiological conditions.

For its side, in **Chapter 4** was presented an enhanced biomimetic platform, and an autonomous closed-loop pumping station. Using the **splenon-on-a-chip version 2**, that may take advantage of laminar CFP, and presents an increased filtering capacity, it was possible to mimic, to some extent, part of the most representative cellular microenvironment of the splenon. In this regard, some blood-tissue interface assays were faced (studying, for instance, platelet adhesion to the coated microfluidic network, or the *in vitro* clot formation), suggesting the fact that this device could perhaps be useful to perform, in the future, certain tests related to vascular interactions. Also, the splenic immune response was, to some extent, partly mimicked, using human spleen macrophages.

As a proof of concept, a first approximation to an obstruction-like scenario was modeled, using several RBCs populations. Additionally, the nanoparticles retention in the slow-flow channel was investigated, and some trials with self-propelled microjets were performed, in order to try to help to position this biomimetic platform as an OCD microfluidic device that could have the potential to make a future impact in the field of biomedical sciences.

Finally, a 3D printed microfluidic device, named **splenon-on-a-chip version 3-D** (and shown in the **Chapter 5**), was designed to create an "industrial concept" of a splenon-like prototype. This device, fabricated using stereolithography, has the particularity that could function with porous membrane filters, with the view to act as the splenon IES; so this version is partly customizable, and reusable, since the membranes can be easily exchangeable. Also, in this framework, and using the presented 3D devices, the first phase of what could be a future "splenon-like filter unit" prototype, working with a solar panel, was designed and shown (as a proof of concept), with the aim that, someday, could perhaps help in facilitating some haematological tests.

Organ-on-a-chip microfluidic devices mimicking human splenic functions

Luis Guillermo Rigat Brugarolas